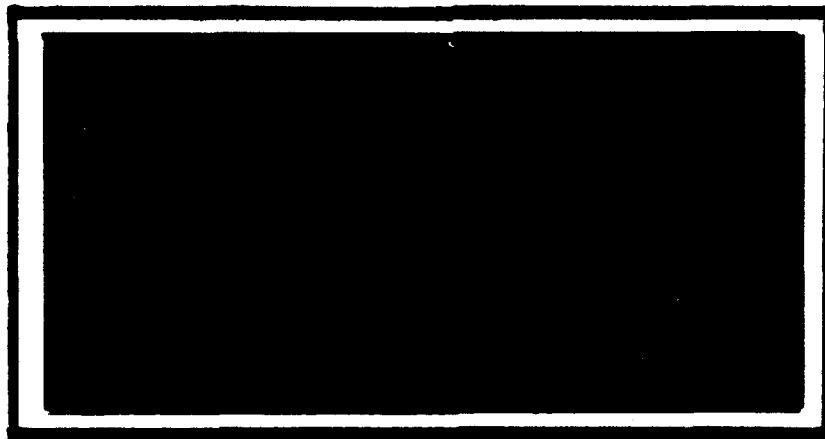AD-A230 628

DTIC
ELECTE
SJAN 0 7. 1991
B
D

DEPARTMENT OF THE AIR FORCE
AIR UNIVERSITY
AIR FORCE INSTITUTE OF TECHNOLOGY

Wright-Patterson Air Force Base, Ohio

PII Redacted

91 1 3 184

AFIT/GAE/ENY/90D-25

MODELLING AND ANALYSIS OF KERNEL FUNCTION AND
DEVELOPMENT OF EQUIVALENT THEODORSEN FUNCTION
FOR THREE-DIMENSIONAL AEROELASTIC ANALYSIS

THESIS

John K. Ryder
Captain, USAF

AFIT/GAE/ENY/90D-25

DTIC
ELECTE
JAN 0 7 1991
S
B
D

AFIT/GAE/ENY/90D-25

MODELLING AND ANALYSIS OF KERNEL FUNCTION AND DEVELOPMENT OF EQUIVALENT

THEODORSEN FUNCTION FOR THREE-DIMENSIONAL AEROELASTIC ANALYSIS

THESIS

Presented to the Faculty of the School of Engineering

of the Air Force Institute of Technology

Air University

In Partial Fulfillment of the

Requirements for the Degree of

Master of Science in Aerospace Engineering

John K. Ryder, M.S., B.M.E.

Captain, USAF

December 1990

Approved for public release; distribution unlimited

Preface

My original objective in performing this thesis was to learn about this strange fractional calculus by applying its principles to unsteady aerodynamics. The original goal was to analytically integrate the pressure-downwash integral equation (a feat which had never been accomplished before) by simplifying the mathematics through the use of the fractional calculus. As the research progressed, the unsteady aerodynamic problem proved to be more challenging than originally anticipated and the analytic integration was not achieved. However, this treatment is the first recorded attempt to model three-dimensional unsteady aerodynamic forces on wings with fractional calculus. By being the first, there was a great deal of ground to cover and a fair amount of dead ends discovered. However, I was able to simplify the unsteady three-dimensional aerodynamic problem by the development of the equivalent Theodorsen function. This development will permit the unsteady aerodynamic loads on a finite airfoil to be written in a compact mathematical form and easily evaluated and applied to control system design. The thesis is written in such a way to allow an individual unfamiliar with the material to read and understand the concepts and to continue the work if desired.

I wish to give a special thanks to Lt Col Ron Bagley for his tolerant listening abilities and strong guidance. I would also like to thank Captain Greg Warhola for providing me with an appreciation of mathematics and for his encouragement and understanding during a

ii

difficult personal crisis. Finally, I would like to express my
heartfelt appreciation to my wife, Suzie, and daughter, Alex, for their
understanding and strong support in helping me achieve one of my goals.

I would like to dedicate this thesis to two special people.
First, to my mother whose strength and determination through a recent
divorce inspired me to continue under difficult circumstances. And to
Alex, on the anniversary of her first birthday, whose accomplishments
will someday outshine my own.

Table of Contents

List of Figures

List of Symbols

AR	aspect ratio, $4\ell^2/S$
a, b, g, f, μ	parameters of fractional calculus model of equivalent Theodorsen function, functions of AR
A_{ij}	area of panel (i,j)
b_0	root semichord, ft
B, B_R, B_I	functions defined by equations (37), (39), (40)
c_{ij}	chord of panel (i,j)
$C_{L,\alpha}$	complex total coefficient of lift associated with pitching
$C_{l,\alpha}$	complex coefficient of lift per unit span associated with pitching
C(k)	Theodorsen Function for two-dimensional unsteady aerodynamic forces
$D^{\alpha+m}[\ ]$	fractional derivative of order α+m, m an integer
$E_\mu(x)$	Mittag-Leffler function of order μ
H(x,y,t)	vertical displacement of airfoil, positive downward, ft/sec
h	plunging motion variable
$h_j(x,y)$	shape function of vertical displacement of j-th mode
$I_0(\ )$	modified Bessel function of first kind of zero order
$I_1(\ )$	modified Bessel function of first kind of first order
I, II, III	regions of spanwise integration, equation (33)
i	$(-1)^{1/2}$
$K_1(\ )$	modified Bessel function of second kind of first order

$K[M,k,x_0,s(y-\eta)]$	kernel function of integral equation, ft^{-2}
$K^*[M,k,x_0,s(y-\eta)]$	modified kernel function
$K^*[k,x_0,s(y-\eta)]$	incompressible modified kernel function
k	reduced frequency, $\omega b_0/V$
$\underline{K}$	kernel function matrix
L	total lift per unit span, positive downward
$L_1()$	modified Struve function of first order
ℓ	wing semispan, ft
$\mathcal{L}$	Laplace transform
$\mathcal{L}^{-1}$	inverse Laplace transform
M	Mach number
N_x, N_y	number of panels in x, y direction
N	total number of panels
$\Delta P(\xi,\eta,t)$	local dynamic pressure between top and bottom surface of wing, lb/sq ft
P_{ij}	dynamic pressure on panel (i,j)
$q_j(t)$	generalized coordinate of j-th degree of freedom, $q_j \exp(i\omega t)$ (j replaced by α denotes pitching)
Q	matrix of constraint
S	area of wing surface, sq ft
s	ratio of wing semispan to root semichord, ℓ/b_0
s	dimensionless Laplace variable, $\hat{s}b_0/V$
$\hat{s}$	Laplace variable
S'	surface used to model wing
t	time, sec
$\bar{t}$	dimensionless time, tV/b_0

$T(k)$	equivalent Theodorsen function
$u_1(t)$	step function
$u_0(t)$	delta function
$u_{-1}(t)$	doublet function
V	velocity of airstream, ft/sec
$w(x,y)$	amplitude function of the prescribed downwash, $w(x,y,t)=w(x,y)\exp(i\omega t)$, ft/sec
x,ξ	chordwise coordinates referred to b_0
$x_0=x-\xi$	
y,η	spanwise coordinate referred to ℓ
$y_0=y-\eta$	
z	vertical coordinate, Figure 1
α	angle of attack
$\alpha(x,y,t)$	pitching mode shape
β	$(1-M^2)^{1/2}$
Γ	gamma function
δ	Dirac delta function
ϵ	small dimensionless spanwise distance
ζ	dummy integration variable
γ	Euler's constant
θ_j	parameters for fractional calculus models of modified kernel function
λ	dummy integration variable
$\xi_{le(\eta)}, \xi_{te(\eta)}$	coordinates of leading and trailing edges, respectively
ρ	fluid density, slugs/cu ft
σ	small dimensionless spanwise distance

x

σ_{ij}	half-width of panel (i,j)
θ	dummy integration variable
ϕ	phase angle between imaginary and real parts of $C_{l,\alpha}$
$\phi(t)$	Wagner Function
$\psi(t)$	Küssner Function
ω	angular frequency, radians/sec
ω_j	angular frequency in j-th mode, radians/sec

Subscripts:

R, I	real and imaginary components
i,j; n,m	panel (i,j); panel (n,m)

Superscripts

T	transpose

AFIT/GAE/ENY/90D-25

Abstract

A fractional calculus model is developed for the kernel function under
incompressible subsonic flow conditions for rectangular planform
airfoils with small aspect ratio. A model valid for restricted regions
of the kernel function for compressible subsonic flow conditions is also
developed. Additionally, a method for numerically solving the pressure-
downwash integral equation for rectangular planform wings of aspect
ratio two through ten in incompressible flow is developed. An
equivalent Theodorsen function for three-dimensional unsteady flow is
developed, enabling the use of the simpler two-dimensional aeroelastic
equations of motion to fully capture the more complicated three-
dimensional effects.

MODELLING AND ANALYSIS OF KERNEL FUNCTION AND DEVELOPMENT OF EQUIVALENT
THEODORSEN FUNCTION FOR 3-D AEROELASTIC ANALYSIS

I. Introduction

This thesis presents the development and results of two
alternative approaches to the prediction of aerodynamic loads produced
by time dependent motions of thin wings in rectilinear subsonic flight.
The first approach taken is an attempt to directly integrate the
pressure-downwash integral equation. The second approach taken is the
development of the equivalent Theodorsen function for three-dimensional
unsteady aerodynamics.

The first of the two approaches was motivated by Bagley (4:16) who
demonstrated the ability of fractional calculus to model the three-
dimensional kernel function at the conditions given in (31:718). The
three-dimensional kernel function is the transfer function relating the
airloads to the downwash (vertical velocity) for a wing. This first
approach is an attempt to model the transcendental nature of the kernel
function with a mathematically simpler function. The kernel function is
defined throughout the complex s-plane, but because of the complicated
mathematics, analysis is usually restricted to the imaginary axis. This
restricts the use of the kernel function to stability analyses such as
flutter and has little benefit to the control system designer. A simple
model which captures fully the behavior of the kernel function
throughout the entire s-plane could be of valuable use in active control

1

algorithms. The model of the kernel function (the transfer function) could be applied directly to control system design to increase the capabilities of active control of unsteady aerodynamic loads.

The second of the two approaches develops the equivalent Theodorsen function. The equivalent Theodorsen function is constructed by relating two- and three-dimensional lift coefficients in unsteady, incompressible flow. The three-dimensional lift coefficients were evaluated numerically by a method developed in this thesis which is a more general form of a method developed by Ueda and Dowell (27:350). A fractional calculus model is used to capture the behavior of the equivalent Theodorsen function. The modelling was motivated by Swinney (24:5) who successfully modelled the two-dimensional Theodorsen function using fractional calculus. The relatively simple form of the equivalent Theodorsen function permits the inclusion of the three-dimensional effects in the two-dimensional equations of motion. Three-dimensional theory produces more accurate results than those of two-dimensional theory. Therefore, the equivalent Theodorsen function in fractional calculus form should prove to increase the accuracy in the two-dimensional equations of motion without greatly increasing the effort required to generate a solution.

This thesis is divided into eight chapters and five appendices. The first chapter is the introduction. Chapter two discusses the background of the kernel function, presents a computational form for the kernel function, and describes the general solution methodology of the three-dimensional aeroelastic problem. The next chapter presents a

2

brief summary of fractional calculus and discusses information necessary to understand the application in this work. References for further study will be given. Chapter four develops the fractional calculus modelling of the modified kernel function for both compressible and incompressible flow conditions. An approximate solution methodology for the pressure-downwash integral equation is developed in Chapter five. The equivalent Theodorsen function is derived in Chapter six along with accompanying fractional calculus models. Chapter seven shows the utility of the equivalent Theodorsen function in fractional calculus form by presenting compact time-domain representations to typical aeroelastic responses. The thesis concludes with Chapter eight.

Six appendices have been included to present additional information without detracting from the flow of the thesis. Appendices A and B supply additional fractional calculus models of the modified kernel function. The parameter variations of the fractional calculus models for the modified kernel function are shown in Appendix C. Fractional calculus models of the coefficient of lift for wings of aspect ratios between two and ten is contained in Appendix D. The variation of the parameters of the equivalent Theodorsen function will be shown in Appendix E. Finally, a presentation of the original development of the pressure-downwash integral equation is included in Appendix F.

II. Background and Definition of Kernel Function

Küssner is generally credited with the development of the pressure-downwash integral equation and the three-dimensional kernel function. A presentation of his development in English is given in (16:1-28) and a summary of the development is shown in Appendix F. His integral equation relating pressure to downwash is the solution to the wave equation written in cartesian coordinates. The dependent variable is chosen to be Prandtl's acceleration potential that is directly related to the perturbation pressure field (16:2). The wing is treated as a nearly plane impenetrable surface S' lying in the x-y plane as shown in Figure 1. It should be mentioned that the convention of the z-axis positive downward was adopted subsequent to the original development to cast the equations into a form which produced results compatible with those of analytical flutter analyses. The x-y-z coordinate system and the surface S' are assumed to move with uniform velocity in the negative x direction. The solution is forced to be unique by satisfying three conditions. First, disturbances must vanish far away from the wing and its wake. Second, the perturbation pressure can only be discontinuous within the region of the surface S'. Finally, the perturbation pressure must vanish along the trailing edge of the surface S' to satisfy the Kutta condition. Assuming a harmonic downwash and satisfying the three conditions just mentioned produces the unique solution written in equation (1). The differential equation can be rewritten as an integral equation relating the downwash $w(x,y,t)$ at any

4
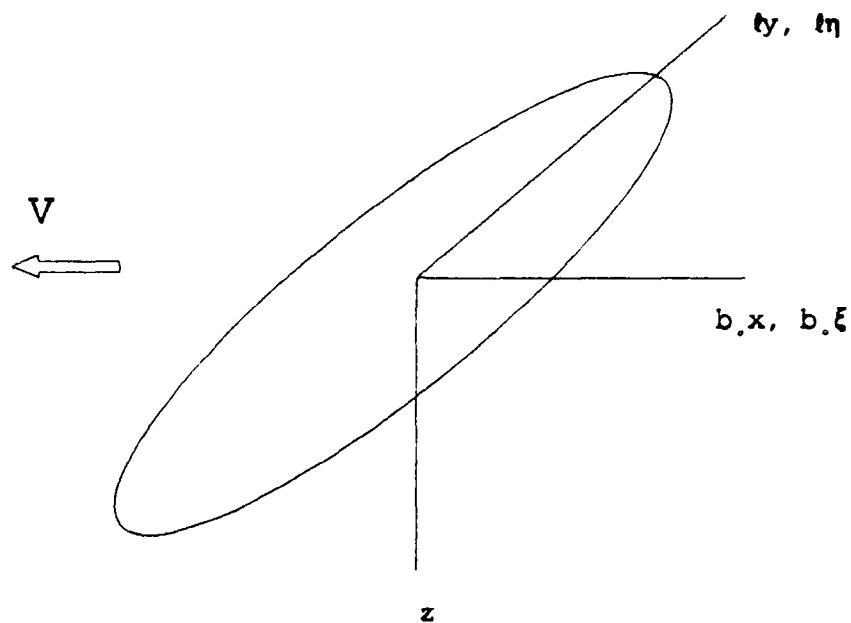
Figure 1: Definition of Coordinate System

point (x,y) on the wing to the perturbation pressure coefficient

$\Delta P(\xi,\eta,t)$ at a point (ξ,η) on the wing.

$$\frac{w(x,y,t)}{V} = \frac{b_0 \ell}{8\pi} \int_{-1}^{+1}$$

(1)

$$\int_{\xi_{le(\eta)}}^{\xi_{te(\eta)}} \Delta P(\xi,\eta,t) \, K[M,k,x-\xi,s(y-\eta)] \, d\xi \, d\eta$$

The variables in equation (1) are defined as follows

ℓ	semispan of wing
ξ_{le}, ξ_{te}	coordinates of leading and trailing edges
M	Mach number
V	velocity
$K[M,k,x-\xi,s(y-\eta)]$	kernel function

5

$x-\xi$	dimensionless chordwise variables referred to root semichord, b_0
$y-\eta$	dimensionless spanwise variables referred to semispan, ℓ
s	ratio of semispan to root semichord
b_0	root semichord

Equation (1) is referred to as the pressure-downwash integral equation in three-dimensional unsteady aerodynamics. The perturbation pressure coefficient Δp in equation (1) is defined as

$$\Delta P(\xi, \eta, t) = \frac{p_- - p_+}{\frac{1}{2}\rho V^2} \tag{2}$$

The downwash and pressure coefficient distributions in equation (1) are both assumed positive downward. When the analysis is restricted to wings of rectangular planform, then $\xi_{le(\eta)}$ and $\xi_{te(\eta)}$ are replaced with -1 and +1 respectively.

The pressure-integral equation (1) is used in the direct sense to solve for the unknown pressure coefficient distribution for a given planform, a known or assumed mode of oscillation, and a prescribed set of stream conditions. A pressure coefficient distribution must be determined which satisfies the edge conditions appropriate to the planform and flow regime under consideration and which, when multiplied by the kernel function and integrated over the planform yields the downwash distribution corresponding to the mode of oscillation (32:5). The pressure-integral equation (1) is used in the direct sense to solve for the downwash distribution for a given planform, an assumed or given pressure coefficient distribution, and given stream conditions. Numerical procedures are usually employed to solve the pressure-downwash

6

integral equation as analytic solutions have not yet been determined for most realistic planforms.

It should be noted that the integration of the spanwise variable will require the use of the finite part of an infinite integral in the Mangler sense (32:13) to handle the double-pole singularity in $y-\eta$ which is evident in equation (5). The generalization to transient motion is accomplished by forming the Laplace transformed version of equation (1). This is accomplished by replacing ik with complex s (2:5)

$$\frac{\hat{w}(x,y;\bar{s})}{V} = \frac{b_0 \ell}{8\pi} \int_{-1}^{+1}$$

(3)

$$\int_{\xi_{le(\eta)}}^{\xi_{te(\eta)}} \Delta \hat{p}(\xi,\eta;\bar{s}) \, \hat{K}[M,\bar{s},x-\xi,s(y-\eta)] \, d\xi \, d\eta$$

Here the circumflex indicates a Laplace transform and $s=\hat{s}b_0/V$ is the dimensionless Laplace parameter.

The majority of references addressing the kernel function have been primarily concerned with numerical computation of the kernel function and numerical integration of the pressure-downwash integral equation. Analytic, closed form solutions of the pressure-downwash equation (1) have been found only a small number of special planforms and flow conditions (32:2). One of the first and most often cited works treating the kernel function is (31:703-718). This pioneering work cast the kernel function into a form more amenable to numerical computation and provided explicit relations for handling limiting cases such as incompressible, sonic, and steady flow conditions. The paper also addressed the nature of the singularities present and provided series

7

representations of the kernel function within regions of its domain.
Two of these authors later added another author and produced (32:1-21)
which presented a systematic procedure for solving the integral
equation. This method involved assuming a plausible pressure mode shape
which added more singularities and difficulties to the problem but the
method does produces satisfactory results. Next a series of at least
twenty different attempts to solve the integral equation reached the
literature. One of the more popular is that of Reissner who developed a
method based on a lifting surface approach to the solution of the
integral equation (21:1-39,22:1-97) that was exact in the limit as the
span approached infinity and resembled lifting line theory at steady
flow. The next series of attempts to solve the integral equation
involved approximate solutions based upon discrete element methods and
was coincident with the development of faster computers. Among these
methods are the vortex lattice (20:1-492), doublet lattice (1:279-285),
doublet point (27:348-355), finite element techniques (12:626-633) and
variational techniques (29:492-498) just to name a few. Landahl and
Stark (13:2049-2060) wrote a complete synopsis of the progress made in
the solution of this problem. Each of these methods produces
satisfactory results, some more easily than others. Coincident with
this development was the development for solutions to the larger class
of problems, namely the non-planar wing (14:1045-1046). The number of
different methods and procedures attempted to obtain the best solution
are a testament to the difficulty of obtaining solutions to the
pressure-downwash integral equation.

8

Computational Form of Kernel Function

Accurate computation of the kernel function is essential if the kernel function is to be modeled with any degree of accuracy. The kernel function poses some numerical impediments that must be carefully avoided for accurate results. The numerical difficulties arise primarily from the presence of both discontinuities and singularities. The kernel function can be written as (32:7)

$$K[M,k,x_0,s(y-\eta)] = \frac{K^*[M,k,x_0,s(y-\eta)]}{b_0^2 s^2 (y-\eta)^2} \tag{4}$$

where K^* is denoted the modified kernel function and the shorthand notation $x_0 = x-\xi$ is adopted for brevity. This form of the modified kernel function is particularly helpful because it shows the second order singularity at $y=\eta$ that exists in the kernel function and admits a less difficult calculation of the modified kernel function, K^*. The modified kernel function is defined in equation (5) (32:7) where K_i and I_i are modified Bessel functions of the first order and first and second kinds respectively, L_1 is the modified Struve function of the first order (8:374-379,495-502) and $\beta = (1-M^2)^{1/2}$. The modified kernel function, K^* does not contain any singularities but it does contain one discontinuity at $x_0 = x-\xi = 0$ and $y_0 = y-\eta = 0$ which can be shown to have the limiting form shown in equation (6) (32:7).

9

$$K^*[M,k,x_0,s(y-\eta)] = e^{-ikx_0}\{-iks|y-\eta| + ks|y-\eta|K_1(ks|y-\eta|)$$

$$+ i\frac{\pi}{2}ks|y-\eta|[I_1(ks|y-\eta|) - L_1(ks|y-\eta|)] + \frac{x_0 e^{\frac{ik}{\beta^2}[x_0 - M\sqrt{x_0^2+\beta^2 s^2(y-\eta)}]}}{\sqrt{x_0^2+\beta^2 s^2(y-\eta)^2}}$$

$$- iks|y-\eta|\int_0^{\frac{1}{\beta^2 s|y-\eta|}[x_0 - M\sqrt{x_0^2+\beta^2 s^2(y-\eta)^2}]} \frac{\tau}{\sqrt{1+\tau^2}} e^{iks|y-\eta|\tau}d\tau\}$$

$$(5)$$

$$\lim_{y-\eta \to 0} K^*[M,k,x_0,s(y-\eta)] = \begin{cases} 2e^{-ikx_0} & x_0>0 \\ \\ 0 & x_0<0 \end{cases} \qquad (6)$$

This form of the modified kernel function as shown in equation (5) exists for steady motion (k=0) as well and can be shown to have the following limiting form (32:7,31:710)

$$K^*[M,0,x_0,s(y-\eta)] = 1 + \frac{x_0}{\sqrt{x_0^2 + s^2(y-\eta)^2}} \qquad (7)$$

Although the calculation of the modified kernel function may seem trivial, there are two numerical problems hidden within the equation. The first problem is the quantity I_1-L_1 and the second is the definite integral term in equation (5). The quantity I_1-L_1 within the modified kernel function is difficult to accurately compute for large argument because both individual functions grow unbounded for large arguments. This problem can be eliminated by using the definition (33:425)

10

$$I_1(ks|y-\eta|) - L_1(ks|y-\eta|) = \frac{2ks|y-\eta|}{\pi}\int_0^1 \sqrt{1-\tau^2}\, e^{-ks|y-\eta|\tau}\, d\tau \qquad (8)$$

This definite integral could be handled by numerical integration but there would be an unknown amount of uncertainty associated with the result depending upon such factors as step size associated with the integration routine. An alternate approach is to approximate the integrand with a function which is integrable in closed form and evaluate the result. This approximation approach is used in this case because the error of the approximation is small. In some instances, accurate approximations to the integrand may not be available and numerical integration would be the only recourse. The result is the following expression (32:8)

$$I_1(ks|y-\eta|) - L_1(ks|y-\eta|) \approx$$

$$\frac{2ks|y-\eta|}{\pi}\left\{ \frac{a_1 ks|y-\eta|}{a_2 + a_3 k^2 s^2 (y-\eta)^2} \right. \qquad (9)$$

$$\left. + \left[\frac{\pi}{4} - a_4 ks|y-\eta|\left(\frac{a_5 + a_6 ks|y-\eta|}{a_2 + k^2 s^2 (y-\eta)^2}\right)\right] e^{-ks|y-\eta|} \right\}$$

where

$$a_1 = 1.0085$$
$$a_2 = 1.3410$$
$$a_3 = 1.0050$$
$$a_4 = 0.8675$$
$$a_5 = 0.4648$$
$$a_6 = 0.9159$$

11

This approximation introduces an error of approximately 0.4 percent in the vicinity of $ks|y_\eta| = 4$ and is less throughout the domain of the function (32:8).

The second numerical difficulty is in the evaluation of the integral term of the modified kernel function, equation (5). This integral has not been solved in closed form to date. Numerical integration once again is possible; instead, an approximation to the integrand, integrable in closed form, exists (32:8) and will be used to minimize the uncertainty in the result. The following approximation can be used to replace the integrand in the integral of the modified kernel function

$$\frac{\tau}{\sqrt{1 + \tau^2}} \approx 1 - a_1 e^{-r_1 \tau} - a_2 e^{-r_2 \tau} - a_3 e^{-r_3 \tau} \sin \pi \tau \qquad (10)$$

where

$$
\begin{aligned}
a_1 &= 0.101 \\
a_2 &= 0.899 \\
a_3 &= 0.09480933 \\
r_1 &= 0.329 \\
r_2 &= 1.4069 \\
r_3 &= 2.90
\end{aligned}
$$

The maximum error of this approximation is about 0.24% near $\tau = 1.5$ and this function possesses the same limiting value as the integrand at the two limits of integration (32:8). However, this expression is only valid for positive values of τ so the integral must be broken up into two regions and a change of variables made on one of the two parts to write the complete integral in terms of positive limits of integration where the limits of integration are defined as follows.

$$\int_0^{a^*-d} \frac{\tau}{\sqrt{1+\tau^2}}\, e^{iks|y-\eta|\tau}\, d\tau \qquad\qquad x_0 > Ms|y-\eta| \qquad\qquad (11)$$

$$\int_0^{d-a^*} \frac{\tau}{\sqrt{1+\tau^2}}\, e^{-iks|y-\eta|\tau}\, d\tau \qquad\qquad x_0 < Ms|y-\eta| \qquad\qquad (12)$$

$$a^* = \frac{x_0}{\beta^2 s|y-\eta|} \qquad\qquad (13)$$

$$d = \frac{M\sqrt{x_0^2 + \beta^2 s^2 (y-\eta)^2}}{\beta^2 s|y-\eta|} \qquad\qquad (14)$$

The modified kernel function is now in a form which can be readily and accurately evaluated throughout the domain of any wing planform.

The solution of the integral equation (1) involves the integration of the kernel function. Although the solution is not specifically addressed in this section, it is appropriate to discuss the special integration required in the spanwise integration. The chordwise ξ integration does contain a finite jump discontinuity which can be easily handled by separating the integral into two regions, solving each individually by appropriate means. The spanwise integration contains a double-pole singularity at $y-\eta=0$ which necessitates the use of the Mangler finite part of an infinite integral (32:13) as shown in equation (15). The integration of a function $F(\eta)$ other than $F(\eta)=1$ is more difficult in general and can only be performed provided the function F is not singular at $\eta=0$. In most instances, the integration is sufficiently difficult to warrant analysis by numerical means. Van

13

$$\int_{y-\zeta}^{y+\zeta} \frac{d\eta}{(y-\eta)^2} = \lim_{e \to 0} \left[\int_{y-\zeta}^{y-e} + \int_{y+e}^{y+\zeta} \frac{d\eta}{(y-\eta)^2} - \frac{2}{e} \right]$$

$$= \lim_{e \to 0} \left\{ \frac{1}{y-\eta} \bigg]_{y-\zeta}^{y-e} + \frac{1}{y-\eta} \bigg]_{y+e}^{y+\zeta} - \frac{2}{e} \right\} = -\frac{2}{\zeta}$$

(15)

Nierkerk (30:1196) and Ueda and Dowell (27:350) have both developed approximate numerical methods capable of accurately evaluating such an integral. The first method by Van Nierkerk (30:1196) uses a special Gauss quadrature rule which is generally accurate with as few as four abscissa points for most functions. The second method by Ueda and Dowell (27:350) develops an equivalent expression for the integrand under the singular integral which can be used in discrete element solutions to the pressure-downwash integral equation.

General Solution Methodology

This section outlines the modification of the general aerodynamic problem into a form suitable for solution by the approximate methods described earlier. The pressure-downwash integral equation is used in the direct sense of lifting surface theory to solve for the unknown pressure coefficient distribution given a known or assumed downwash distribution. As there are only a very limited number of special cases for which closed form solutions are exist, the general problem must be solved by approximate numerical procedures as discussed in the previous section. The wing is assumed to be undergoing a displacement $H(x,y,t)$ which is represented as the superposition of rigid body and elastic modes of vibration

14

$$H(x,y,t) = h_1(x,y)\,q_1(t) + h_2(x,y)\,q_2(t) + \ldots$$
$$+ h_j(x,y)\,q_j(t) + \ldots \qquad (16)$$

Linear superposition is possible because the boundary conditions used by Küssner were linear, preserving the linearity of the wave equation operator and hence the solution, the integral equation (1), is itself a linear operator. For sinusoidal oscillations we have the following

$$q_j(t) = \tilde{q}_j\, e^{i\omega t} \qquad (17)$$

where the tilde indicates the magnitude of the displacement in the j-th mode, ω is the frequency of oscillation, $h_j(x,y)$ describes the shape of the j-th mode and $i=(-1)^{1/2}$. The downwash $w(x,y,t)$ for a given displacement $H(x,y,t)$ is given by the following (32:5)

$$w(x,y,t) = \left(\frac{V}{b_0}\frac{\partial}{\partial x} + \frac{\partial}{\partial t}\right)H(x,y,t) \qquad (18)$$

This can be rewritten using the above relations in equations (16) and (17) for the j-th mode of vibration.

$$\frac{w_j(x,y,t)}{V} = \left(\frac{\partial}{\partial x} + ik\right)h_j(x,y)\,\frac{q_j(t)}{b_0} \qquad (19)$$

Seeking the downwash as the product of a shape function and an unknown time dependent magnitude reduces the expression above to the following

$$\frac{\tilde{w}_j(x,y)}{V} = \left(\frac{\partial}{\partial x} + ik\right)h_j(x,y) \qquad (20)$$

where the downwash has been assumed as

15

$$w(x, y, t) = \tilde{w}(x, y) e^{i\omega t} \tag{21}$$

The pressure coefficient distribution on the wing can also be put into a similar form

$$\Delta P(\xi, \eta, t) = \Delta \tilde{P}(\xi, \eta; k) e^{i\omega t} \tag{22}$$

The shape function in equation (22) is shown with k, the reduced frequency, as parameter. By choosing the downwash mode shape, the pressure coefficient is forced to behave as specified by the kernel function. The pressure coefficient is a function of reduced frequency to counter the frequency-dependence in the kernel function. The type of notation in equation (22) allows for easy transition to the Laplace domain formulation in equation (3). The use of these equations produces the following relationship between the shape of the downwash and the shape of the pressure distribution throughout the spatial domain of the airfoil

$$\frac{\tilde{w}(x, y)}{V} = \frac{b_0 \ell}{8\pi} \int_{-1}^{+1}$$
$$\int_{\xi_{le}(\eta)}^{\xi_{te}(\eta)} \Delta \tilde{P}(\xi, \eta; k) K[M, k, x-\xi, s(y-\eta)] \, d\xi \, d\eta \tag{23}$$

For a general problem, the general displacement shape is decomposed into a finite number of modes (either rigid body or elastic modes). Each mode shape is handled separately, solving the integral equation by an appropriate means for the pressure coefficient distribution responsible for the assumed downwash distribution. The summation of the individual modal pressure coefficient distributions produce the total resultant

16

pressure coefficient distribution for the general condition. The pressure coefficient distribution can in turn be used to compute generalized aerodynamic forces acting on the wing.

III. Fractional Calculus

The mathematics of fractional calculus is nearly as old as that of classical calculus. The fractional calculus treats derivatives and integrals of fractional order and is not solely restricted to integer order as is the classical calculus (23:115). An interesting discussion of the historical development of fractional calculus has been written by Ross (23:115-122). The early engineering applications of fractional calculus were precipitated by the observation that the stress relaxation phenomenon of viscoelastic materials appeared to proportional to time raised to the fractional power. This observation in turn suggested a fractional order time derivative rather than an integer order time derivative in the equations of motion for a system comprised of the material. This discovery spawned a renewed interest in the fractional calculus in the twentieth century. The fractional derivative can be defined as the inverse operation of fractional integration attributed to Reimann and Liouville (3:203)

$$D^{\alpha+m}[x(t)] \doteq \frac{1}{\Gamma(1-\alpha)} \frac{d^{1+m}}{dt^{1+m}} \int_0^t \frac{x(\tau)}{(t-\tau)^{\alpha}} d\tau ; \tag{24}$$

$$0 < \alpha < 1 , \quad m \in \mathbf{N}$$

One especially convenient feature of the fractional derivative is

$$\mathcal{L}\{D^{\alpha+m}[x(t)]\} = s^{\alpha+m} \mathcal{L}\{x(t)\} \tag{25}$$

which shows differentiation in the Laplace domain is equivalent to multiplication by the quantity $s^{\alpha+m}$ (3:203), s being the general Laplace

18

variable. A similar relation holds in the Fourier domain when s is replaced by $i\omega$ and Fourier transforms are used instead of Laplace transforms in equation (25). For example, the Laplace domain representation of the fractional derivative of order one half of the function $f(t)=e^{-at}$ is $s^{1/2}/(s+a)$. These mathematical features, coupled with the apparent correct description of viscoelastic phenomenon, have generated the renewed interest in fractional calculus and its applications to engineering problems. The fractional derivative operator $D^{\alpha+\beta}[\ ]$ is a linear operator so all the mathematical conveniences associated with linearized problems can still be utilized when the fractional calculus is included in the problem.

IV. Model of the Modified Kernel Function

The primary emphasis of this portion of research is to develop a
model which accurately describes the frequency dependent and chordwise
and spanwise spatially dependent behavior of the kernel function. It
should be emphasized that the modelling will be performed on computed
values of the kernel function in an attempt to simplify the mathematics
involved in its analysis and is not performed to actual test data. One
major goal is to substitute relatively simple functions for
transcendental ones, reducing the effort presently required to calculate
the kernel function along the imaginary axis and throughout the complex
s-plane. Additionally, if a suitable model could be found which was
more amenable to analytic integration than the kernel function itself,
equations of motion for the finite airfoil could be written directly as
functions of this integration and evaluated directly in closed form.
Finally, given the first two goals, if the model is of a form which has
a closed form inverse Laplace transform, then this transform can be used
as the transfer function in control system analyses. The kernel
function can be thought of as a transfer function spatially convolved
with the pressure coefficient distribution to produce the downwash
distribution. A model which describes the behavior of the kernel
function along the imaginary axis, integrable in closed form, and
available for analytic continuation into the complex plane is the target
of the project. Given this descriptive model can be developed, a
tractable, analytically integrable transfer function that can be

20

spatially convolved to produce the response of the system to general input will be obtained.

Model Development

The candidate model must be capable of capturing the variation of the kernel function over a wide range of reduced frequencies along the imaginary axis with the ability to be analytically continued into the entire complex plane without difficulty. The range of reduced frequency has to be sufficiently large to insure that both the small and large argument asymptotic behavior of the kernel function was captured. As shown earlier, the kernel function has the second order singularity which could cause problems in developing an accurate model, especially in the vicinity of the singularity. Therefore, the modified kernel function shown in equation (5) earlier will be modelled as it is more well behaved mathematically. It should be noted, however, that the singular nature of the kernel function shown in equation (4) can be included before the integration is performed.

The modified kernel function will be modelled with the functional form shown in eqaution (26). K_0^* is given by the steady value computed using equation (7). This equation will be shown later in Chapter VII to be comprised of two functions which are derivatives of two general order Mittag-Leffler functions (17:102) with step functions as the leading coefficients. Bagley (5:742) has shown a model similar in form is appropriate for describing the frequency dependent behavior of the modulus of a viscoelastic material. In Bagley's model (5:742), a

21

$$K^*[M,k,x_0,y_0] = K_0^* - \frac{\theta_1(M,x_0,y_0)\,(ik)^{\theta_2(M,x_0,y_0)}}{1 + \theta_3(M,x_0,y_0)\,(ik)^{\theta_4(M,x_0,y_0)}}$$

(26)

$$- \frac{\theta_5(M,x_0,y_0)\,(ik)^{\theta_6(M,x_0,y_0)}}{1 + \theta_7(M,x_0,y_0)\,(ik)^{\theta_8(M,x_0,y_0)}}$$

single Mittag-Leffler function was sufficient to capture the behavior of
the modulus. Swinney (25:5) was able to capture fully the frequency
dependent behavior of the Theodorsen function for two-dimensional flow
(25 :418) using a single Mittag-Leffler function. The Theodorsen
function relates the variation of circulatory lift to downwash of a flat
plate undergoing simple harmonic motion (25:1). Swinney's model was
also extended to include the laplace variable for arbitrary motion. The
success in modeling the two-dimensional aerodynamic function led Bagley
(4:16) to suppose the three-dimensional kernel function could be
modelled with a similar functional form. Early investigation over a
broad band of reduced frequencies demonstrated Bagley's form of model
(4:16) was incapable of capturing the behavior in the higher subsonic
region of the kernel function (M=0.8+). The model shown in equation
(26) with two terms rather than one was adopted in an attempt to capture
better the properties of the modified kernel function over a wide range
of reduced frequencies. The fractional calculus based model is
especially convenient because the analytic continuation is automatic
with the substitution of the general Laplace parameter for the purely
imaginary argument. Additionally, this type of functional relationship

22

is capable of capturing two independent phase lags because of the two independent derivatives of the Mittag-Leffler functions present.

There is actually some empirical foundation for a model of this form. In two-dimensional flow, the wing is considered infinite in span and the only wake produced is along the trailing edge. Under steady flow conditions, the wake leaves the trailing edge smoothly. As the reduced frequency is increased, the wake no longer leaves smoothly but instead produces disturbances along the trailing edge which propagate forward and change the effective angle of attack of the wing. For wings of finite span, the wing tips may also create disturbances independent of those along the trailing edge which cause additional disruption in the motion of the airfoil. This type of phenomenon may require two functions with two separate phase lags. The functions in equation (26) are capable of representing two separate phase lags because the θ_2 and θ_6 values are independent, one capturing the trailing edge effects and the other capturing the wing tip effects.

The model shown in equation (26) is a direct function of reduced frequency with the parameters being functions of Mach number and dimensionless chordwise and spanwise spatial variables. The Mach numbers of interest ranged from incompressible (M=0) up to high subsonic (M=0.8+). The range of the dimensionless chordwise variable would have to include values ranging from $x_0 \in [-2,2]$. The range of the dimensionless spanwise variable would depend upon the aspect ratio of the given airfoil $sy_0 \in [-2s,2s]$ where s is the ratio of semispan to root semichord. A general comprehensive model which could describe the

23

entire range of the modified kernel function was not discovered. The large number of independent variables created additional difficulties in determining a suitable functional form for the model parameters, θ_j. However, many regions were adequately modelled and all regions were fully investigated and analyzed.

As evidenced by the form of the model in equation (26) and the nature of the modified kernel function discussed in equation (5), this curve fitting is a highly nonlinear problem and a suitable method of nonlinear optimization had to be found to solve the problem in a timely manner. For models with a small number of parameters, it is sometimes sufficient to perform manual regression. However, in this case with eight independent parameters, a nonlinear least squares regression routine using the modified Levenberg-Marquardt algorithm (18:431-441) to generate a sequence of approximations to the minimum point was used to expedite the process. This algorithm uses a "trust region" approach with a bounded step. The Jacobian is needed to optimize the parameters of the model and is computed numerically in this instance by forward finite differences (10:243). The IMSL routine RNLIN which implements this algorithm was used (10:239) in the present analysis. There is a certain amount of insight required to use such a routine in this type of application.

This routine is designed for regression of real valued functions, not complex valued functions. In performing a modelling of the modified kernel function a model must be constructed which adequately predicts the behavior of both the real and imaginary parts of the function. A

24

simultaneous regression performed on both the real and imaginary parts is desired. Unfortunately, in this present work, the simultaneous regression was not readily programmable and was not used.

Two different attempts were made to trick the routine into performing a simultaneous regression. The routine requires a real-valued function which computes the error between the function and the model at a discrete number of points. This is the only possible input to the routine which could potentially be modified to achieve a simultaneous fit. The first attempt was to return to the routine the magnitude of the complex error between the points. The real part caused the routine to diverge in this instance. Another attempt was made to treat the real and imaginary parts as one real-valued curve by translating the imaginary part to begin at the tail of the real part. This failed as well because the derivative of the curve was, in general, discontinuous at the point where the two parts were joined. Without a quick method of performing simultaneous regression, the regression was performed solely on the imaginary part. The imaginary part proved to be more amenable to fitting than the real part. When the real part of the model (based upon the regression of the imaginary part) was compared to the real part of the modified kernel function it was generally observed to produce a satisfactory fit as well. Normally, the real part of a complex function would not be well modelled by specifying the imaginary part. However, given a linear transfer function, the imaginary and real parts can be shown to be related through derivative operators using Fourier transforms. In this work, a good model for the imaginary

25

produced a good model for the real part as well, evidence of the strong linear nature of the modified kernel function.

Another obstacle in this IMSL routine is the requirement for a starting point in the optimization space. A good initial point would produce good regression results and a bad initial vector would produce no regression result and unfortunately no information regarding how to improve the initial value. The real difficulty in the procedure is determining the correct initial vector; because this function has not been modelled in this manner before, the selection of the initial trial vector was something gained by experience and practice. One recommendation for further investigation in this area is the use of a complex regression algorithm for evaluating models of the modified kernel function.

There are several advantages associated with this IMSL routine as well. First, as the routine is available internationally and used extensively, the routine probably has been extensively tested against established test cases and has no errors. Creating a routine takes a large amount of time to code and test. Another advantage is speed. The IMSL routines are coded for efficient operation. The routine was one of the better nonlinear regression routines available in either pre-coded or algorithm format.

One interesting and helpful result discovered during the modelling process was the nature of the regression parameters, θ_j. Given a good regression for one particular Mach number, x_0 and y_0, a reasonable initial value for another x_0 and y_0 value for the same Mach number could

26

be interpolated quite readily . This resulted in family of regression curves for the various parameters of the model. Unfortunately, this behavior was not observed fo. all regions of the modified kernel function using this form of model, possibly suggesting the present form of model is not quite appropriate in the region. The existence of the strong relationship between the parameters of the model in many regions suggests the existence of some type of fractional derivative model that could adequately represent the complicated and highly intractable modified kernel function.

The goodness of fits of the fractional calculus models were minimized using a least squares type of error calculation. The error is calculated using the following

$$ err = \frac{1}{N_D} \left\{ \sum_{p=0}^{p=N_D} [f(x_p) - f_c(x_p)]^2 \right\}^{1/2} \qquad (27) $$

where $f(x_p)$ is the value of the modified kernel function at the p-th point, $f_c(x_p)$ is the value of the fractional calculus model at the p-th point in the interval, N_D indicates the total number of points in the interval, and p is an index locating the point of comparison. The errors for the models will be given when the model is presented. The number of points used to compute the error varies in the thesis. The models and functions throughout the thesis were compared at intervals of 5 percent of reduced frequency (the independent variable). Hence, for an interval between zero and one, there would be twenty-one points compared and for an interval between zero and three, there would be sixty-one points of comparison between the target points and the model.

27

Model Results

The results presented are restricted to thin rectangular planform
airfoils. It should also be pointed out that the modelling of the
modified kernel function was performed to calculated values and not
actual test data.

Compressible Flow. The modelling of the modified kernel function
was generally unsuccessful for compressible flow conditions using the
form of model in equation (26). There were a number of obstacles
encountered in attempting to model the modified kernel function. The
first attempt at modelling was performed at Mach number 0.8. This
proved to be extremely difficult with the form of model shown in
equation (26). The model would predict behavior well in regions of x_0
between 0.7 and 1.0; in other regions, the overall trends of the
modified kernel function were followed but the actual functional values
were generally not achieved. One possible reason for the difficulty is
the compressibility effects beginning to dominate at the higher Mach
numbers. As the Mach number approaches one, shock waves will begin to
form on the wing. Shock waves are viewed as a non-linear phenomenon and
as such, the kernel function, which is a linear operator, would probably
have difficulty capturing these effects. It can be shown that the
modified kernel function at Mach number 1.0 (sonic) is equal to zero
($x_0 \leq 0$, all sy_0) compared to the subsonic case where the modified kernel
function was equal to zero for ($x_0 \leq 0$, $sy_0 \to 0$) equation (6). It is
postulated that possibly a third function would need to be added to the
two function model to help capture the shock formation phenomenon. The

28

investigation at Mach number 0.8 was abandoned for lack of complex non-linear regression software to perform the statistical regression on a increasingly difficult problem. It was evident at this point that the global modified kernel function model would not be obtained. Another Mach number in the compressible regime was analyzed in an attempt to characterize the modified kernel function at least one Mach number.

The Mach number was reduced to 0.5 in an attempt to decrease the dominance of the compressibility effects, but still retain enough compressibility to attempt to capture the subdominant effects. The modelling at this Mach number produced some very good results. The modified kernel function was best modelled in the regions with small x_0, small sy_0 and large x_0, large sy_0. Acceptable models were obtained in the vicinity of small x_0, large sy_0 and poorer fits were found for large x_0, small sy_0. Negative x_0 values were not analyzed for this case because the modelling was determined to be insufficient to capture fully all of the behavior.

The resulting model for two of the regions will be shown in the main body of the text and samples from the remaining two regions contained in Appendix A. A sample comparison between the real and imaginary parts of the model and modified kernel function in the small x_0, small sy_0 region is shown in Figure 2. The model is shown below

$$K^*[0.5,k,0.1,0.05] = K_0^* - \frac{\theta_1 (ik)^{\theta_2}}{1 + \theta_3 (ik)^{\theta_4}} - \frac{\theta_5 (ik)^{\theta_6}}{1 + \theta_7 (ik)^{\theta_8}} \quad (28)$$

29

where

$$K_0^* = 1.917$$
$$\theta_1 = -0.027 \qquad\qquad \theta_2 = 1.205$$
$$\theta_3 = 0.154 \qquad\qquad \theta_4 = 0.094$$
$$\theta_5 = 0.236 \qquad\qquad \theta_6 = 1.01$$
$$\theta_7 = 0.064 \qquad\qquad \theta_8 = 0.95$$

The error for the real and imaginary parts is 2.6×10^{-3} and 1.3×10^{-3} respectively. The steady value is computed using the relationship in equation (7). As shown in the figure, there is excellent correspondence between the model and the modified kernel function for both real and imaginary parts. In this region, the exponential limiting form of equation (6) is dominant and this behavior is evidenced in the figures shown. If the curves were extended to include values of negative frequency, the beginning of a finite jump discontinuity could be seen, resembling a travelling wave at this point. As mentioned earlier, other values of the modified kernel function in the vicinity of this chordwise and spanwise location can be interpolated with a certain amount of accuracy. There appear to be a substantial number of local minima in the nonlinear least squares minimization function created by the model and the modified kernel function. Therefore, the modelling of one region of the function does not necessarily produce good results for another region. The compressibility effects are thought to be contributing to the large number of local minima present. A true complex regression algorithm might be more beneficial.

Another region investigated was small x_0 and large sy_0. The model had increasing difficulty capturing the behavior of the modified kernel function for larger sy_0 primarily due to the more oscillatory nature of
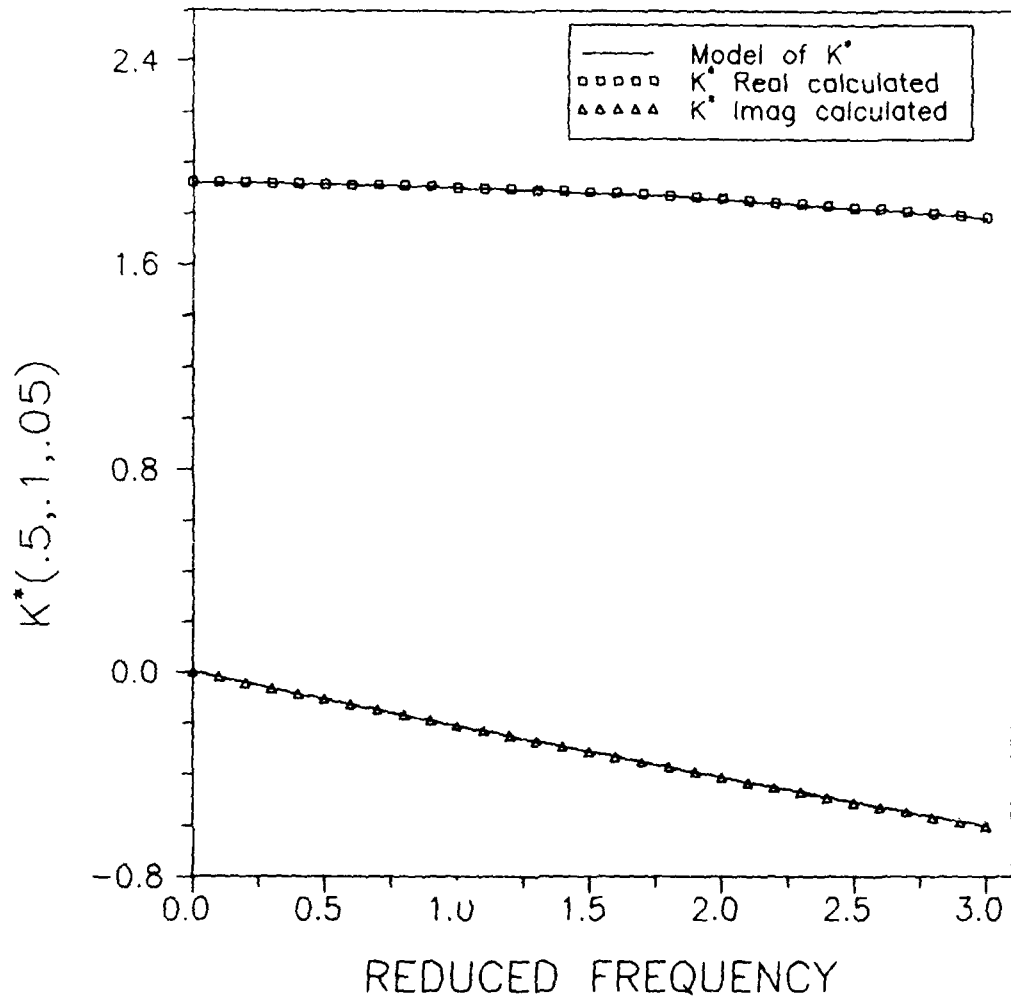
30

Figure 2: Model of $K^*[0.5, 0.1, 0.05]$

the kernel function for large arguments (26:174). A sample of the model in the larger sy_0 domain is shown in Figure 3. The model has the form shown in equation (29) with the real and imaginary parts having errors of 3.2×10^{-2} and 7.1×10^{-3} respectively. As the reduced frequency is increased, the modified kernel function becomes oscillatory which would
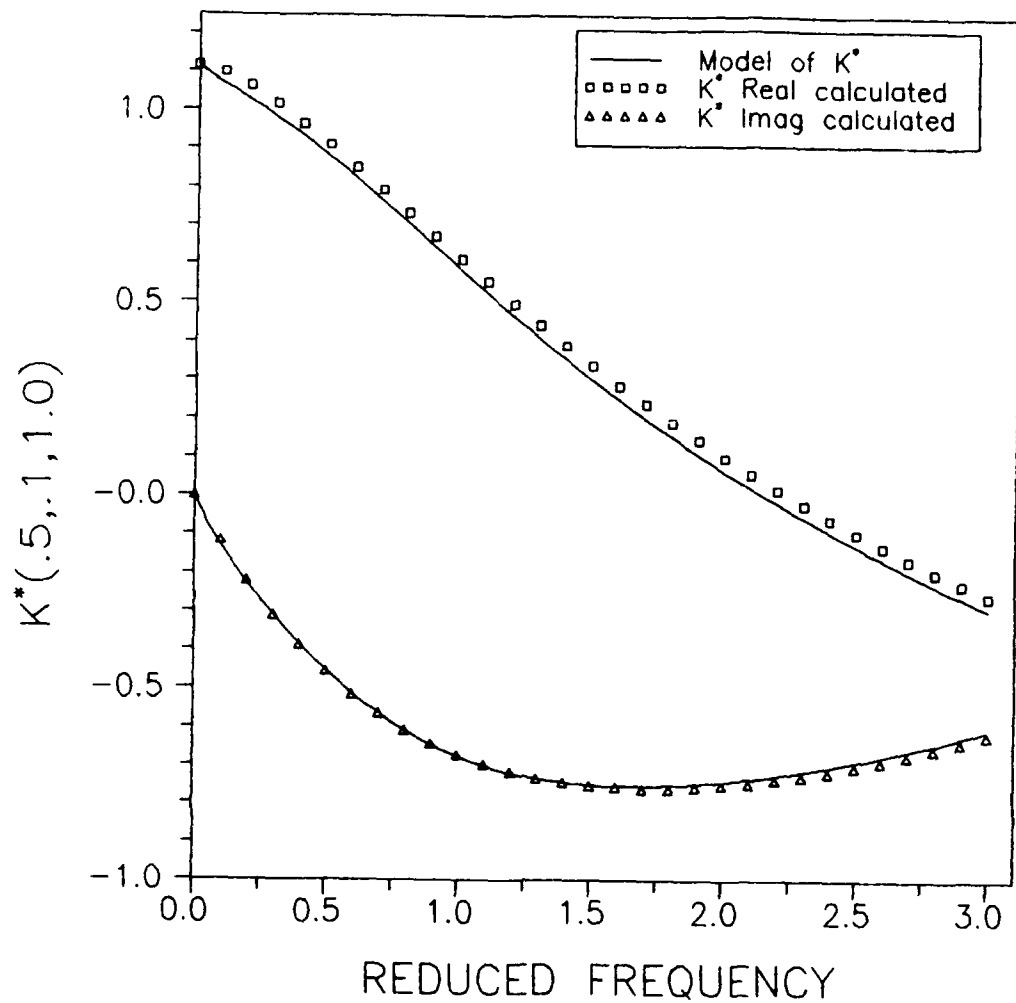
31

Figure 3: Model of $K^*[0.5, 0.1, 1.0]$

$$K^*[0.5, k, 0.1, 0.05] = K_0^* - \frac{\theta_1 (ik)^{\theta_2}}{1 + \theta_3 (ik)^{\theta_4}} - \frac{\theta_5 (ik)^{\theta_6}}{1 + \theta_7 (ik)^{\theta_8}} \quad (29)$$

where

$K_0^* = 1.1147$
$\theta_1 = 0.647$ $\theta_2 = 0.888$
$\theta_3 = 0.549$ $\theta_4 = 1.04$
$\theta_5 = 0.263$ $\theta_6 = 0.263$
$\theta_7 = 0.109$ $\theta_8 = 1.37$

require successively more terms in the model. This may suggest an infinite series with an argument consisting of a function similar to the one used in the model. This is an area that could be further developed. The large k behavior is important because the large asymptotes must be sufficiently modelled to have an accurate inverse Laplace transform (the Laplace transform and its inverse are defined over the infinite complex frequency plane).

The region of large x_0 and small sy_0 is shown in Figure 17 located in Appendix A. Once again, in this region the exponential limiting term is dominant and the modified kernel function is highly oscillatory, causing difficulty in the modelling. Although the imaginary part is following the function quite nicely, the real part is losing its ability to describe the function. A true simultaneous regression of both real and imaginary parts of the model might have overcome this deficiency.

The region comprising both large x_0 and large sy_0 was handled reasonably well for the particular values investigated but the performance of the model will degrade as the reduced frequency is increased because of the oscillatory nature of the modified kernel function mentioned earlier. Figure 18 in Appendix A show the behavior in this region.

Overall, the modelling of the modified kernel function for Mach number 0.5 was not completely satisfactory and did not provide a complete modelling over the domain of the wing. Further analysis into the possibility of analytic integration of the integral equation as originally planned was not performed because of time constraints.

33

However, the modelling and investigation do give promise that such a model could exist, given the correct form could be determined. As mentioned earlier, a complex non-linear regression routine would greatly increase the ability to explore other model forms. Lack of total success in the compressible domain led to the investigation of the modified kernel function for incompressible flow. The supposition that compressibility of any magnitude greatly increased the complexity of the problem will be tested in the next section.

Incompressible Flow. The incompressible case would require another model. The model given in equation (26), when tried in this case, had too many parameters for the regression to be performed with any degree of consistency. The following model was adopted for the incompressible flow conditions where, once again, the K_0^t value is given

$$K^*[k, x_0, y_0] = K_0^* - \frac{\theta_1(x_0, y_0)(ik)^{\theta_2(x_0, y_0)}}{1 + \theta_3(x_0, y_0)(ik)^{\theta_4(x_0, y_0)}} \tag{30}$$

by the steady limiting form in equation (7) and the Mach number, M, has been eliminated from the argument for brevity. A more thorough study was conducted on the incompressible case than on the other compressible cases previously conducted because the incompressible case provided the most opportunity for complete modelling of the modified kernel function. One model describing the modified kernel for incompressible flow conditions throughout its entire domain was not found either. However, the model in equation (30) shows a very strong potential for modelling wings of small aspect ratios (aspect ratios less than one-half) such as those found in the late stages in turbomachinery. The modelling of the

34

modified kernel function in the incompressible regime discussed in this section was shown to be very capable of describing the smaller aspect ratio wings throughout the domain of the airfoil. However, the asymptotic behavior of the model with respect to the modified kernel function for small and large asymptotic values of reduced frequency has not established and is currently under investigation. Ueda (26:169-174,28:346-347) provides asymptotic expansions of the kernel function for both small and large arguments. These behaviors need to be verified before the model can be said to fully describe the modified kernel function for small aspect ratio wings. Samples of the model in specific regions are presented here and in Appendix B.

A sample of the model for small sy_0 and large x_0 is shown in Figure 4. The model has the following representation

$$K^*[k, -0.1, 0.5] = K_0^* - \frac{\theta_1 (ik)^{\theta_2}}{1 + \theta_3 (ik)^{\theta_4}} \tag{31}$$

where

$K_0^* = 1.9987$
$\theta_1 = 1.729$ $\theta_2 = 0.81$
$\theta_3 = 0.267$ $\theta_4 = 1.34$

with errors of 9.9×10^{-2} and 2.4×10^{-2} for the real and imaginary parts. The agreement between the model and the computed modified kernel function is much better than the same case for the Mach number 0.5 case, indirectly supporting the supposition that compressibility effects cause difficulty in the modelling of the modified kernel function. This particular case represents the worst agreement between model and modified kernel function for the incompressible case. Although not
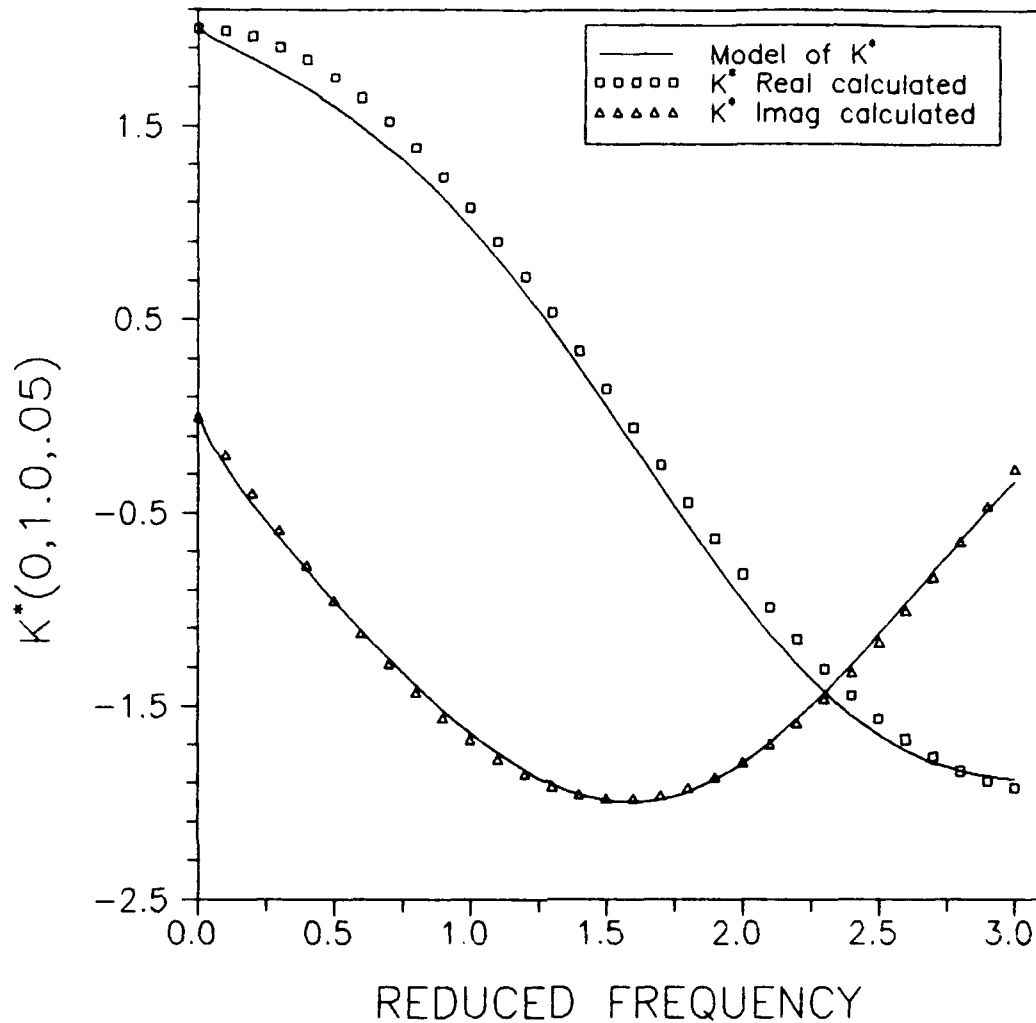
35

Figure 4: Model of $K^{*}[0,1.0,0.05]$

perfect, it is reasonable considering the relative time required to evaluate equation (30) and equation (5). The model also worked reasonably well for large x_0 and large sy_0. The small x_0 and large sy_0 behavior was modelled very well using equation (30) as shown in Figure 5. The model for this particular case is written in equation (32) with errors of 1.1×10^{-2} and 4.7×10^{-3} respectively for the real and
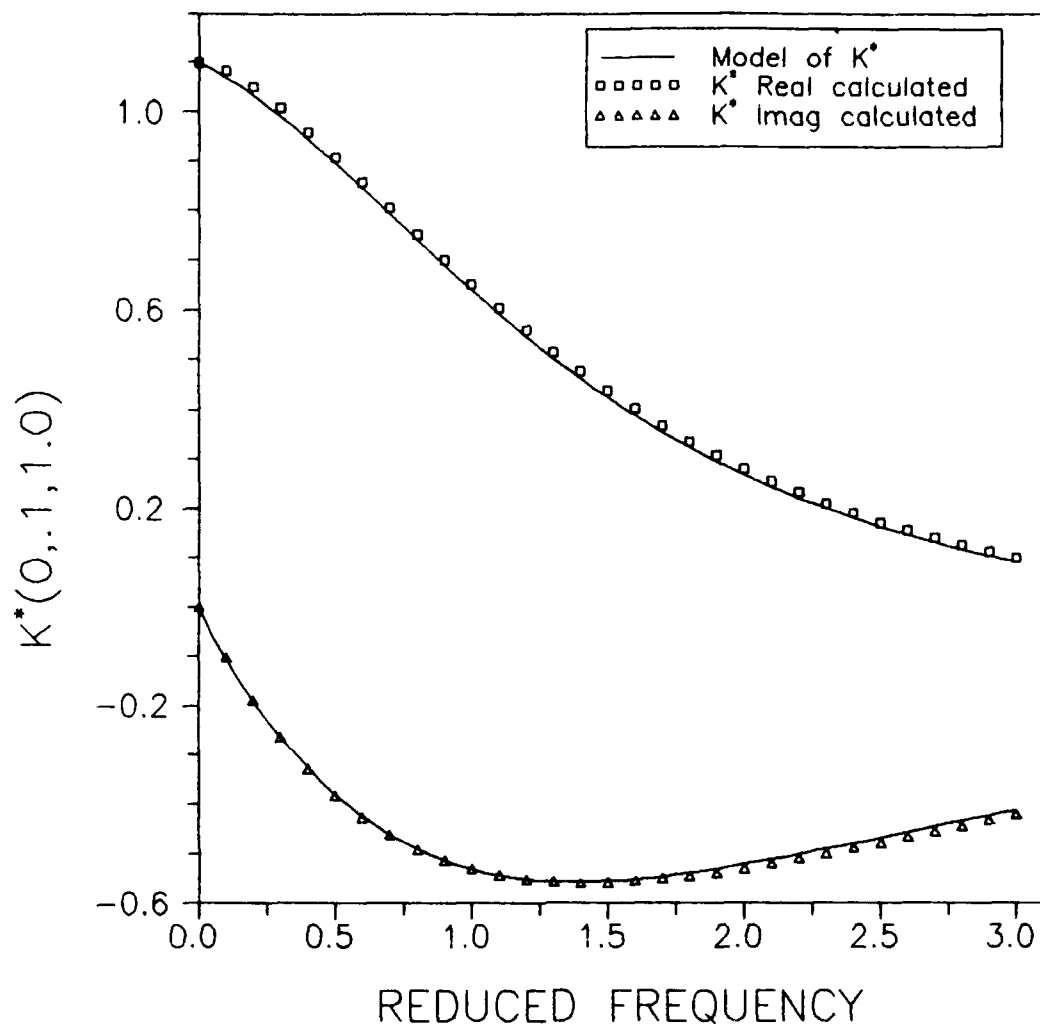
Figure 5: Model of K^i[0,0.1,1.0]

imaginary parts.

$$K^*[k, -0.1, 0.5] = K_0^i - \frac{\theta_1 (ik)^{\theta_2}}{1 + \theta_3 (ik)^{\theta_4}} \qquad (32)$$

where

$K_0^i = 1.099$
$\theta_1 = 0.837$ $\theta_2 = 0.871$
$\theta_3 = 0.582$ $\theta_4 = 0.956$

Comparing this figure to the corresponding case at M=0.5 (Figure 3)

shows the higher Mach number case has a much sharper curve than the

respective incompressible case, demonstrating the more complex behavior

due to compressibility effects. In addition to investigating the

positive x_0 behavior, negative x_0 behavior was also analyzed. The

behavior for small values of negative x_0 and small sy_0 is given in

Figure 19 which is included in Appendix B. The model clearly captures

the behavior of the modified kernel function in this region. Note that

these curves will be forced to zero as the sy_0 values are decreased

toward zero in keeping with the limiting form given in equation (6). In

this region, where the dominant behavior is characterized by a step

function of magnitude two, it is important to include some negative

reduced frequency values in the regression process to insure that the

step behavior, the small argument asymptotic behavior, is fully

captured. The advantage of the fractional derivative model is that it

is capable of representing a step function type of behavior quite

easily. This particular type of behavior in the modified kernel

function has just been initially investigated but is not presented here.

Figure 20 shows an example of the model in this region. The

difficulties associated with the modelling of the modified kernel

function occurred in the regions of the step function and the region

containing negative x_0 and large values of sy_0. As stated earlier, the

restriction to values of sy_0 less than one merely suggests the

suitability of the model for smaller aspect ratio wings. Another form

of model might be necessary to successfully model rectangular airfoils of higher aspect ratio.

It is possible to construct curves describing the dependence of the parameters of the model upon x_0 and sy_0. A sample of the variation of the parameters of the model for the incompressible case is contained in Appendix C. These curves can in turn be fit with polynomials of up to order five quite easily. However, rather than viewing these as polynomial curves, it is more convenient to view the terms of the polynomial models as the first few terms in an infinite power series of some unknown function which would fully describe the behavior of the parameters. If the infinite series can be shown to represent a mathematically convenient functional expression, it could facilitate the direct analytic integration of the integral equation or, at least, allow for an easier inverse Laplace transformation. These ideas have been initially studied in this work and continued work in this vein is planned to determine if this is a viable approach to the solution of the problem.

The modelling of the modified kernel function with fractional calculus types of functions has promise. It has been demonstrated that models can be developed which are sufficient for describing much of the behavior for moderate Mach number but not totally descriptive over all the domain of the kernel function. Higher Mach number behavior is more difficult to capture but some behavior was captured with a very simple model suggesting further investigation. The modified kernel function for incompressible flow was found to be modelled quite well for small

39

aspect ratio rectangular airfoils by a fractional calculus model with as few as four parameters. Although the model asymptotes for small and large values of reduced frequency have not yet been veri/i~d, ~.e result that the majority of the domain of the modified kernel function could be captured with a simple fractional calculus makes an import~..it thrust into a new area of application for fractional calculus.

One additional topic which must be addressed before the model can be deemed complete is the comparison with the modified kernel function in the complex s-plane. Ashley (2:7-8) provide forms of the modified kernel function suitable for evaluation throughout the complex plane, one of which has been used here as equation (5). If this model is shown to predict the behavior of the modified kernel function in the complex s-plane, then the model will be suitable for control analyses, not just stability analyses.

This particular work was only successful in modelling wings of very small aspect ratios under one-half. The goal of finding a directly integrable model of the kernel function does seem unlikely but the development of a model that can be inverted in the Laplace or Fourier sense seems very feasible. This type of model would be of extreme importance as it would permit the incorporation of the model of the kernel function into the equations of motion of the airfoil. If the model can be extended analytically into the left half s-plane, then equations of motion for general motion, not just stability, could be solved using the simple model of the kernel function. There is a great

need for more work in this area as this was the first attempt at
performing such a modelling on this function.

V. Approximate Solution of the Pressure-Downwash Integral Equation

Although the approximate solution of the integral equation (3) or
(23) was not a direct goal of the thesis, it became necessary after the
lack of success experienced in Section IV discussed earlier. The
approximate method is used to calculate the inverse kernel function K^{-1}
by sampling the integral equation and reducing the problem to a linear
system of equations. The inverse kernel function can then be used to
calculate numerically the generalized aerodynamic forces which will be
used to determine the equivalent Theodorsen function for three-
dimensional aerodynamics.

This chapter outlines the development of a method to evaluate
numerically the integral equation (3) or (23) which will collapse down
to a form similar to the doublet point method developed by Ueda and
Dowell (27:348-355). The doublet point method (27:348-355) is a
variation of the doublet lattice method (1:279-285) which is easier to
apply. Although the doublet point method was not used directly, the
result of the author's method reduces to a form which is close to that
of the doublet point formulation warranting the reference and credit for
the original work.

The procedure involves dividing the wing into a finite number of
panels and representing the entire pressure coefficient and downwash
distributions over the small panel by a single concentrated load with a
yet to be determined magnitude. This is mathematically equivalent to
treating the pressure coefficient distribution as a series of

42

acceleration doublet points (27:349) represented as Dirac delta functions. A downwash mode is assumed and a linear system of equations is formed by the sampling caused by the delta functions. The linear system is solved to determine the unknown coefficients of the delta functions which define the pressure coefficient distribution in a discrete sense.

The integral equation (23) is separated as shown in equation (33) to permit special treatment of the second order singularity present in the denominator when $sy_0 = 0$.

$$\frac{\tilde{w}(x,y)}{V} = \frac{b_0 \ell}{8\pi} \int_{-1}^{+1}$$

$$\left\{ \int_{-1}^{y-\sigma} + \int_{y-\sigma}^{y+\sigma} + \int_{y+\sigma}^{+1} \Delta \tilde{P}(\xi,\eta;k) \, K[k,x-\xi,s(y-\eta)] \, d\eta \right\} d\xi \tag{33}$$

The singular $d\eta$ integration in equation (33) will have to be performed by taking the finite part of an infinite integral in the Mangler sense (32:13) and σ in this instance indicates a small distance away from y. Note that the Mach number dependence has been omitted from the kernel function because the flow conditions have been specified to be incompressible. However, the procedure described in this chapter is applicable to compressible cases as well, provided the proper form of the kernel function is used. The airfoil surface is divided into η-integration regions to facilitate the integration process: the region containing the singularity will be referred to as Region II, the region to the left of this Region I, and to the right, Region III as shown in Figure 6. As mentioned previously, the modified kernel function
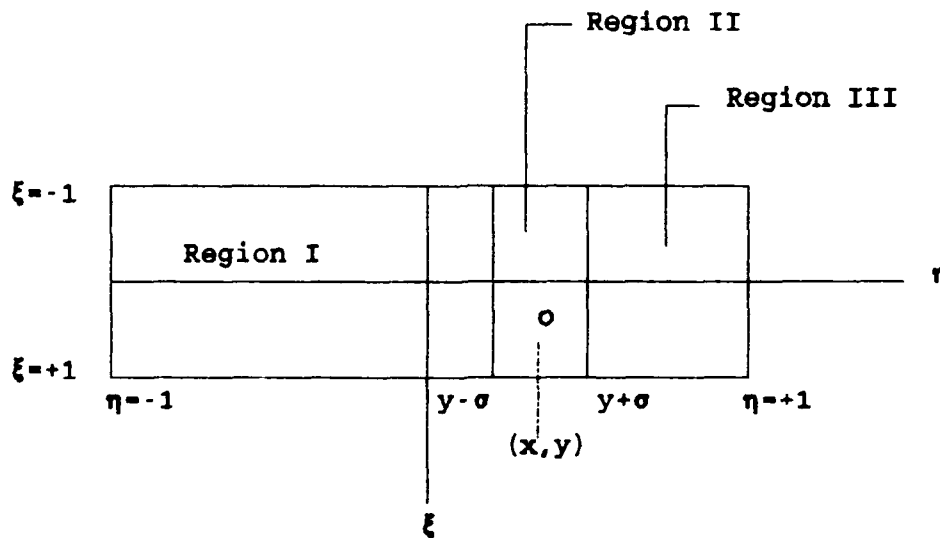
43

Figure 6: Integration Regions

possesses a finite jump discontinuity as $x-\xi \to 0$ and $y-\eta \to 0$. Otherwise the $d\xi$ integration poses no extreme challenges. The wing is now divided into N panels as shown in Figure 7. The number of panels in the x-direction is denoted by N_x and in the y-direction by N_y such that $N=N_x$ X N_y. The pressure coefficient information for the entire panel (i,j) will .e concentrated at the point (ξ,η) located at the one quarter chord and mid-span position on the panel and the downwash information concentrated at the panel three quarter chord and mid-span point (x,y) as shown in Figure 8. The convention of utilizing the one-quarter/
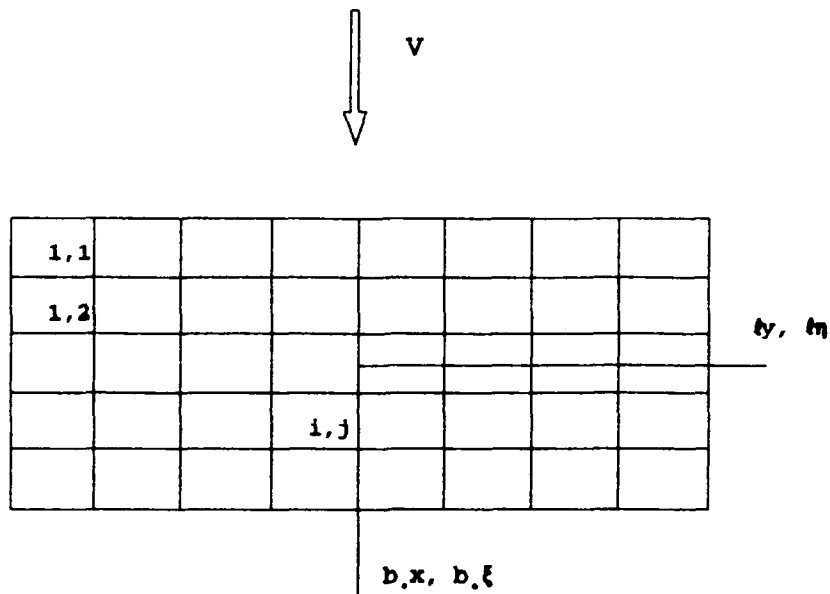
44

Figure 7: Discretization of Airfoil Surface

three-quarter chord rule for doublet and downwash location has been used successfully for years by both the vortex and doublet lattice methods (20:2) but the rigorous analytical justification for such an assumption is lacking to date (20:325-342).

Hence, the pressure coefficient distribution can be written in the following form shown in equation (34).

$$\Delta \tilde{P}(\xi,\eta;k) = P_{ij}(k)\delta(\xi-\xi_i,\eta-\eta_j) \qquad \textit{Regions I, III}$$

$$\Delta \tilde{P}(\xi,\eta;k) = P_i(k)\delta(\xi-\xi_i) \qquad \textit{Region II}$$

(34)

45

y

x

Doublet point (ξ, η)

Downwash point (x,y)
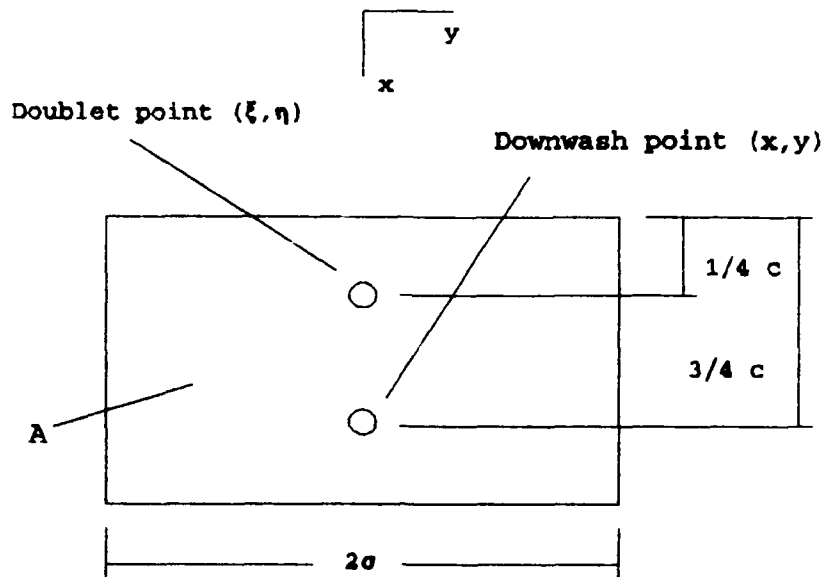
1/4 c

3/4 c

A

2σ

Figure 8: Airfoil panel

Using equation (34) for the pressure coefficient distribution and a similar type of formulation for the downwash distribution produces the following system of linear equations relating the coefficients of the downwash and pressure coefficient distributions.

In equation (35) the A_{ij} indicates the area of the (i,j) panel, P_{ij} indicates the undetermined pressure coefficient strength on the (i,j) panel and ℓ_i is the length of the panel (i,j) along the spanwise coordinate strip containing the singularity. The quantity $w(x_n, y_m)$ indicates the downwash strength on the (n,m) panel. This approach still requires the evaluation of the finite part of an infinite integral but it does avoid having to treat the jump discontinuity in the modified

46

$$\hat{w}(x_n, y_m) \approx \frac{b_0 \ell}{8\pi} \left\{ \sum_{i=1}^{N_x} \sum_{j=1}^{m-1} P_{ij} \frac{K^* [k, x_n - \xi_i, s(y_m - \eta_j)]}{b_0^2 s^2 (y - \eta)^2} A_{ij} \right.$$

$$+ \sum_{i=1}^{N_x} P_i \ell_i \int_{y_m - \sigma}^{y_m + \sigma} \frac{K^* [k, x_n - \xi_i, s(y_m - \eta)]}{b_0^2 s^2 (y_m - \eta)^2} d\eta \qquad (35)$$

$$\left. + \sum_{i=1}^{N_x} \sum_{j=m+1}^{N_y} P_{ij} \frac{K^* [k, x_n - \xi_i, s(y_m - \eta_j)]}{b_0^2 s^2 (y_m - \eta_j)^2} A_{ij} \right\}$$

kernel function because the locations of the downwash and pressure coefficient sample points are not coincident and hence $x_0 \neq 0$.

The Mangler integration can be handled in one of two ways as mentioned previously. The first method by Ueda (27:350) involves determining an equivalent non-singular expression for the kernel function at $y - \eta = 0$ based upon a discrete treatment of the Mangler integration and an asymptotic expansion for small argument of the kernel function. The second approach is to utilize a modified Gauss quadrature rule to capture the finite part of the integral (25:1196) in which the kernel function is evaluated at the abscissa points by any accurate means. Both methods were compared and produced comparable results using as few as six abscissa points with the quadrature rule. The former method was chosen, however, because it is more consistent with the sampling of the kernel function for the other two regions of the airfoil. This step collapses the present methodology into the doublet point method (27:349).

47

The method used in this thesis permits the Mangler integration to be performed by any appropriate means. Another distinction from the doublet point method (27:349) is the manner in which the kernel function is evaluated. The present method computed the kernel function in the non-singular regions by first computing the modified kernel function, equation (5) by methods described in Section II and then dividing by the double-pole singularity term (equation (4)). The kernel function in the singular region was handled by the approximation given in equation (46). The doublet point method (27:349) utilizes the asymptotic expansions, equations (39) through (44) to compute the kernel function throughout the domain of the airfoil. The series converge at different rates depending on the values of the arguments, requiring special treatment of summation computationally. Rather than work with this, the alternate method was used which did not require any series evaluations.

Ueda has shown (26:169) the kernel function can be written as follows for incompressible flow conditions

$$K[k, x-\xi, s(y-\eta)] = e^{-ikx_0} B(k, x-\xi, s(y-\eta)) \tag{36}$$

48

where the function B(k,x-ξ,s(y-η)) is defined

$$B(k,x-\xi,s(y-\eta)) = \int_{-\infty}^{x-\xi} \frac{e^{ikv}}{[v^2+s^2(y-\eta)^2]^{3/2}} dv \qquad (37)$$

If this integral is separated into its real and imaginary parts, the real part contains a double-pole singularity in η as $\eta \to 0$ as shown in equation (38) which was obtained by making a change of variables on equation (37).

$$B(k,x_0,s(y-\eta)) = \frac{1}{s^2(y-\eta)^2} \int_{-\infty}^{(x-\xi)/s(y-\eta)} \frac{e^{iks(y-\eta)\lambda}}{(1+\lambda^2)^{3/2}} d\lambda \qquad (38)$$

Ueda has expanded both the real and imaginary parts of equation in an asymptotic series about small ks(y-η). The series is written as the following (21:170)

$$B_R(k,x_0,sy_0) = \sum_{n=0}^{\infty} (-1)^n U_{2n}$$

$$\qquad (39)$$

$$- \frac{k^2}{2} \sum_{n=0}^{\infty} \frac{\left(\frac{kr}{2}\right)^{2n}}{(n+1)(n!)^2} \times \left\{ \sum_{m=1}^{n} \frac{1}{m} + \frac{1}{2(n+1)} - \gamma - \ln\frac{k}{2} \right\}$$

$$B_I(k,x_0,sy_0) = \sum_{n=0}^{\infty} (-1)^n U_{2n+1} + \frac{\pi}{4} k^2 \sum_{n=0}^{\infty} \frac{\left(\frac{kr}{2}\right)^{2n}}{(n+1)(n!)^2} \qquad (40)$$

$$U_0 = \frac{1}{\sqrt{x_0^2+s^2 y_0^2}\left(\sqrt{x_0^2+s^2 y_0^2} - x_0\right)} \qquad (41)$$

49

$$U_1 = -\frac{k}{\sqrt{x_0^2 + s^2 y_0^2}} \tag{42}$$

$$U_2 = -\frac{k^2}{2} \left\{ \frac{x_0}{\sqrt{x_0^2 + s^2 y_0^2}} + \ln\left(\sqrt{x_0^2 + s^2 y_0^2} - x_0\right) \right\} \tag{43}$$

$$U_m = \frac{k}{(m-2)m!} \frac{(kx_0)^{m-1}}{\sqrt{x_0^2 + s^2 y_0^2}} - \frac{(ksy_0)^2}{m(m-2)} U_{m-2} \; ; \qquad m \geq 3 \tag{44}$$

One attractive feature of these series is that every singular part is explicitly written as an initial term (26:169). These expressions can be inserted in the η integral and the integrations can be performed in the Mangler sense.

$$\int_{-\sigma}^{\sigma} B_R(k, x_0, sy_0) \, d(sy_0) = \lim_{\zeta \to 0} \left[\int_{-\sigma}^{-\zeta} + \int_{\zeta}^{\sigma} B_R(k, x_0, sy_0) \, d(sy_0) - \frac{4}{\zeta} \right]$$

$$x_0 > 0$$

(45)

Ueda has shown an equivalent expression for B_R after including the effects of the Mangler integral performed in a discrete sense can be written as the following (27:350)

$$B_R(k, x_0, sy_0) \to B_R(k, -x_0, 0) - \frac{\pi^2}{6\sigma^2} + k^2 \left(\ln\frac{k\sigma}{2} + \gamma - \frac{3}{2} \right) \tag{46}$$

$$(sy_0 < \sigma, \quad x_0 > 0)$$

This provides a method of evaluating the kernel function when $sy_0=0$ and can be substituted into the second summation expression in equation (35). Replace the integration in the second expression in equation (35) with a discrete sampling of the kernel function as done previously in equation (34). This permits the panel numbering system (i,j) to collapse to a single because it is no longer required to track specially the spanwise coordinate of the modified kernel function for integration purposes as there exists a way to evaluate the kernel function at $sy_0=0$ and no special integration treatment is now required for the kernel function. Hence, the (i,j) panel will be relabeled as the i-th panel with a doublet point at ξ_i, η_i and downwash at point x_i, y_i. This simplification allows the system of equations in equation (35) to be expressed in a much simpler form

$$\vec{w} = \underline{K}\vec{p} \tag{47}$$

$$\vec{p} = \{p_j\} = \{\Delta \hat{p}(\xi_j, \eta_j; k)\} \tag{48}$$

$$\vec{w} = \{w_i\} = \{\hat{w}(x_i, y_i)\} \tag{49}$$

$$\underline{K} = [K_{ij}] = \frac{A_{ij}}{8\pi} K[k, x_i - \xi_j, s(y_i - \eta_j)] \tag{50}$$

where i and j can index from 1 to $N=N_x \times N_y$ panels. The $\rightarrow$ indicates a vector quantity and $\underline{K}$ distinguishes the matrix quantity from the continuous quantity. This system of equations (47) through (50) is presented as the doublet point method (27:349). This linear system of

51

equations can be solved given an assumed downwash modeshape vector w_i.
The beauty in this method is evidenced by not having to presume an
appropriate form for the pressure coefficient distribution. This method
relies on the mathematics embodied inside the kernel function to
determine the correct pressure coefficient distribution. An
illustration of the ability of the procedure to compute the pressure
coefficient distribution is seen in Figure 9 below. Most methods
discussed previously such as the vortex and doublet lattice methods and
all assumed mode methods, involve assuming some form for the pressure
coefficient distribution. This distribution is generally singular,
creating even more difficulties using one of these other approximate
methods. The pressure coefficient Δp shown is for a thin rectangular of
aspect ratio two in steady flow. The pressure distribution on an
airfoil of this type under steady flow conditions should possess two
distinct features: first, the flow should exhibit a singularity of the
type $\epsilon^{-\frac{1}{2}}$, $\epsilon \rightarrow 0$ at the leading edge of the airfoil (32:5) and the flow to
go to zero at the wing tips with an infinite slope as $\epsilon^{\frac{1}{2}}$, $\epsilon \rightarrow 0$ (32:5).
The first type of behavior is demonstrated in Figure 9, becoming more
pronounced as the number of chordwise panels N_x is increased. The
second type of behavior is seen in Figure 10 where $C_{l,\alpha}$ is shown as a
function of the number of spanwise panels, N_y. The coefficient of lift
is calculated using equation (60) which will be introduced shortly. The
behavior is more pronounced as the number of panels is increased, as
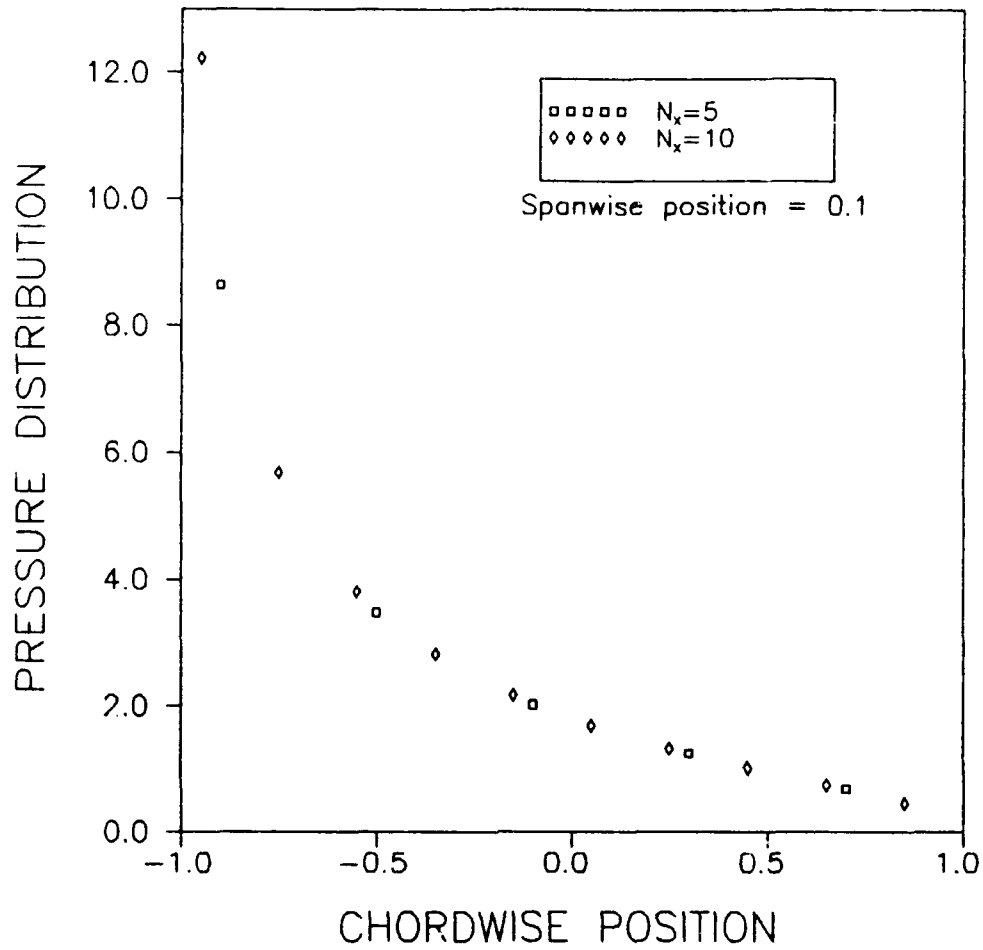observed in the previous figure.

52

Figure 9: Dependence on N_x

The total pitching lift coefficient for the case $N_y=10$ is 2.78 compared with the previously reported value of 2.65 when $N_y=20$. This demonstrates the dependence between the total pitching lift coefficient and the number of panels in the spanwise direction. The total pitching lift coefficient for the $N_x=5$ case was 2.65 compared to the $N_x=10$ case

with a value of 2.64. This shows the total pitching lift coefficient is
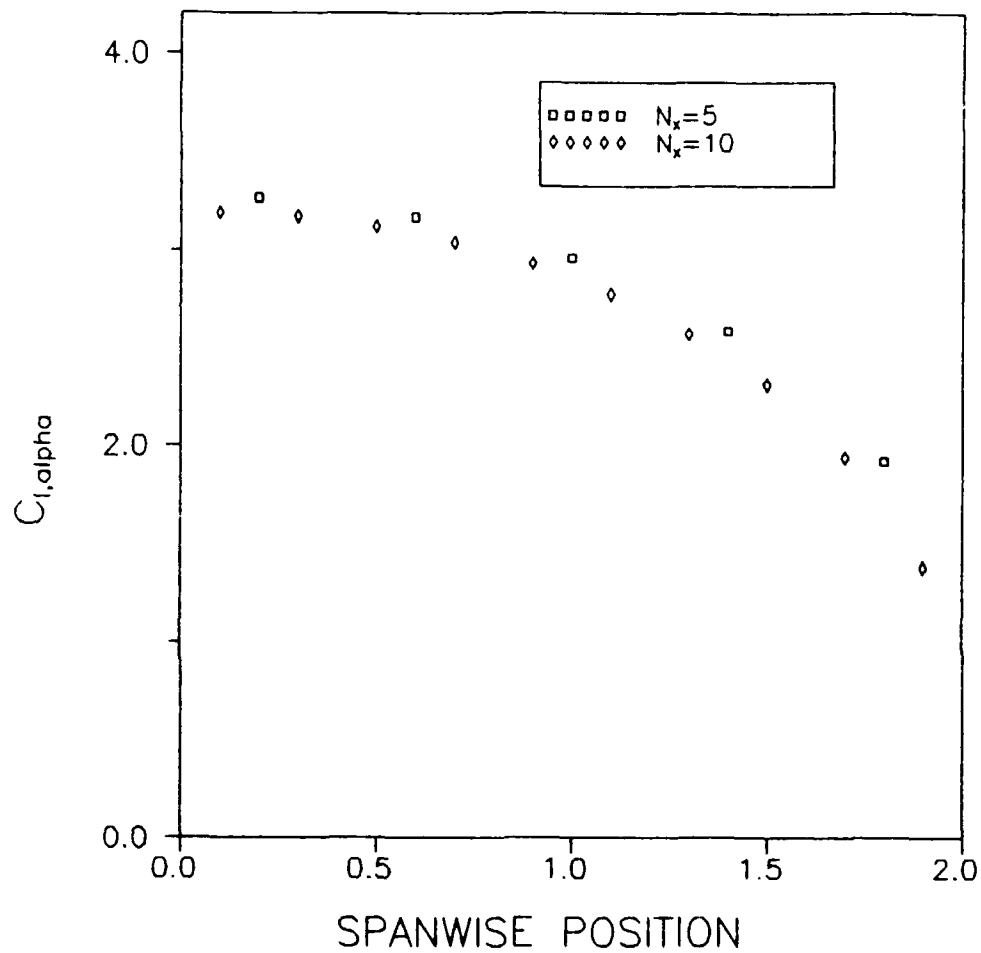little changed by the number of panels.

Figure 10: Dependence on N_y

These examples serve to show the increased accuracy in the local
pitching lift coefficient achieved by the larger number of panels in the
chordwise direction and little effect the number of chordwise panels has

54

on the same. The unsteady cases also have a similar type of dependence upon the number of spanwise and chordwise panels.

This procedure is not compared to actual test data here, but is compared to other approximate methods. Test data such as that in reference (34) is difficult to compare with at lower reduced frequencies. This is due to the very high velocities necessary to achieve low reduced frequencies ($k=\omega b_0/V$) inside the wind tunnel. These higher velocities result in high mach numbers, violating the incompressible flow assumptions upon which the procedure is based. Even Mach number corrections are not very helpful because the higher Mach numbers feature shock waves traveling along the airfoil which is a non-linear problem not handled by this theory. Comparisons of the computed steady values of total pitching lift coefficient with those of modified lifting line theory (20:338) and an approximate method by Graham (7:93) show a maximum error of approximately six percent and a minimum error of about 0.3 percent for aspect ratios ranging from two through ten with $N_x=5$ and $N_y=20$. Although these appear large, the results are respectable for unsteady aerodynamic analysis. The unsteady results over a range of reduced frequency from zero to one for the aspect ratio two cases were compared with those of another approximate method by Lawrence (15:769-781) and the agreement was good.

There is a desire to use a large number of elements to achieve higher accuracy. However, this increases the size of the linear system and significantly increases the solution time, especially when the computations must be done over a wide range of reduced frequencies. The

aspect ratio two case was solved using a 100 panel (5 X 20) wing and aspect ratio ten was solved using a 600 panel (5 X 100) airfoil. The dependence upon the N_γ for each aspect ratio was determined by keeping the N_γ/AR ratio constant. This method presented in this section and the doublet point method (27:349) is much less time consuming computationally than any of the procedures mentioned earlier. Another option that exists for wings with spanwise symmetry is to reduce the number of degrees of freedom by utilizing a constraint matrix (27:351) If the pressure coefficient distribution can be represented by a smaller number of degrees of freedom

$$\vec{p} = Q\overline{p} \tag{51}$$

where Q is the constraint matrix. This allows equation (47) to be written as

$$Q^T\vec{w} = [Q^T K Q]\overline{p} \tag{52}$$

where the number of degrees of freedom is reduced by an amount determined by the Q matrix. Generally, for rectangular, spanwise symmetry, the number of degrees of freedom will be reduced by a factor of one-half.

An important feature of this procedure is direct input into finite element types of aeroelastic analyses. Once the structural grid is established, this routine can be used to obtain reasonably accurate structural applied loads by computing the pressure coefficient vector for the structure and multiplying by $\frac{1}{2}\rho V^2 S$. The finite element technique can then be used to solve the aeroelastic problem.

56

Ashley and Boyd (2:8) have demonstrated the expression for the modified kernel function in equation (5) is an appropriate form for computing values throughout the complex s-plane provided special precautions are taken in computing the modified kernel function in certain regions of the s-plane. Hence, the generalized forces computed using this method can be treated as Laplace transformed aerodynamic forces. Modelled with fractional calculus, the generalized forces can now be used more easily to determine the forced response of the airfoil which will be discussed in Section VI.

VI. Equivalent Theodorsen Function for Three-dimensional Aerodynamics

Theodorsen's function is the transfer function relating the unsteady circulatory lift to the downwash of an infinitely thin, harmonically oscillating plate in inviscid, incompressible, two-dimensional flow (25:418). The Theodorsen function is a ratio of Bessel functions with no known analytic inverse transform whose arguments are defined in terms of the reduced frequency and taken as purely imaginary for stability analysis (4:5). Swinney (24:5) has developed a fractional calculus model of the Theodorsen function which is valid in the entire s-plane with the appropriate substitution of the dimensionless Laplace variable s for ik. Unfortunately, no direct functional analog to the Theodorsen function in three-dimensional aerodynamics has been established. The integral equation (3) shows the transfer function is part of a spatial convolution with the transform of the pressure coefficient distribution on the airfoil. This transfer function is not as mathematically clean as the Theodorsen function and little investigation and progress has been made toward the simplification of the three-dimensional unsteady aerodynamic transfer function.

This chapter will describe an approach taken to simplify the determination of the transfer function in three-dimensional aerodynamics. As stated above, this transfer function is embedded in the spatial convolution in the integral equation (3). The approach taken is to express the generalized aerodynamic forces in three-dimensional flow in terms of the forces found in two-dimensional flow by

appropriate use of a new function, the equivalent Theodorsen function for three-dimensional unsteady aerodynamics. The equivalent Theodorsen function will be developed and its properties explained. Additionally, since the equivalent Theodorsen function exists in the Laplace domain, the accompanying time domain functions used in aeroelastic analysis will be developed as well.

The idea of relating the two- and three-dimensional aerodynamic forces is not new. Many different theories have been authored describing how to establish such a relationship. Watkins, Runyan and Woolston established that the kernel function does collapse to the two-dimensional case as the span is increased to infinity (31:713), which may suggest the existence of some type of mathematical link between the finite span wing and infinite airfoil unsteady aerodynamic phenomena. Reissner (21:32) has established an integral correction factor based upon an strip formula type of approach similar to that of lifting-line theory which modifies the two-dimensional Theodorsen function to produce the generalized forces on a finite wing. Another method has been developed by Lawrence (15:771) which modifies the Theodorsen function to produce three-dimensional effects. These methods are based upon different underlying assumptions regarding the connection between the two-and three-dimensional flow conditions. Reissner's theory establishes the non-circulatory portion of the lift on an infinite wing remains unchanged as the span becomes finite (6:389). The non-circulatory flow produces no wake and therefore, the induction effects associated with it are relatively small. In regions of the wing where

59

the induction effects are small compared to the purely circulatory ones, this is certainly true. However, this is not true in the immediate wing tip region because of the larger induction effects from the tip vortices present. Reissner has also established the unimportance of induction effects on the accurate prediction of airloads on wings for large values of reduced frequency since the non-circulatory effects are proportional to k^2 (6:389). However, induction effects are dominant for small values of k and for small aspect ratio wings. These observations and theories led to the postulation of the equivalent three-dimensional Theodorsen function.

Development

Two-dimensional unsteady aerodynamic equations are an appropriate starting point to begin a search for an appropriate form of the equivalent Theodorsen function. Lift generated by pure pitching motion was selected as a generalized aerodynamic force with which to compare the two- and three-dimensional unsteady aerodynamics. The lift per unit span of an airfoil in pure pitch is given by (6:272)

$$L = \pi \rho b_0^2 \left[V\dot{\alpha} \right] + 2\pi \rho U b_0 C(k) \left[V\alpha + \frac{b_0}{2}\dot{\alpha} \right] \tag{53}$$

where $C(k)$ is the Theodorsen function for two-dimensional aerodynamics. The first term in equation (53) represents the non-circulatory portion and the second term represent the circulatory portion of lift per unit span. In this case the downwash function $w(x,y,t)=\alpha(x,y,t)$ has taken on

the following form to insure positive angle at the leading edge of the airfoil and to be consistent with equation (53)

$$w(x, y, t) = \alpha(x, y, t) = -\alpha_0 x e^{i\omega t} \qquad (54)$$

Noting that lift per unit span for the finite rectangular airfoil can be approximated by the following expression while still being consistent with the original assumptions of the integral equation (1), it is possible to directly relate the integral equation for three-dimensional flow to the Theodorsen function.

$$L = \frac{1}{2}\rho V^2 C_{L_\alpha} \alpha (2b_0)$$
$$\alpha = \frac{w(x, y, t)}{V} \qquad (55)$$

Here the $T(k)$ has been substituted for the usual $C(k)$ and will now be referred to as the equivalent Theodorsen function for three-dimensional unsteady aerodynamics because the coefficient of lift, $C_{L,\alpha}$, is computed using the three-dimensional theory. Substituting these expressions into equation (53) and simplifying yields

$$C_{L_\alpha} = \pi \left\{ ik + 2T(k)\left[1 + \frac{ik}{2}\right] \right\} \qquad (56)$$

Note that this model presumes the changes between two-and three-dimensional flow exists purely in the equivalent Theodorsen function. The initial model was constructed with no constraints placed on the non-circulatory and circulatory lift, allowing the two to vary independently of one another. The initial model was found to be suboptimal. Next, the model in equation (56) in which the non-circulatory lift is fixed

61

and the circulatory lift is allowed to vary was used. This model was shown to yield satisfactory results and is an incomplete confirmation of Reissner's conjecture mentioned earlier which stated that the non-circulatory lift does not change. This will elaborated upon further after the fractional calculus model of the equivalent Theodorsen function is presented in the next section. Given the relationship shown in equation (56), discrete values of $T(k)$ can be computed from the discrete values of the coefficient of lift and modelled using fractional calculus. Given a convenient form for $T(k)$, time domain response will be calculable as is the case with $C(k)$. It should be noted that pure pitching motion is only one form of motion for which this relationship should exist. Another form being pure plunge, for example.

Fractional Calculus Model and Results

A fractional calculus model for the two-dimensional Theodorsen function (24:5) suggested a fractional calculus form for the equivalent three-dimensional function since the two have been presumed to be mathematically related as shown in equation (56). Also, as shown earlier, the kernel function for incompressible flow conditions was shown to possess fractional derivative properties which further suggested the resulting lift and hence, the equivalent Theodorsen function $T(k)$, should have these same trends.

The equivalent Theodorsen function is highly nonlinear and there is a number of possible forms of models. In this case, Swinney's model of the Theodorsen function was used as a suitable form with which to begin. Before the modelling can begin, the coefficient of lift must be

62

computed. The next paragraph will elaborate on the exact method used to determine the coefficient of lift.

The mode shape for pure pitching about midchord can be written in a form consistent with equation (19) as

$$\alpha(x, y, t) = -\alpha_0 x \frac{q_\alpha(t)}{b_0} \tag{57}$$

where $\alpha_0 x$ is the shape function describing the position of all points on the airfoil experiencing pure pitching motion and the minus sign is included to produce positive angle for positive α_0 at the leading edge. The subscript α makes reference to the pitching amplitude function $q_j(t)$. There is no y dependence in the shape function because there is pure rigid body pitching and no spanwise bending or torsion is present. This downwash can be cast into the form in equation (49) as

$$\vec{\alpha} = \vec{W} = \{\vec{W}(x_i, y_i)\} = \{-\alpha_0(1 + ikx_i)\} \tag{58}$$

Using the relationship defined previously in equation (50) for $\underline{K}$, the unknown pressure coefficient can now be solved via standard linear system procedures. The $\underline{K}$ matrix is well conditioned and solutions were obtained using the IMSL routine LSACG which solves complex general systems of linear equations by Gaussian elimination with iterative refinement (9:31). Given the pressure coefficient, the following definitions can be used to obtain the complex lift coefficient per unit span and total lift coefficient as shown in equations (59) and (60). The coefficients of lift in equations (59) and (60) above can be treated as

63

$$C_l(y_j) = \frac{\sum_{i=1}^{N_x} p_{ij} A_i}{\sum_{i=1}^{N_x} A_i} \qquad (59)$$

$$C_L = \frac{1}{S} \sum_{j=1}^{N_y} \left\{ C_l(y_j) \sum_{i=1}^{N_x} A_{ij} \right\} \qquad (60)$$

derivatives with respect to angle of attack, α, because the coefficients of pressure upon which they are based are only known to an arbitrary magnitude, α_0, of the pitching motion.

The equivalent Theodorsen function modelling was accomplished using the same procedure as was performed for modelling the modified kernel function, the only difference being the real part was used for regression in this instance versus the imaginary part in the prior case. The real part inexplicably seemed to produce more consistent results in this case. The functional form used to model the equivalent Theodorsen function is

$$T(k, AR) = T_0 + \frac{a(AR) \, (ik)^{\mu(AR)}}{1 + b(AR) \, (ik)^{\mu(AR)}} \qquad (61)$$

$$- g(AR) \, (ik) + f(AR) \, (ik)^2$$

where T_0 is given by the steady value of $C_{L,\alpha}$ as determined in equation (56) divided by π. The results once again yielded a family of curves, the parameters in this instance being functions of aspect ratio only. The accuracy of the modelling of the equivalent Theodorsen function is shown below and in Appendix D. The equivalent Theodorsen function

64

models for aspect ratio two and ten along with the two-dimensional C(k) are shown in Figure 11 and Figure 12 below.
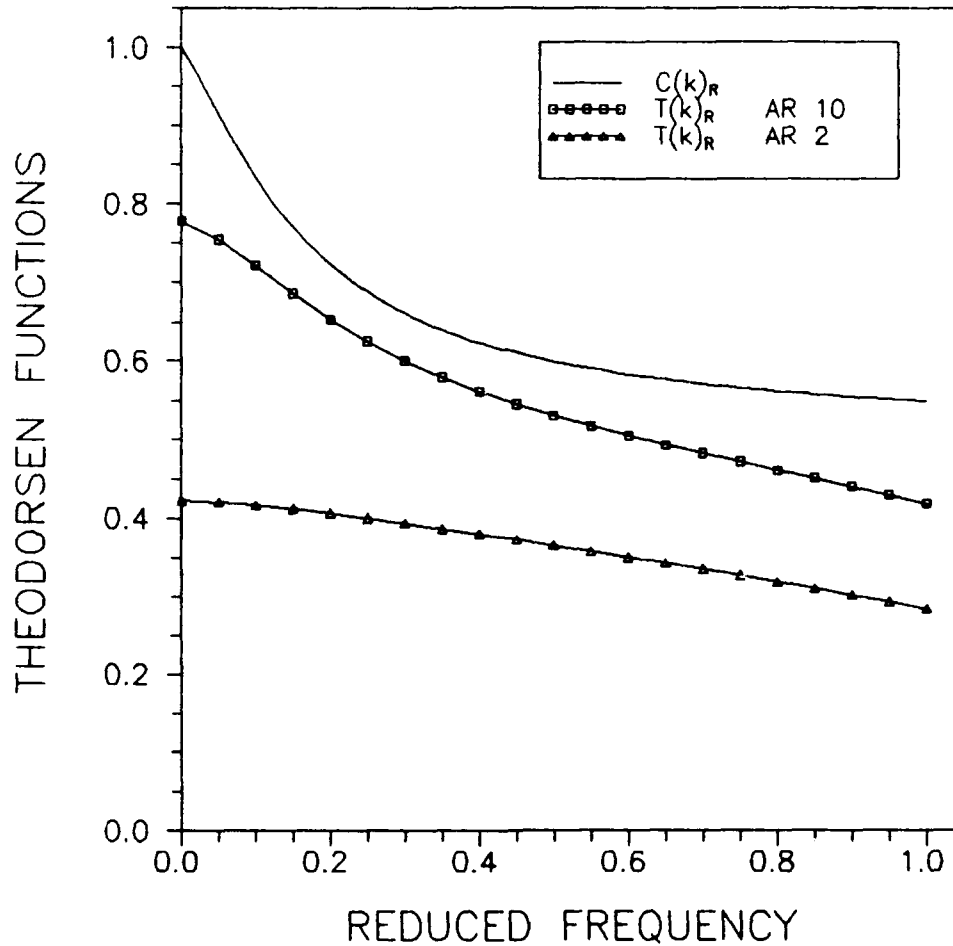

Figure 11: Real Parts of Theodorsen Functions

The resulting model of the coefficient of lift for aspect ratio ten is given in equation (62) and is shown in Figure 13. One interesting observation made from these figures is the apparent relationship between the different Theodorsen functions. It appears the equivalent
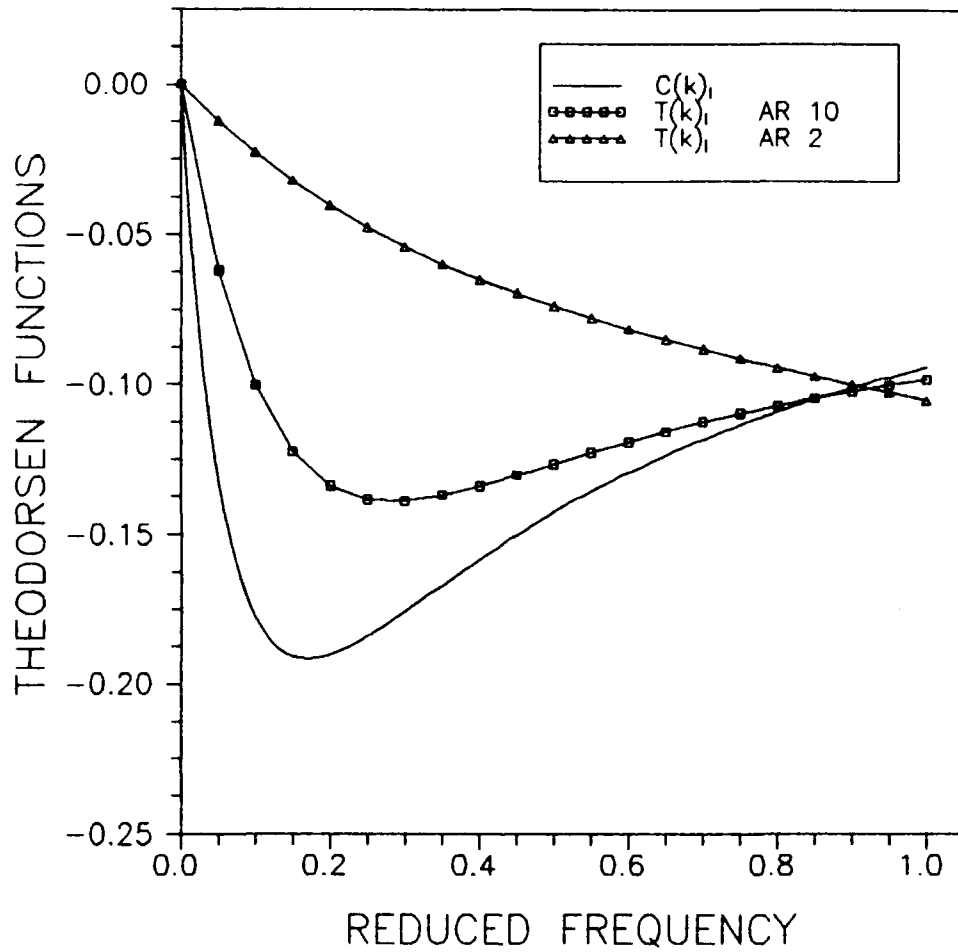
65

Figure 12: Imaginary Parts of Theodorsen Functions

Theodorsen function T(k) tends toward the two-dimensional C(k) in the limit as the aspect ratio is increased from two to ten; this was not verified or proven in this work.

$$T(ik) = T_0 + \frac{a(ik)^\mu}{1 + b(ik)^\mu} - g(ik) + f(ik)^2 \qquad (62)$$

where

$$T_0 = 0.778$$
$$a = 1.034 \qquad\qquad \mu = 0.904$$
$$b = 3.32 \qquad\qquad f = 0.085$$
$$g = 0.017$$
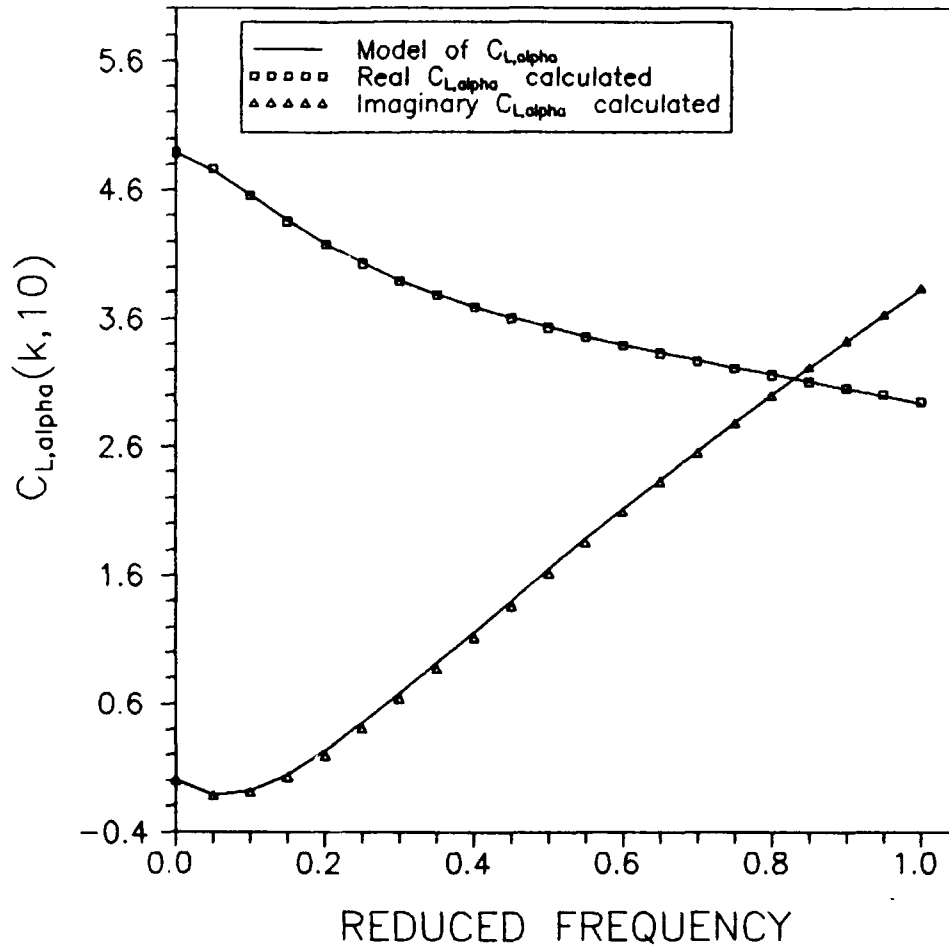
Figure 13: $C_{L,\alpha}$ for Wing of Aspect Ratio 10

It would be interesting to see the results for higher aspect ratio such as twenty or fifty. This type of analysis was not pursued further here because of a lack of available computer memory. This limiting

67

relationship was not proven here but does suggest a topic for further study. As mentioned earlier, Reissner (22:14-18) has developed a relationship between the two-dimensional Theodorsen function and three-dimensional unsteady aerodynamics. This relationship consists of modifying the Theodorsen function by multiplication with a factor consisting of an integral factor and a combination of Bessel functions. The integrals in Reissner's relationship are quite difficult to evaluate and have been tabulated for easier use (22:70-72). It is believed the behavior within the fractional calculus model may fully capture the adjustment Reissner made to the Theodorsen function with his correction factor. The theory by Reissner presumes the non-circulatory effects of the flow remain unchanged between the two- and three-dimensional flow (6:389). The mathematics of the modelling process suggested this phenomenon as well. In numerous attempts to force the three-dimensional effects to be contained in an additional non-circulatory term, the models would not converge uniformly for both the real and imaginary parts of the coefficients of lift. Many different types of additive non-circulatory terms and many different trial vectors were tried with no success. It was only when the flow modifications were restricted to the circulatory portion of the flow that good convergence for both the real and imaginary parts was obtained. The Theodorsen function is the transfer function for the circulatory portion of two-dimensional flow. The relative contribution of circulatory lift to the coefficient of lift, the quantity [1+ik/2] in equation (53), which multiplies the Theodorsen function for pure pitching motion as shown in equation

68

remained unchanged and all differences between the two- and three-dimensional flow were placed in the equivalent Theodorsen function.

Another interesting result from this analysis is the relationship established among the parameters of the model. This relationship can be used to determine other values of the equivalent Theodorsen function for rectangular wings of aspect ratios between two and ten. The curves relating the parameters are contained in Appendix E with a sample shown in Figure 14 and Figure 15. These results are good only for rectangular planforms but it is believed such a relationship might exist for other planforms such as tapered and swept-tapered.

The parameter a was well behaved but the μ parameter was more complicated. More is to be gained mathematically by viewing the polynomial model of these parameters as the first portion of an infinite power series of some unknown function which fully describes the behavior. A cubic spline is plotted through the μ points as the order of the polynomial was continually increasing. The coefficients of the polynomial were decreasing toward zero quite rapidly, typical of a convergent series. It is postulated that the unusual behavior of the parameter μ may smooth out if the modelled range of reduced frequency is increased.
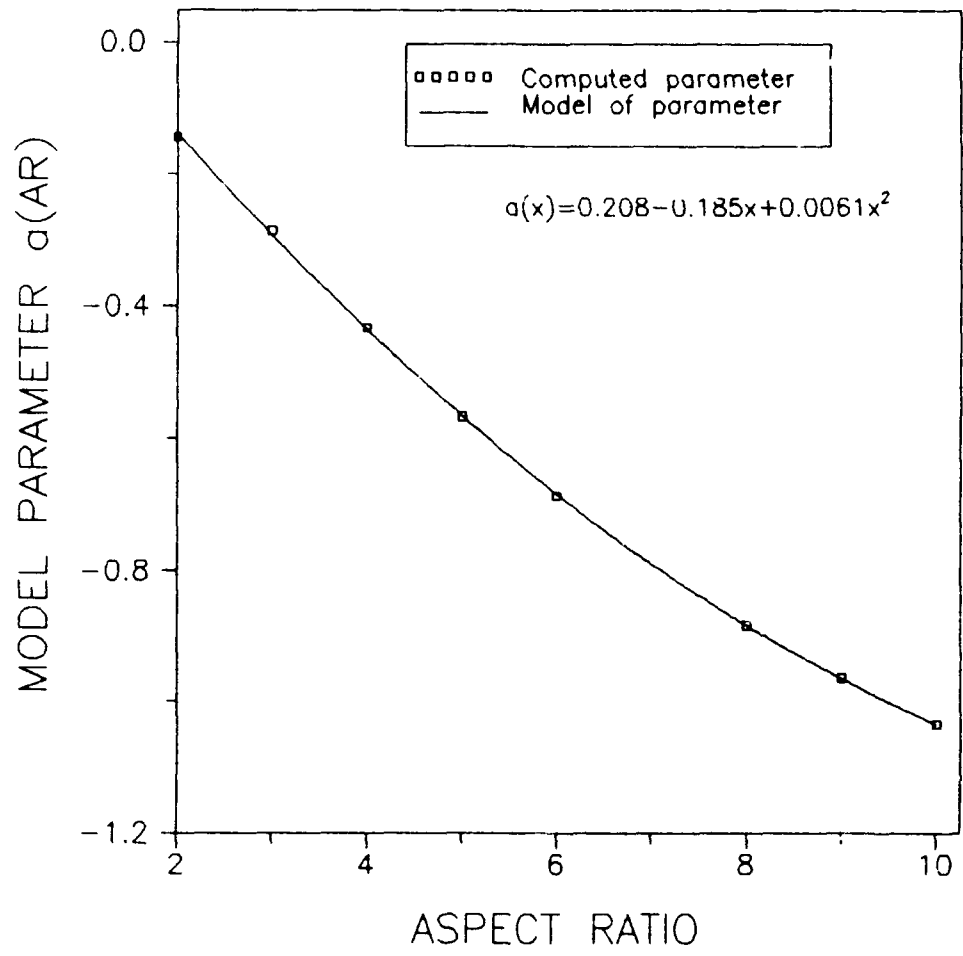
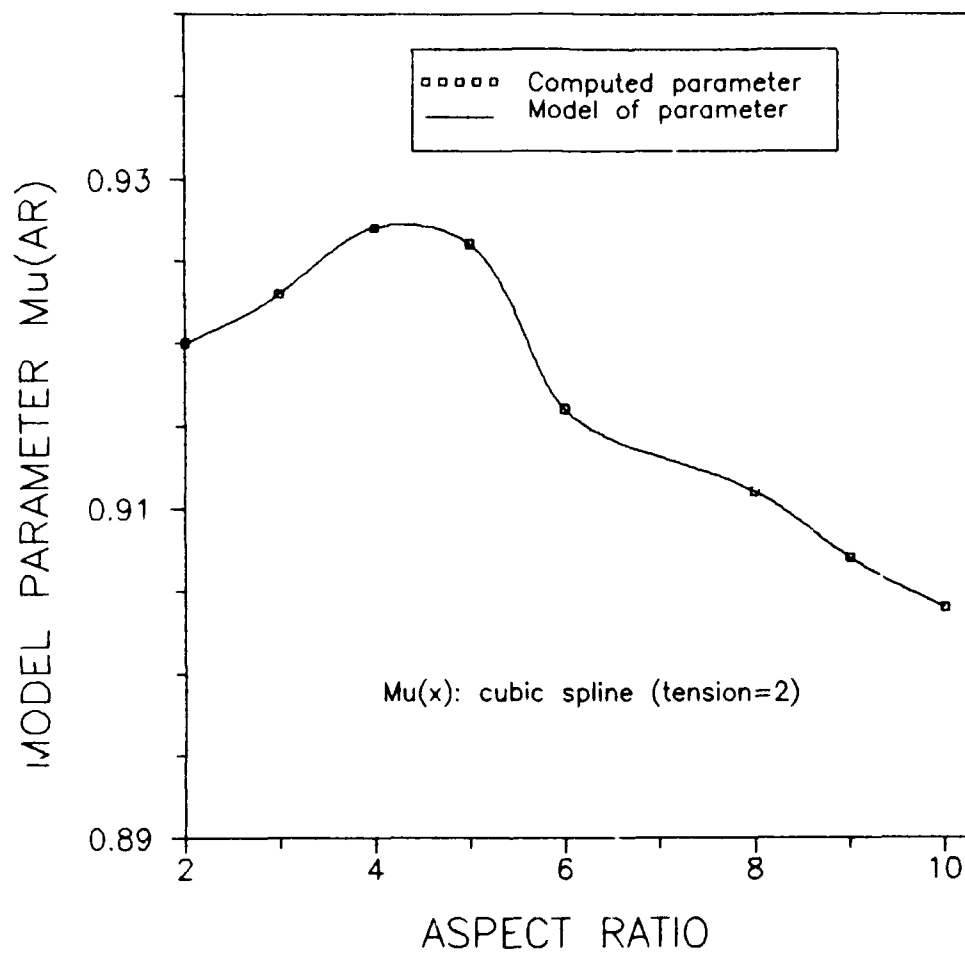Figure 14: Parameter a vs. Aspect Ratio

Figure 15: Parameter μ vs. Aspect Ratio

VII. Time Domain Responses Based Upon Equivalent Theodorsen Function

In general, it is difficult to get an accurate time domain representation of unsteady aerodynamic loads using the three-dimensional pressure-downwash integral equation (1). Usually, the solution of this equation is only presented for frequency only since most of the work with the kernel function has been restricted to stability or flutter analyses which are only defined along the positive imaginary axis. In two-dimensional unsteady aerodynamics, the Theodorsen function has been approximated with a model that has an elementary inverse Laplace transform to permit forced response analysis. As this is the first time the circulatory properties of the three-dimensional aerodynamics have been cast into a mathematically tractable form, this will be the first time the forced responses for wings of finite span will be written in a mathematically accurate and compact form.

Wagner Function

The advantage of this fractional calculus model is the reasonably compact time domain representation of the unsteady aerodynamic loads. The other approximate methods used to compute the generalized aerodynamic forces, such as Reissner's (21:1-39) and Lawrence's (15:769-781), do not have this unique and beneficial feature. The time-dependent lift is posed in terms of the Wagner function (6:285), $\phi(t)$, which is defined in equation (63). The Wagner function represents the lift resulting from a unit step change in angle of attack (sometimes called indicial lift).

72

$$\phi(t) = \mathscr{L}^{-1}\left[\frac{C(\overline{s})}{\hat{s}}\right] \tag{63}$$

The fractional calculus model of the equivalent Theodorsen function, $T(k)$, in equation (61) can be represented in the Laplace domain as

$$T(\overline{s}) = T_0 + \frac{a(\overline{s})^\mu}{1 + b(\overline{s})^\mu} - g(\overline{s}) + f(\overline{s})^2 \tag{64}$$

where the dimensionless Laplace variable $s = \hat{s}b_0/V = ik$ indicates the change into the Laplace plane, $\hat{s}$ the general Laplace variable, and where the AR dependence of the parameters is not shown for compactness. Equation (64) can manipulated into a form more suitable for inverse Laplace transformation

$$T(\overline{s}) = T_0 - \frac{a}{b} + \frac{a}{b}\frac{1}{b(\overline{s})^\mu + 1} - g(\overline{s}) + f(\overline{s})^2 \tag{65}$$

By recognizing the binomial series present, this can be further expressed by the following power series

$$T(\overline{s}) = T_0 - \frac{a}{b}\sum_{n=0}^{\infty}\left(\frac{-1}{b(\overline{s})^\mu}\right)^n - g(\overline{s}) + f(\overline{s})^2 \tag{66}$$

These simplifications lead to the following Laplace domain expression for the Wagner function

$$\frac{T(\overline{s})}{\hat{s}} = \frac{T_0}{\hat{s}} - \frac{a}{b}\sum_{n=0}^{\infty}\left(\frac{-1}{b}\right)^n\frac{1}{\overline{s}^{n\mu}}\frac{1}{\hat{s}} - g\frac{\overline{s}}{\hat{s}} + f\frac{\overline{s}^2}{\hat{s}} \tag{67}$$

Making a substitution for s the Wagner function can be written in terms of the Laplace variable $\hat{s}$

73

$$\frac{T(\bar{s})}{\bar{s}} = \frac{T_0}{\bar{s}} - \frac{a}{b} \sum_{n=0}^{\infty} \left(\frac{-V^{\mu}}{b_0^{\mu} b}\right)^n \frac{1}{\bar{s}^{n\mu+1}} - \frac{b_0}{V} g + \left(\frac{b_0}{V^2}\right) f\bar{s} \qquad (68)$$

Taking the inverse Laplace transform yields

$$\phi(t) = T_0 u_{-1}(t) - \frac{a}{b} \sum_{n=0}^{\infty} \left(\frac{-1}{b}\right)^n \left(\frac{Vt}{b_0}\right)^{\mu n} \frac{1}{\Gamma(\mu n + 1)}$$
$$- \frac{b_0}{V} g u_0(t) + \left(\frac{b_0}{V}\right)^2 f u_{+1}(t) \qquad (69)$$

The term u_{-1} is a unit step function, the u_0 term is the unit delta function, and the u_{+1} term is the unit doublet function. The doublet function is the derivative of the delta function. The μ order Mittag-Leffler function is defined as (15:102)

$$E_{\mu}(x) = \sum_{n=0}^{\infty} \frac{x^n}{\Gamma(1+\mu n)} \qquad (70)$$

The μ order Mittag-Leffler function shown in equation (70) can be considered as the generalized μ order exponential function (4:12) as setting μ equal to one produces the Taylor series for the exponential function e^x. Using this notation to represent the time series in the Wagner function produces

$$\phi(t) = T_0 u_{-1}(t) - \frac{a}{b} E_{\mu}\left[\frac{-1}{b}\left(\frac{Vt}{b_0}\right)^{\mu}\right] - \frac{b_0}{V} g u_0(t)$$
$$+ \left(\frac{b_0}{V}\right)^2 f u_{+1}(t) \qquad (71)$$

74

The Wagner function is shown in terms of dimensionless time, $\bar{t}=Vt/b_0$, in equation (72).

$$\phi(\bar{t}) = T_0 u_{-1}(\bar{t}) - \frac{a}{b} E_\mu \left[\frac{-\bar{t}^\mu}{b} \right] - \frac{b_0}{V} g u_0(\bar{t}) \qquad (72)$$

$$+ \left(\frac{b_0}{V} \right)^2 f u_{+1}(\bar{t})$$

This expression is similar to the Wagner function determined by Swinney (24:22) with the addition of the discontinuous Dirac delta function and doublet function. The approximation to Wagner's function in three-dimensional flow (72) is shown with the Wagner function model developed by Swinney (24:22) for two-dimensional flow in Figure 16. It should be noted that only the continuous portions of the Wagner function representation in equation (72) are shown in Figure 16. The figure illustrates the response to a step input in angle of attack reaches a steady-state value faster in three-dimensional flow than in two-dimensional flow. This is expected as the finite wing has wing tip effects working to dampen motion in addition to the trailing edge effects it has in common with the infinite wing.

75
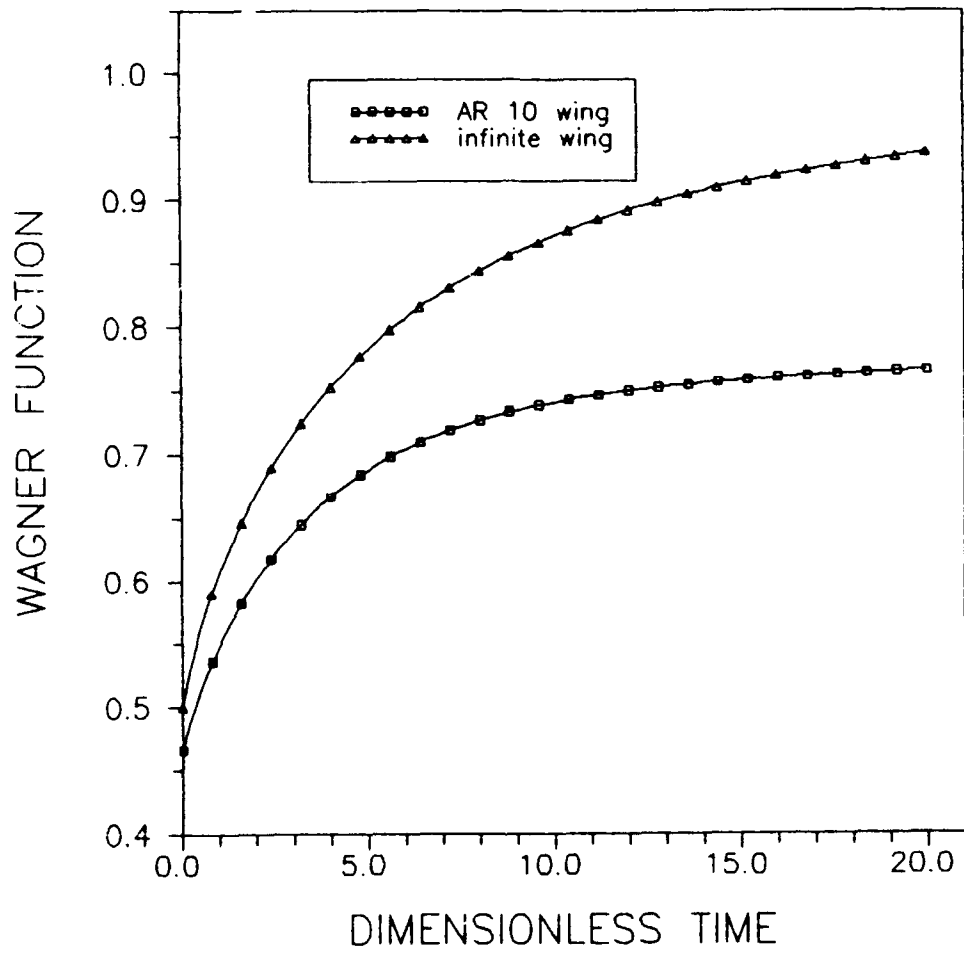
Figure 16: Time Domain Representation of Wagner Function

Time Dependent Lift in Terms of Wagner Function

The lift for a wing can be developed using the Wagner function quite easily. The lift per unit span for an airfoil was given in equation (53) for pure pitching motion. Generalizing this equation to include vertical translation as well and constructing the Laplace transform yields equation (73).

$$L(\vartheta) = \pi \rho b_0^2 \mathcal{L}[\ddot{h}(t) + V\dot{\alpha}(t)]$$

$$+ 2\pi \rho V b_0 \mathcal{L}\left[\dot{h}(t) + V\alpha + \frac{b_0}{2}\dot{\alpha}(t)\right] T(\bar{s}) \qquad (73)$$

Substituting the expression in equation (64) for $T(s)$ and taking the inverse Laplace transform produces equation (74).

$$L(t) = \pi \rho b_0^2 [\ddot{h}(t) + V\dot{\alpha}(t)]$$

$$+ 2\pi \rho V b_0 \left(T_0 - \frac{a}{b}\right)\left[\dot{h}(t) + V\dot{\alpha}(t) + \frac{b_0}{2}\dot{\alpha}(t)\right]$$

$$- 2\pi \rho b_0^2 g \int_0^t \frac{d}{d\tau}\left[\dot{h}(t-\tau) + V\dot{\alpha}(t-\tau) + \frac{b_0}{2}\dot{\alpha}(t-\tau)\right]d\tau \qquad (74)$$

$$+ \frac{2\pi \rho b_0^3}{V} f \int_0^t \frac{d^2}{d\tau^2}\left[\dot{h}(t-\tau) + V\dot{\alpha}(t-\tau) + \frac{b_0}{2}\dot{\alpha}(t-\tau)\right]d\tau$$

$$- 2\pi \rho V b_0 \int_0^t \left[\dot{h}(\tau) + V\dot{\alpha}(\tau) + \frac{b_0}{2}\dot{\alpha}(\tau)\right]\dot{E}_\mu\left[\frac{-1}{b}\left(\frac{V(t-\tau)}{b_0}\right)^\mu\right]d\tau$$

The dot over the Mittag-Leffler function implies the continuous portion of the derivative as the discontinuous portions are contained in the second term.

77

Küssner Function

A similar time-dependent lift function is the Küssner function which describes the lift created by a sharp-edged gust striking the leading edge of an airfoil. The Küssner function $\psi(t)$ is defined as (6:287)

$$\psi(t) = \mathcal{L}^{-1}\left\{ e^{-\beta}\left[(I_0(\beta) - I_1(\beta))T(\overline{s}) + I_1(\beta) \right] \right\} \qquad (75)$$

Taking the inverse transform of equation (75) yields the time domain representation of the Küssner function.

Hence, for rectangular geometry wings between aspect ratio two and ten, it is beneficial to utilize the equivalent Theodorsen function inserted into equations of motion developed for two-dimensional flow to compute aerodynamic loads and responses for three-dimensional flow conditions. With the development of the equivalent Theodorsen function for finite span wings, the three-dimensional unsteady aerodynamic analysis of response to arbitrary motion can be easily obtained, a task which was extremely difficult to accomplish with the methods described previously. The advantage of the equivalent Theodorsen function is that it permits the aerodynamic loads to be written in a mathematically compact form and convenient, closed form inverse Laplace transforms exist for the equivalent Theodorsen function, making its use quite attractive.

78

VIII. Conclusions

This thesis has investigated two alternative approaches to predicting the aerodynamic loads produced by time-dependent motions of thin wings in rectilinear subsonic flight. The first method was an attempt to directly integrate the pressure-downwash integral equation in three-dimensional unsteady aerodynamics. This method consisted of finding a model of the three-dimensional kernel function to capture the behavior in a more mathematically convenient form to facilitate the spatial convolution. The model was sought in a fractional calculus form to capture better the frequency dependent properties and to make the analytic continuation from the imaginary axis into the entire complex s-plane easier. It was found that the compressibility effects within the kernel function made the modelling at higher Mach numbers extremely difficult. The kernel function in incompressible flow was shown to be modelled by a simple four-parameter model throughout most of the domain of small aspect ratio airfoils; however, the small and large asymptotes of reduced frequency have not yet been verified. Initial investigations suggest this should be successful as well. Additionally, the determination of appropriate behavior for the model in the complex s-plane has not been verified yet either should be accomplished in the future. The four-parameter model began to worsen as the values of the spanwise variable were increased above those of aspect ratio one-half. The higher cases of aspect ratio need further investigation with different forms of fractional calculus models. The implementation of a

complex, nonlinear, least-squares regression algorithm with adaptive search methods would greatly enhance the capability of examining these models. The three-dimensional kernel function contains fractional calculus behavior and it is only a matter of time before a suitable model, mathematically simpler in form than the kernel function itself, will be found and successfully applied to the active control system design of aircraft.

The second approach taken to the prediction of unsteady aerodynamic loads on finite span rectangular airfoils was to develop an equivalent Theodorsen function. The equivalent Theodorsen can then be substituted into the two-dimensional air load equations and thus inserted into the equations of motion to capture three-dimensional induction effects. The equivalent Theodorsen function was constructed with a convenient fractional calculus form to facilitate the capturing of the frequency-dependent properties of the generalized aerodynamic forces. The coefficient of lift resulting from pure pitching motion was computed using a method presen 1 which collapses to the modified Doublet point method (27:348-355). The coefficient of lift was then used to calculate values of the equivalent Theodorsen function by utilizing two-dimensional generalized aerodynamic force equations. The values of the equivalent Theodorsen function were in turn modelled using the fractional calculus model. The fractional calculus model fully captured the behavior of the computed values of the equivalent Theodorsen function and coefficient of lift for rectangular wings with aspect ratios between two and ten. The equivalent Theodorsen function

80

was generalized into the complex s-plane and the Wagner function and the Küssner function, time-dependent response functions for indicial lift and sharp-edge gusts, were determined and compared to their two-dimensional counterparts. The success of capturing the properties of the coefficient of lift for pure pitching motion for rectangular airfoils suggests further investigation of other generalized aerodynamic forces caused by other types of downwash for more complex wing geometries. The important calculations in aeroelastic analysis are the determination of the airloads and the structural stiffness and damping matrices. The equivalent Theodorsen function allows the use of the more realistic three-dimensional aerodynamic loads, rather than the two-dimensional approximate loads, in control system designs. The development of the equivalent Theodorsen function for finite span airfoils permits the general response to be written in a mathematically tractable form. It also enables the active coupling between the automatic control system and aeroelastic phenomenon like flutter and unsteady structural loading which is not available presently in a practical form.

Bibliography

1. Albano, E. and Rodden, W. P., "A Doublet-Lattice Method for Calculating Lift Distributions on Oscillating Surfaces in Subsonic Flows," AIAA Journal, Vol 7, pp. 279-285, February 1969.

2. Ashley, H. and Boyd, W. N., "On Choosing the Best Approximations for Unsteady Potential Theory," presented to Colloquium on Unsteady Aerodynamics in honor of the 80th birthday of Prof. H. G. Küssner, September 24, 1980; Proceedings of Colloquium on Unsteady Aerodynamics, Institut für Aeroelastik, DFVLR, Göttingen, Germany, 1981, pp. 25-44.

3. Bagley, R. L., "A Theoretical Basis for the Application of Fractional Calculus to Viscoelasticity," Journal of Rhealogy, Vol. 27, pp. 201-210, 1983.

4. Bagley, R. L., Swinney, D. V. and Griffin, K. E., "Fractional Calculus-A New Approach to Modeling Unsteady Aerodynamic Forces," AIAA Paper No. 91-0748, 29th Aerospace Sciences Meeting, Reno, Nevada, 7-10 January, 1991, pp. 1-30.

5. Bagley, R. L. and Torvik, P. J., "Fractional ,Calculus - A Different Approach to the Analysis of Viscoelastically Damped Structures," AIAA Journal, Vol. 21, May 1983, pp. 741-748.

6. Bisplinghoff, R. L., Ashley, H., and Halfman, R. L., Aeroelasticity, Addison-Wesley Publishing Company, Inc, Cambridge, MA 1955.

7. Graham, J. M. R., "A Lifting-Surface Theory for the Rectangular Wing in Non-Stationary Flow," The Aeronautical Quarterly, Vol. 12, February 1971, pp. 83-100.

8. Handbook of Mathematical Functions, edited by M. Abramowitz and I. A. Stegun, Dover Publications, Inc, New York, 1972.

9. IMSL Math/Library: Fortran Subroutines for Mathematical Applications, Version 1.0, IMSL Inc., April 1987.

10. IMSL Statistical/Library: Fortran Subroutines for Statistical Applications, Version 1.1, IMSL Inc., 1989.

11. Jones, R. T., "The Unsteady Lift of a Wing of Finite Aspect Ratio," NACA Report 681, June 1939.

12. Jordan, P. F., "Reliable Lifting Surface Solutions for Unsteady Flow," Journal of Aircraft, Vol. 15, pp. 626-633, September 1978.

13. Landahl, M. T., "Kernel Function for Non-Planar Oscillating Surfaces in Subsonic Flow," AIAA Journal, Vol. 5, May 1967, pp. 1045-1046.

14. Landahl, M. T. and Stark, J. E., "Numerical Lifting Surface Theory -Problems and Progress," AIAA Journal, Vol. 6, pp. 2049-2060, November 1968.

15. Lawrence, H. R. and Gerber, E. H., "The Aerodynamic Forces on Low Aspect Ratio Wings Oscillating in an Incompressible Flow," Journal of Aeronautical Sciences, Vol. 19, pp. 769-781, November 1952 (errata issued Vol. 20, p. 296, April 1953).

16. Küssner, H. G., "General Airfoil Theory," NACA Technical Memorandum 979, 1940. (translated from the original "Allgemeine Tragflächentheorie," Luftfahrtforschung, Vol. 17, no. 11/12, December 10, 1940, pp. 370-378.)

17. Mittag-Leffler, G., "Sur La Représentation Analytique D'une Branch Uniforme D'une Function Monagine," Acta Mathematica, Vol. 29, 1905, pp. 101-182.

18. Marquardt, D., "An Algorithm for Least-Squares Estimation of Non-Linear Parameters," SIAM Journal on Applied Mathematics, Vol. 11, 1963, pp. 431-441.

19. Murrow, H. N., Kermit, G. P., and Drischler, J. A., "Numerical Technique to Lifting-Surface Theory for Calculation of Unsteady Aerodynamic Forces Due to Continuous Sinusoidal Gusts on Several Wing Planforms," NASA Technical Note D-1501, August 1962.

20. "Vortex-Lattice Utilization," NASA SP-405, 1976.

21. Reissner, E., "Effect of Finite Span on the Airload Distributions for Oscillating Wings I - Aerodynamic Theory of Oscillating Wings of Finite Span," NACA Technical Note 1194, March 1947.

22. Reissner, E., "Effect of Finite Span on the Airload Distributions for Oscillating Wings II - Aerodynamic Theory of Oscillating Wings of Finite Span," NACA Technical Note 1195, October 1947.

23. Ross, B., "Fractional Calculus," Mathematics Magazine, Vol. 50, pp. 115-122, May 1977.

24. Swinney, D. V., A Fractional Calculus Model of Aeroelasticity, Master's Thesis, AFIT/GA/ENY/89D-5, Air Force Institute of Technology, OH, 1989.

25. Theodorsen, T., "General Theory of Aerodynamic Instability and the Mechanism of Flutter," NACA Report 496, 1934, pp. 413-433.

26. Ueda, T., "Asymptotic Expansion of the Kernel Function in Subsonic Unsteady Lifting Surface Theory," Journal of Japan Society of Aero/Space Sciences, Vol. 29, pp. 169-174, 1981.

27. Ueda, T. and Dowell, E. H., "A New Solution Method for Lifting Surfaces in Subsonic Flow," AIAA Journal, Vol. 20, pp. 348-355, March 1982.

28. Ueda, T., "Expansion Series of Integral Functions Occurring in Unsteady Aerodynamics," Journal of Aircraft, Vol. 19, pp. 345-347, 1982.

29. Van Nierkerk, B., "Computation of Second-Order Accurate Unsteady Aerodynamic Generalized Forces," AIAA Journal, Vol. 24, pp. 492-498, March 1986.

30. Van Nierkerk, B., "Integration of Singular Functions Associated with Lifting Surface Theory," AIAA Journal, Vol. 24, pp. 1194-1196, July 1986.

31. Watkins, C. E., Runyan, H. L. and Woolston, D. S., "On the Kernel Function of the Integral Equation Relating the Lift and Downwash Distributions of Oscillating Finite Wings in Subsonic Flow," NACA Report 1234, 1955, pp. 703-718.

32. Watkins, C. E., Woolston, D. S. and Cunningham, H. J., "A Systematic Kernel Function Procedure for Determining Aerodynamic Forces on Oscillating or Steady Finite Wings at Subsonic Speeds," NASA Technical Report R-48, June 1959, pp. 1-21.

33. Watson, G. N., A Treatise on the Theory of Bessel Functions, Second Ed., The Macmillan Co., 1944.

34. Widmayer, E., Clevenson, S. A., and Leadbetter, S. A., "Some Measurements of Aerodynamic Forces and Moments at Subsonic Speeds on a Rectangular Wing of Aspect Ratio 2 Oscillating About the Midchord," NACA Technical Note 4240, June 1953.

Appendix A: Additional Model and Modified Kernel Function Comparisons for Mach Number 0.5

Model results for the M=0.5 case based on equation (26) are further presented in this appendix. The original discussion was presented in Chapter IV, compressible flow subsection.

The model used to produce the fit in Figure 17 is

$$K^*[0.5, k, 0.1, 0.05] = K_0^* - \frac{\theta_1 (ik)^{\theta_2}}{1 + \theta_3 (ik)^{\theta_4}} - \frac{\theta_5 (ik)^{\theta_6}}{1 + \theta_7 (ik)^{\theta_8}} \quad (76)$$

where

$K_0^* = 1.9991$
$\theta_1 = 0.534$ $\theta_2 = 0.523$
$\theta_3 = 0.116$ $\theta_4 = 1.62$
$\theta_5 = 1.24$ $\theta_6 = 0.902$
$\theta_7 = 0.331$ $\theta_8 = 1.34$

The error is 2.2×10^{-1} and 2.2×10^{-2} for the real and imaginary parts.
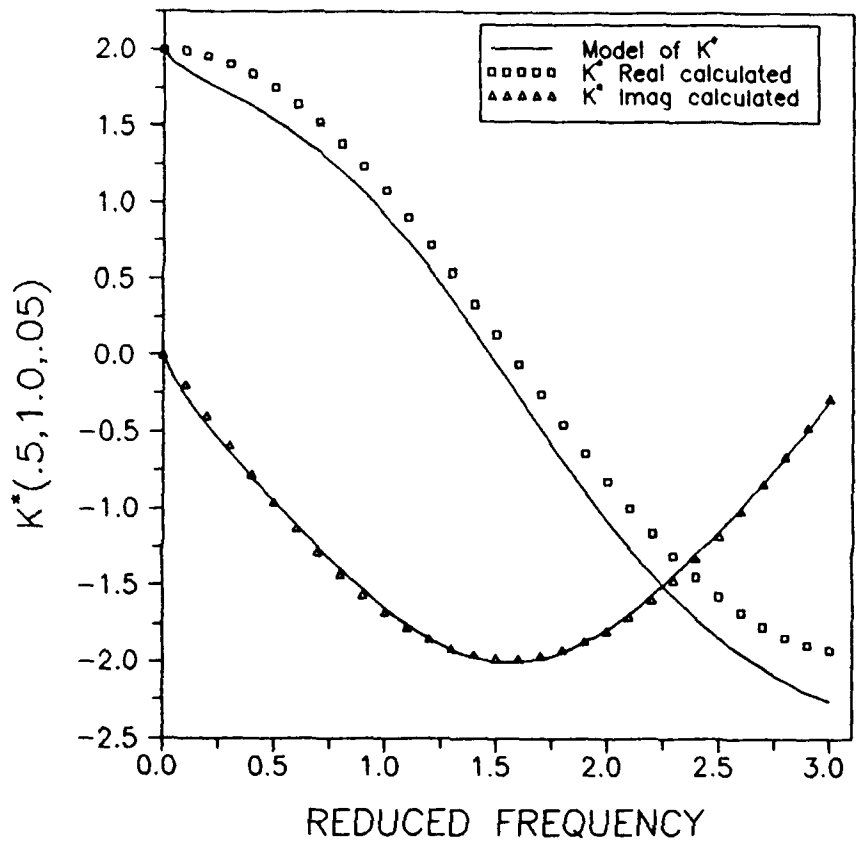
Figure 17: Model of K'[0.5,1.0,0.05]
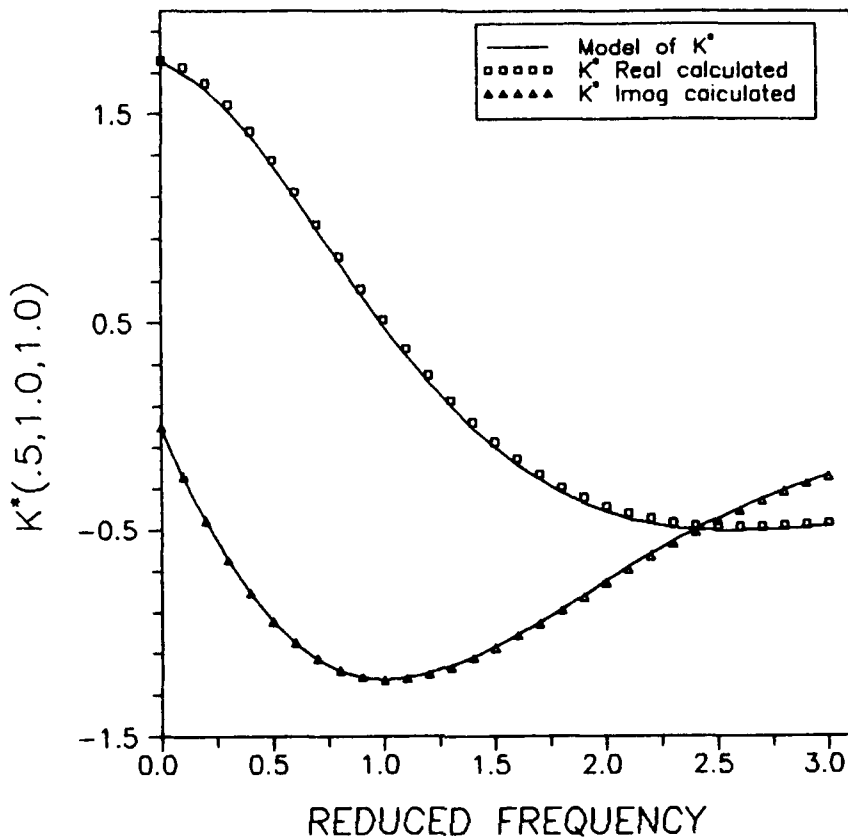
Figure 18: Model of K^*[0.5,1.0,1.0]

The model for this particular case in Figure 18 is given by

$$K^*[0.5, k, 0.1, 0.05] = K_0^* - \frac{\theta_1 (ik)^{\theta_2}}{1 + \theta_3 (ik)^{\theta_4}} - \frac{\theta_5 (ik)^{\theta_6}}{1 + \theta_7 (ik)^{\theta_8}} \quad (77)$$

where

$K_0^* = 1.7559$
$\theta_1 = 0.205$ $\theta_2 = 0.600$
$\theta_3 = 0.302$ $\theta_4 = 1.43$
$\theta_5 = 1.87$ $\theta_6 = 0.954$
$\theta_7 = 0.808$ $\theta_8 = 1.06$

Errors are 2.4×10^{-2} and 7.9×10^{-3} for the real and imaginary parts.

87

Appendix B: Additional Model and Modified Kernel Function Comparisons for Incompressible Flow Conditions

Additional samples of the modified kernel function models for other regions in incompressible flow are presented in this appendix. The original discussion is contained in the incompressible subsection of Chapter IV. The form of model was given in equation (30). The model used for Figure 19 is

$$K^*[k, -0.1, 0.5] = K_0^* - \frac{\theta_1 (ik)^{\theta_2}}{1 + \theta_3 (ik)^{\theta_4}} \tag{78}$$

where

$K_0^* = 0.804$
$\theta_1 = 0.353$ $\qquad\qquad \theta_2 = 0.93$
$\theta_3 = 0.447$ $\qquad\qquad \theta_4 = 0.876$

producing errors of 2.3×10^{-3} and 1.8×10^{-3} respectively.
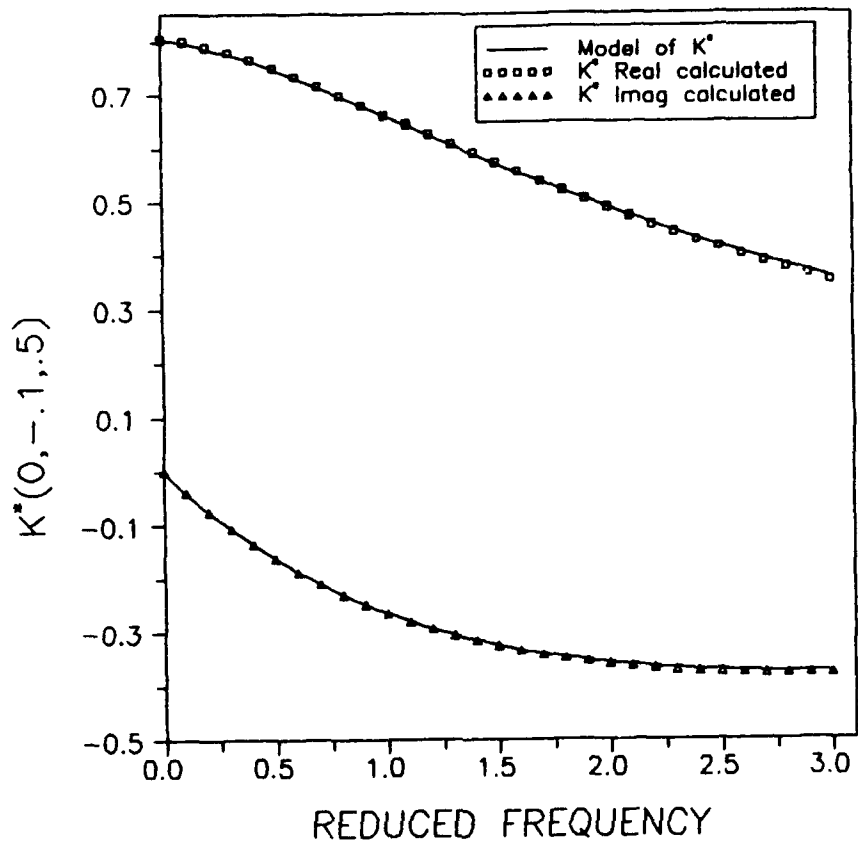
Figure 19: Model of $K^*[0,-0.1,0.5]$

89
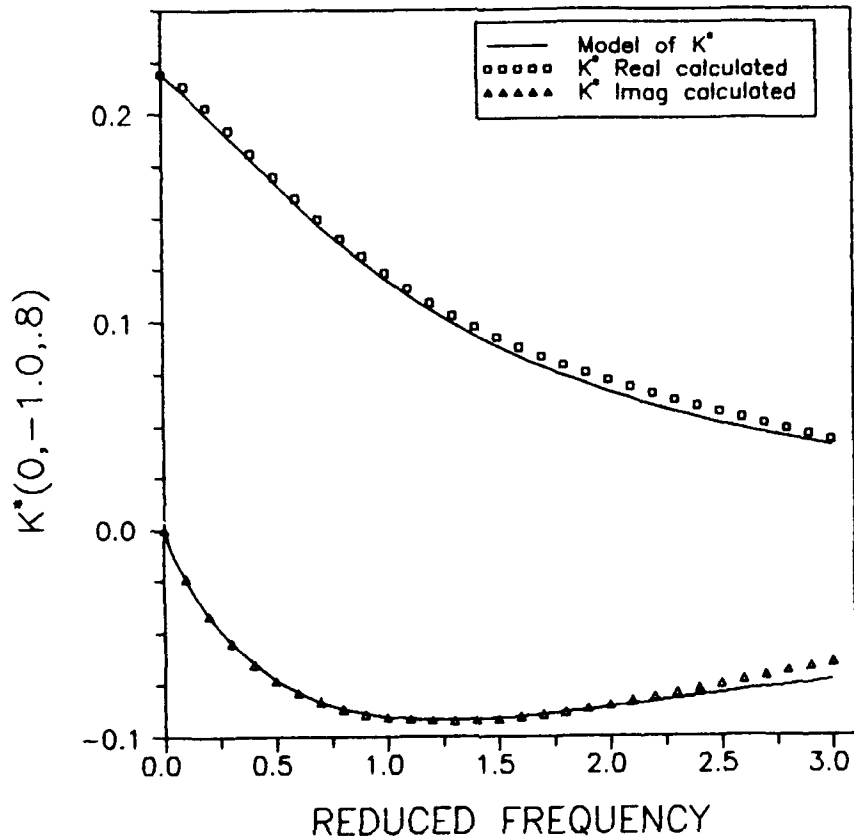
Figure 20: Model of $K^{*}[C,-1.0,0.8]$

The model used to produce Figure 20 is

$$K^{*}[k,-0.1,0.5] = K_{0}^{*} - \frac{\theta_{1}(ik)^{\theta_{2}}}{1 + \theta_{3}(ik)^{\theta_{4}}} \tag{79}$$

where

$K_{0}^{*}=0.219$

$\theta_{1}=0.188$ $\theta_{2}=0.841$

$\theta_{3}=0.791$ $\theta_{4}=0.854$

with errors of 3.8×10^{-3} and 1.7×10^{-3}.

90

Appendix C: Model Parameters for Incompressible Case

Additional figures describing the variation of the different parameters θ_1 through θ_4 of the model for the modified kernel function in incompressible flow is further presented in this appendix. Other figures were presented along with the initial discussion in Chapter IV. The four-parameter model is given in equation (30).
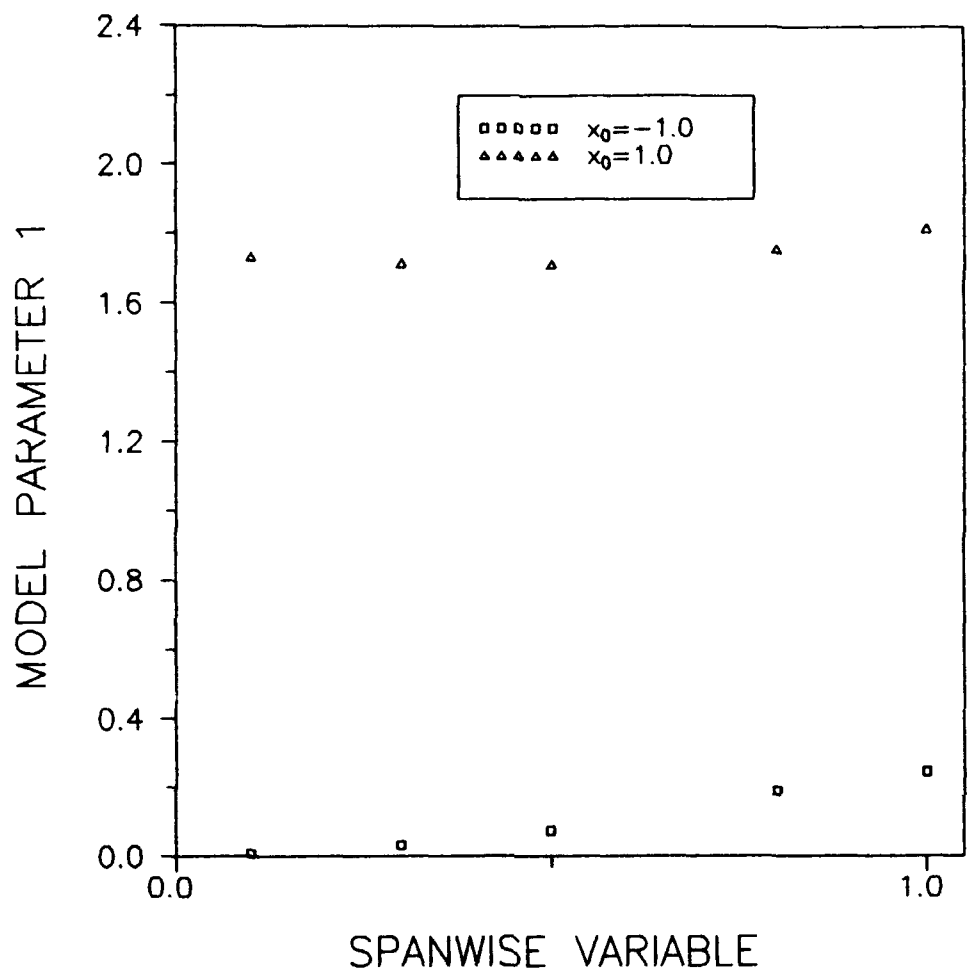
Figure 21: Parameter 1 Dependence on sy_0
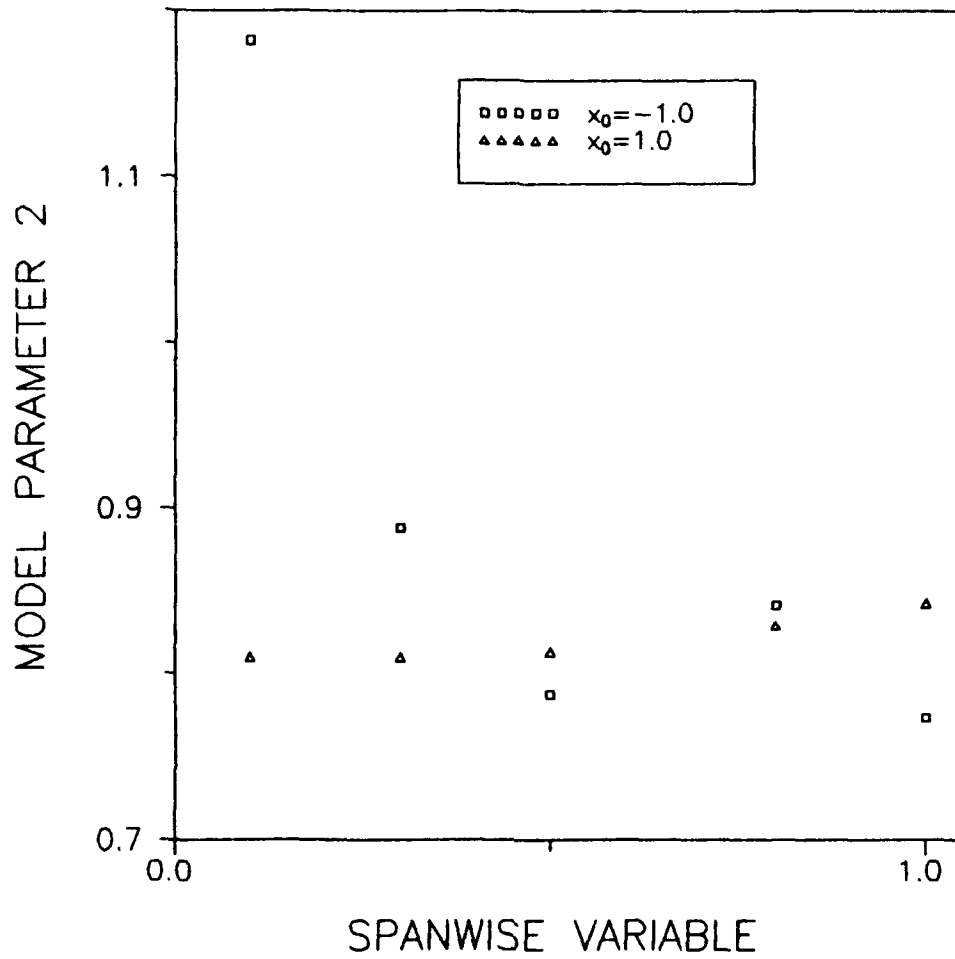
Figure 22: Parameter 2 Dependence on sy_0
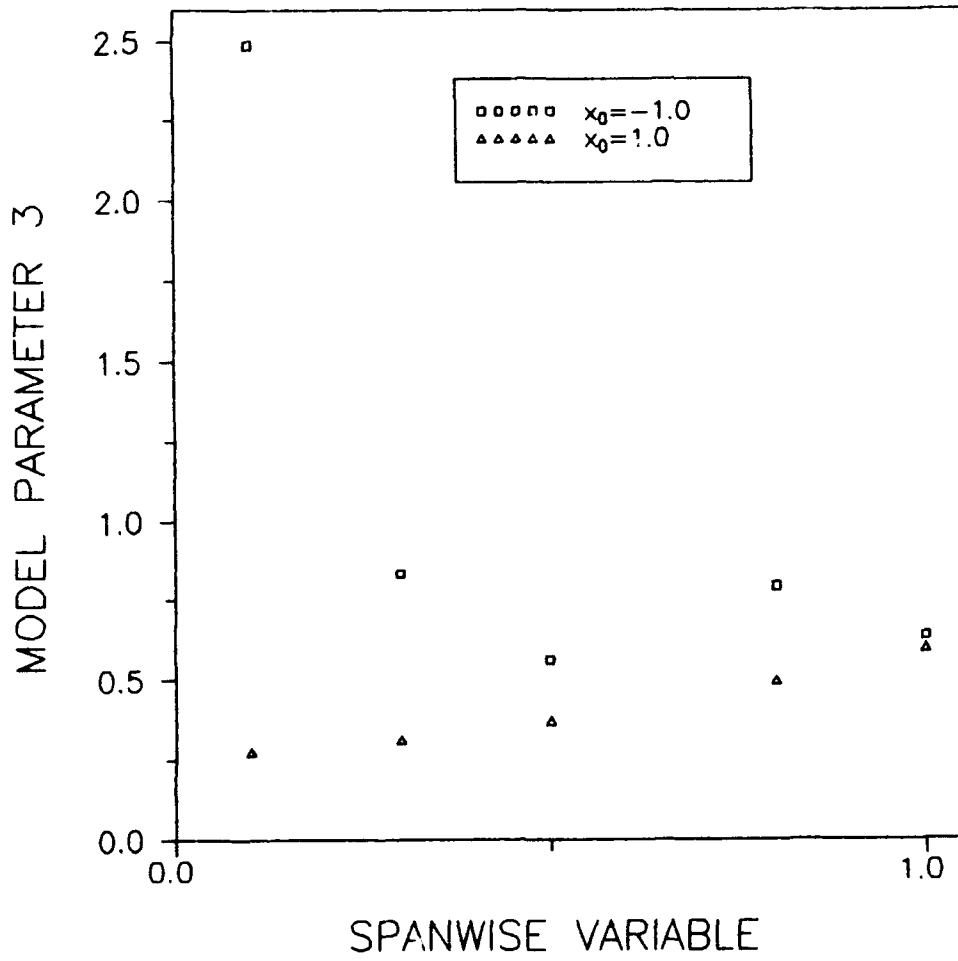
Figure 23: Parameter 3 Dependence on sy₀

.
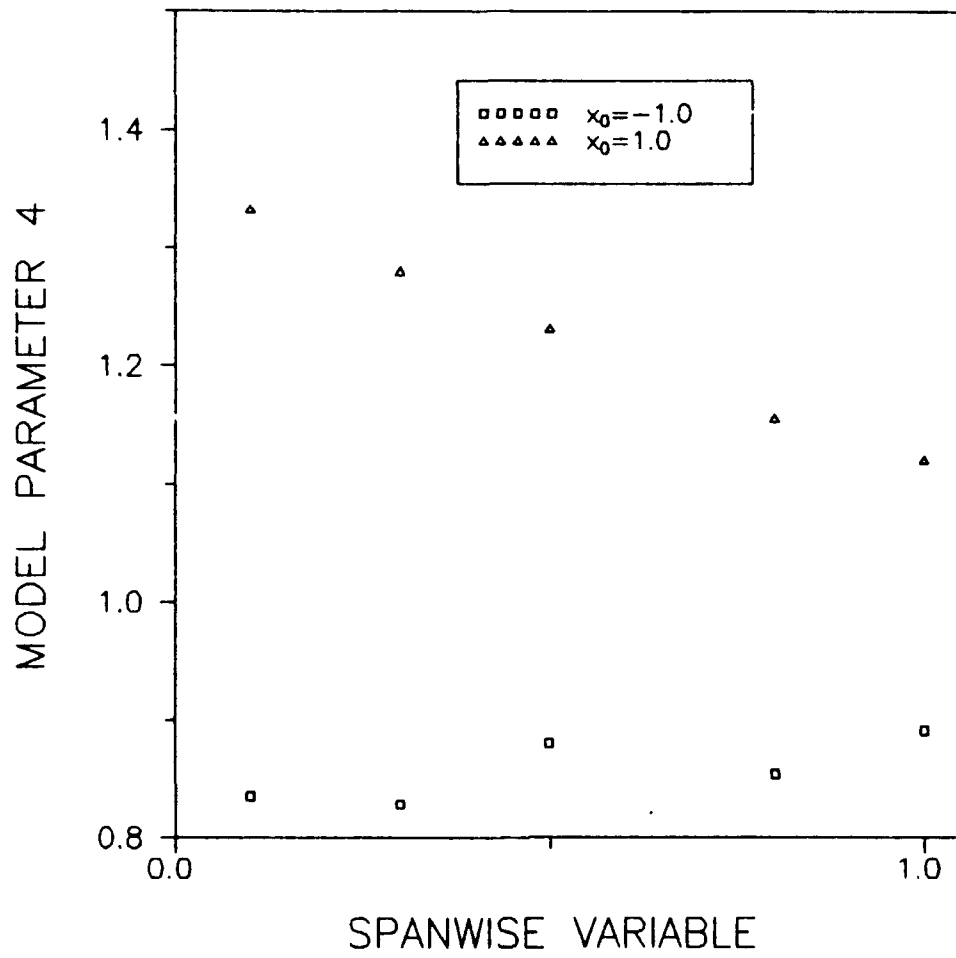
Figure 24: Parameter 4 Dependence on sy_0
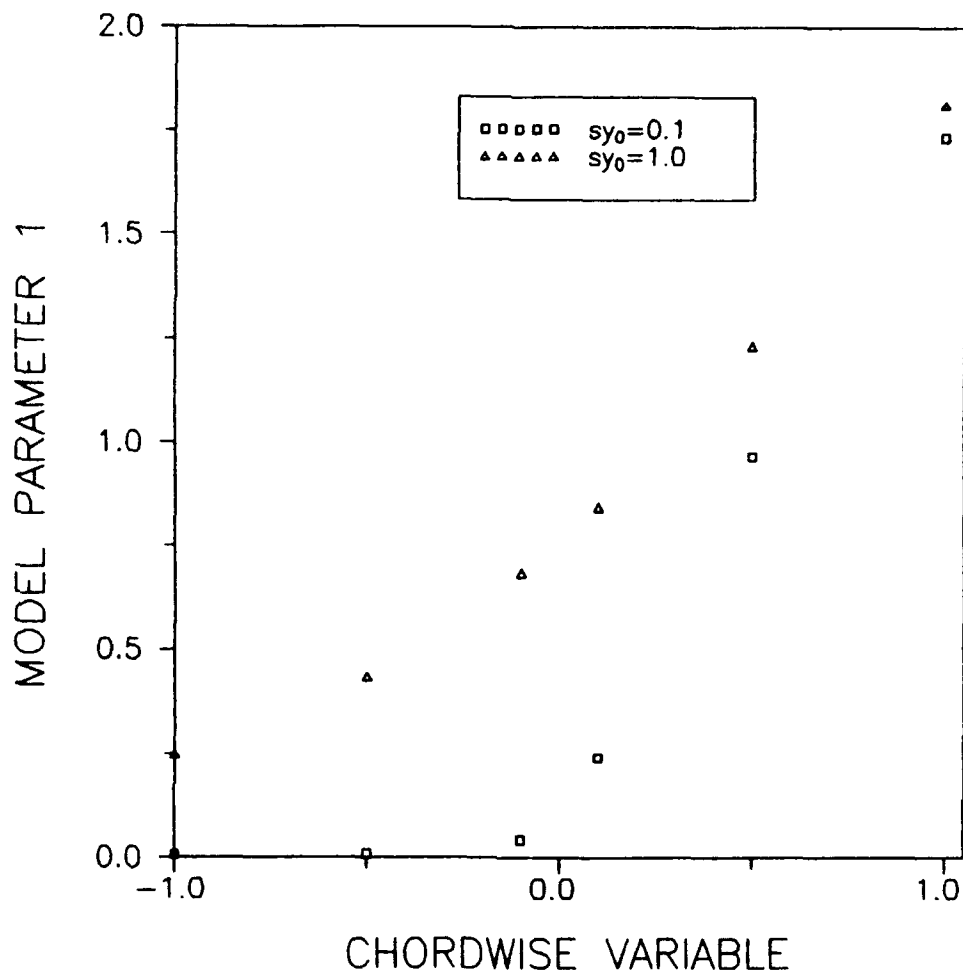
Figure 25: Parameter 1 Dependence on x_0
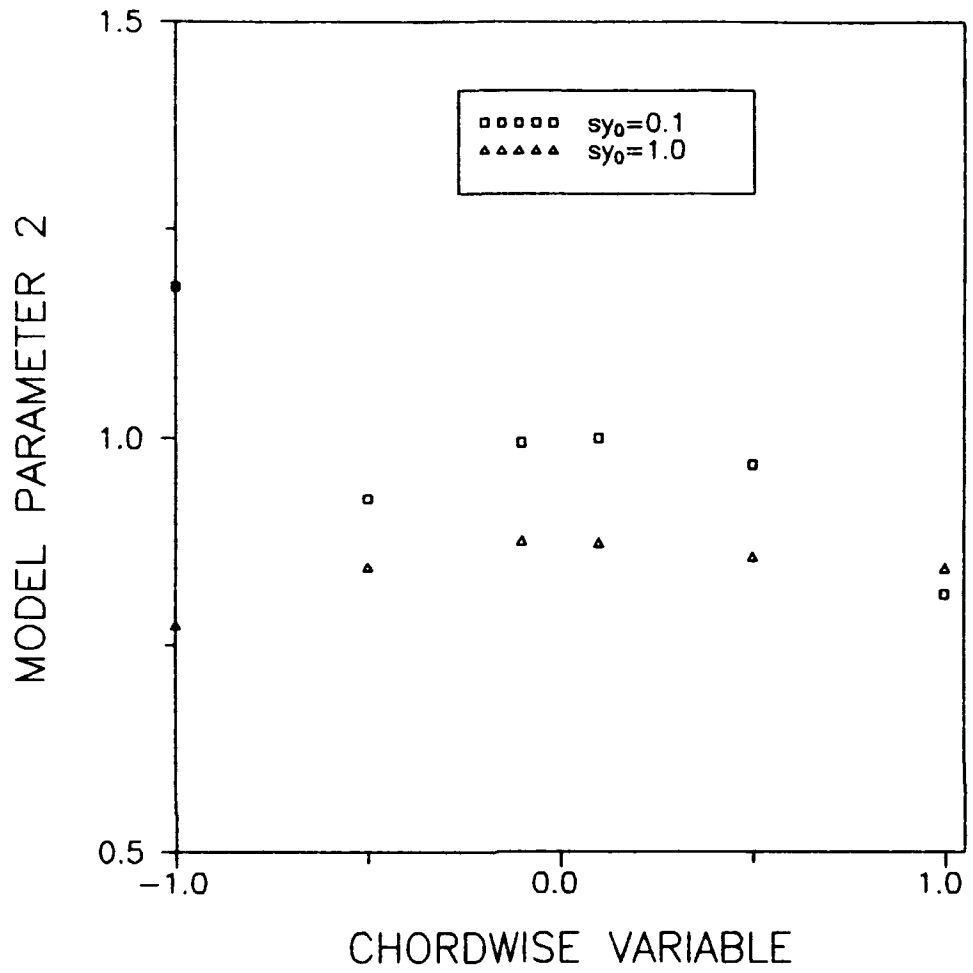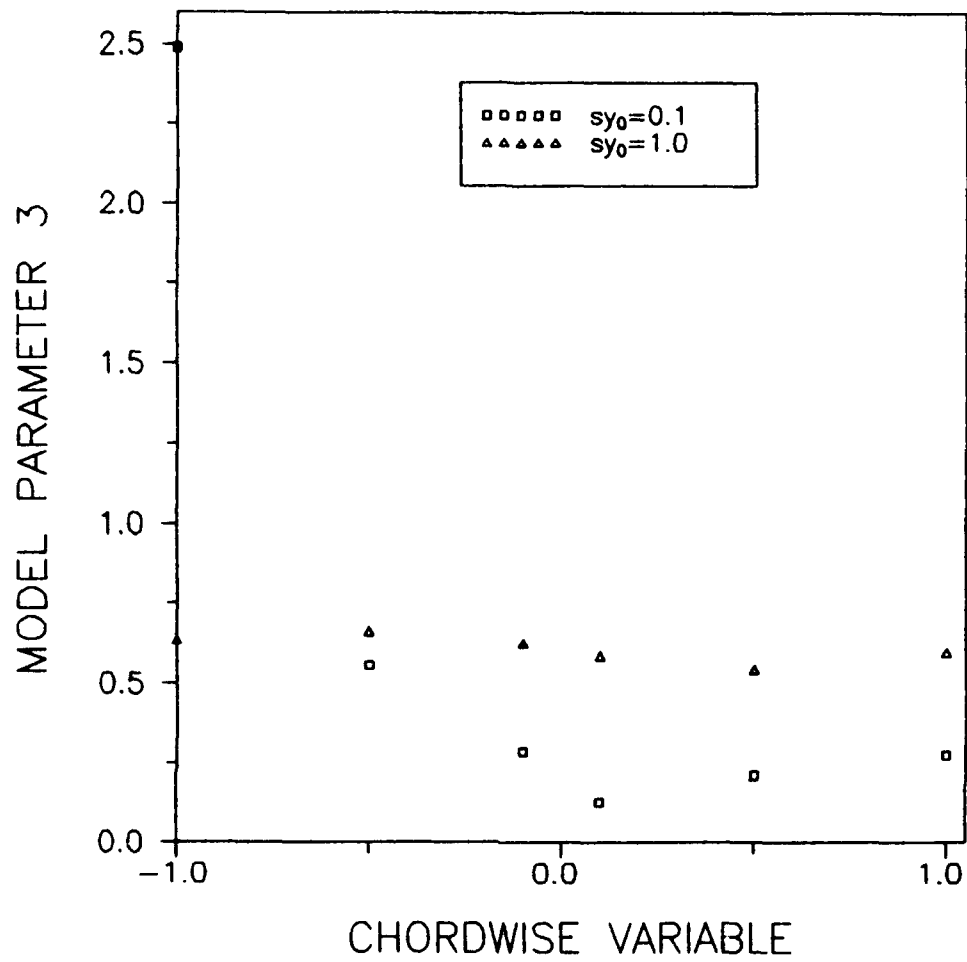
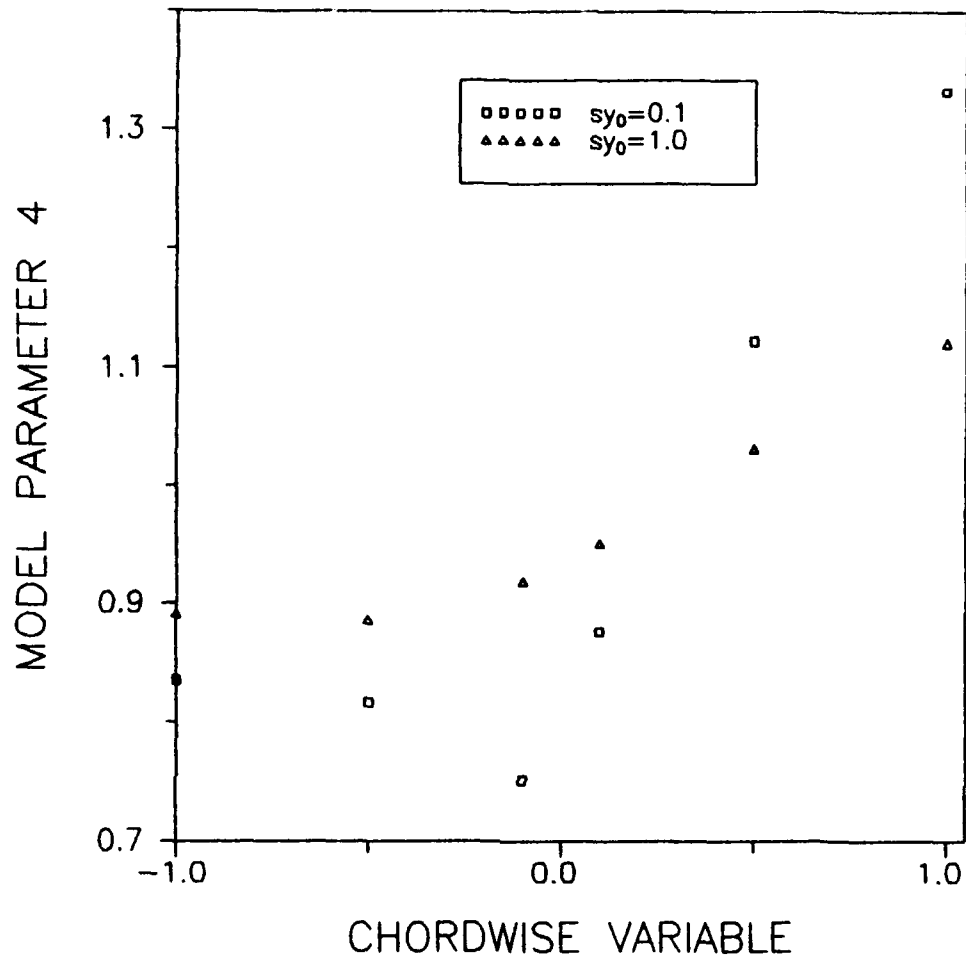Figure 26: Parameter 2 Dependence on x_0

Figure 27: Parameter 3 Dependence on x_0

Figure 28: Parameter 4 Dependence on x_0

Appendix D: Lift Coefficient Model at Various Aspect Ratios

The coefficients of lift for rectangular wings of various aspect ratios between two and ten are shown modelled in this appendix. The initial discussion and development of these models is presented in Chapter VI. The general form of the fractional calculus model is

$$C_{L_\alpha} = \pi \left\{ ik + 2 T(k) \left[1 + \frac{ik}{2} \right] \right\} \tag{80}$$

where the equivalent Theodorsen function $T(k)$ is defined as follows.

$$T(ik) = T_0 + \frac{a(ik)^\mu}{1 + b(ik)^\mu} - g(ik) + f(ik)^2 \tag{81}$$

This appendix will present a series of different figures showing the superb agreement between the model and the calculated lift coefficients for various aspect ratios. Each figure on the following pages will be accompanied with an equation showing the model of $T(k)$ used to produce the fit. The error associated with each plot is not explicitly stated. However, the error on the real parts was of the order of 10^{-3} and the error on the imaginary part of the order of 10^{-4} for all the cases shown.
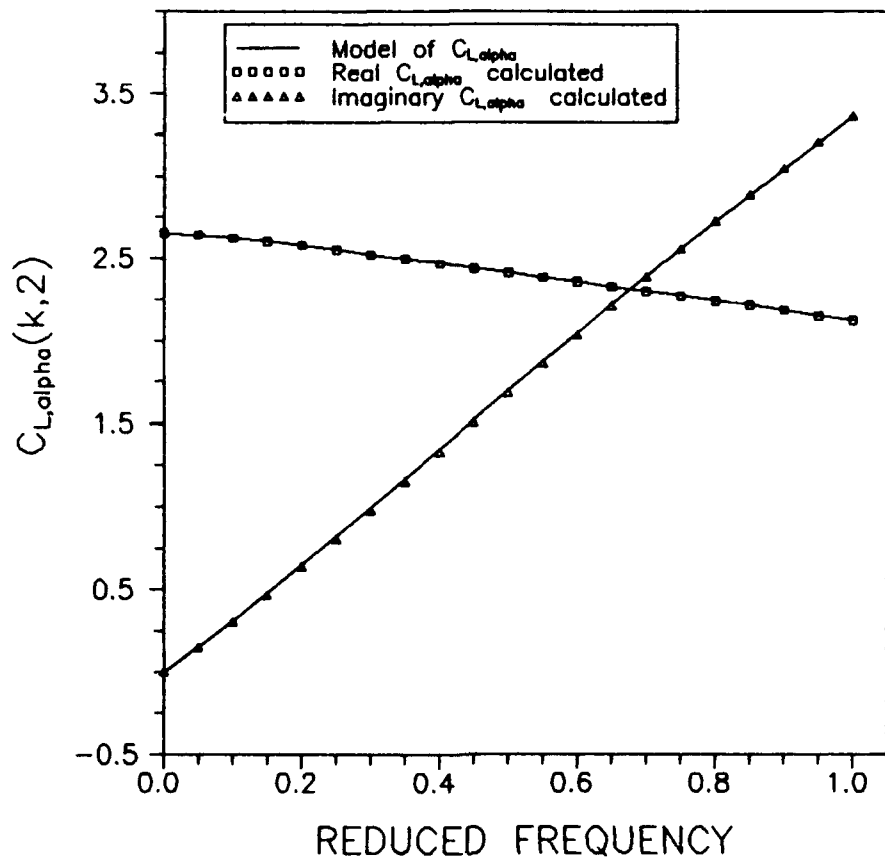
Figure 29: C_{L_α} for Wing of Aspect Ratio 2

$$C_{L_\alpha} = \pi \left\{ ik + 2T(k)\left[1 + \frac{ik}{2}\right] \right\} \qquad (82)$$

$$T(ik) = T_0 + \frac{a(ik)^\mu}{1 + b(ik)^\mu} - g(ik) + f(ik)^2 \qquad (83)$$

where

$T_0 = 0.422$
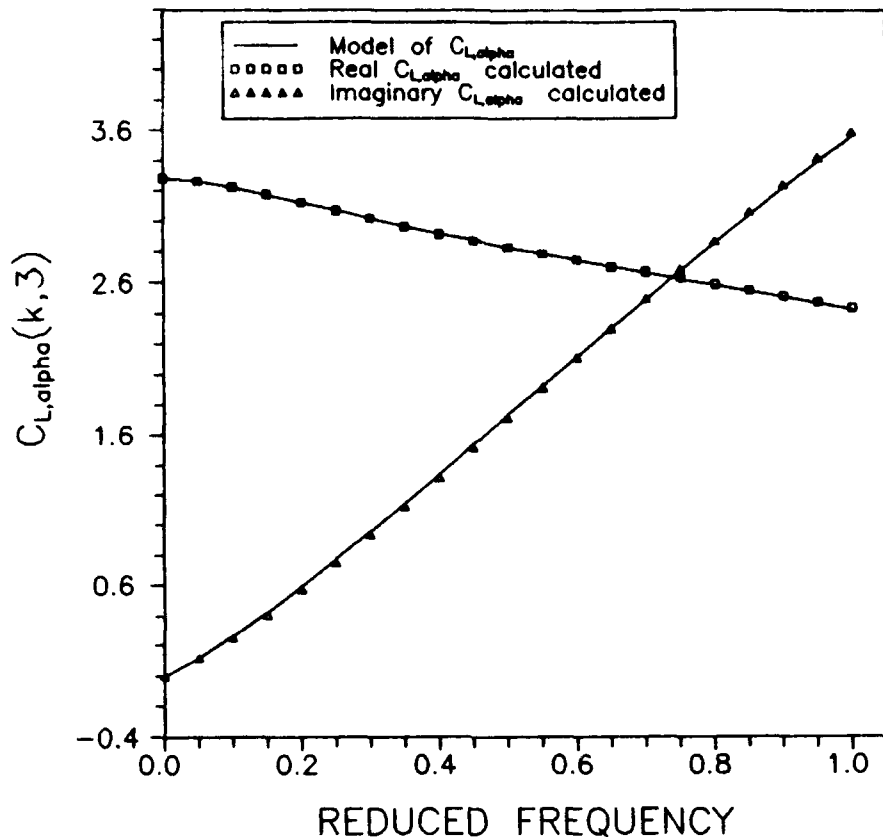$a = 0.144$ $\mu = 0.92$
$b = 1.58$ $f = 0.075$
$g = 0.068$

Figure 30: $C_{l,\alpha}$ for Wing of Aspect Ratio 3

$$C_{L_\alpha} = \pi\left\{ik + 2T(k)\left[1 + \frac{ik}{2}\right]\right\} \tag{84}$$

$$T(ik) = T_0 + \frac{a(ik)^\mu}{1 + b(ik)^\mu} - g(ik) + f(ik)^2 \tag{85}$$

where

$T_0=0.523$
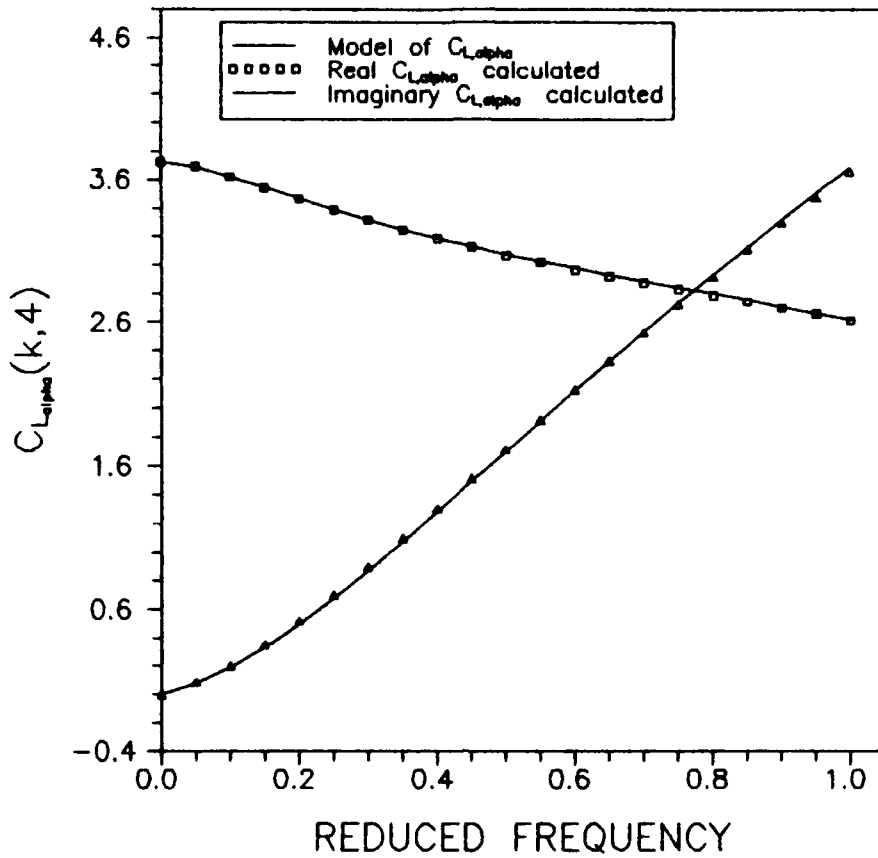$a=0.286$ $\mu=0.923$
$b=2.053$ $f=0.078$
$g=0.047$

102

Figure 31: $C_{L,\alpha}$ for Wing of Aspect Ratio 4

$$C_{L_\alpha} = \pi \left\{ ik + 2T(k)\left[1 + \frac{ik}{2}\right]\right\} \tag{86}$$

$$T(ik) = T_0 + \frac{a(ik)^\mu}{1 + b(ik)^\mu} - g(ik) + f(ik)^2 \tag{87}$$

where

$T_0 = 0.593$
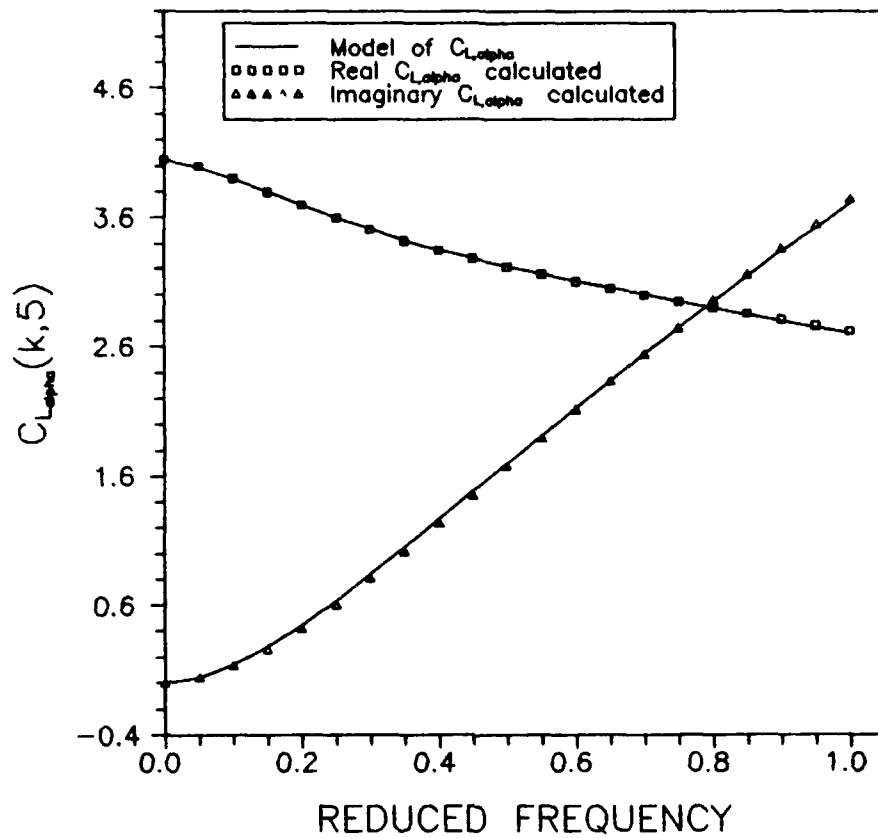$a = 0.433$ $\mu = 0.927$
$b = 2.49$ $f = 0.0804$
$g = 0.042$

103

Figure 32: C_{L_α} for Wing of Aspect Ratio 5

$$C_{L_\alpha} = \pi \left\{ ik + 2T(k)\left[1 + \frac{ik}{2}\right] \right\}$$ (88)

$$T(ik) = T_0 + \frac{a(ik)^\mu}{1 + b(ik)^\mu} - g(ik) + f(ik)^2$$ (89)

where

T_0=0.644
a=0.568   μ=0.926
b=2.69   f=0.0821
g=0.032

104

Figure 33: $C_{L,\ell}$ for Wing of Aspect Ratio 6

$$C_{L_\alpha} = \pi \left\{ ik + 2T(k)\left[1 + \frac{ik}{2}\right]\right\} \tag{90}$$

$$T(ik) = T_0 + \frac{a(ik)^\mu}{1 + b(ik)^\mu} - g(ik) + f(ik)^2 \tag{91}$$

where

$T_0 = 0.684$
$a = 0.688$ $\mu = 0.9167$
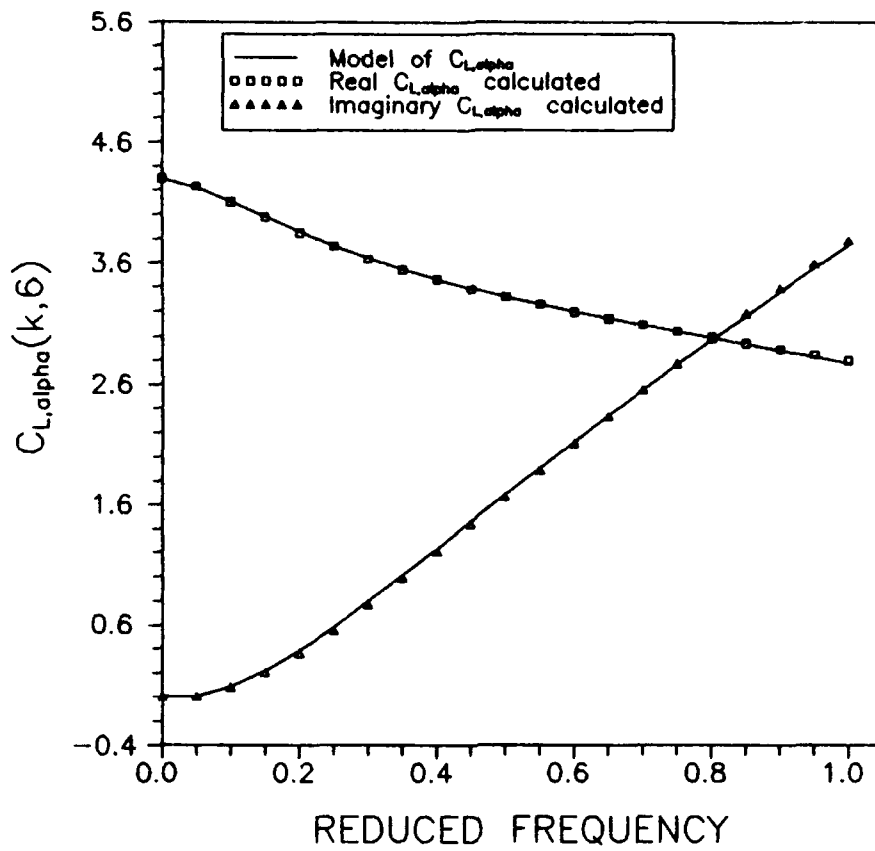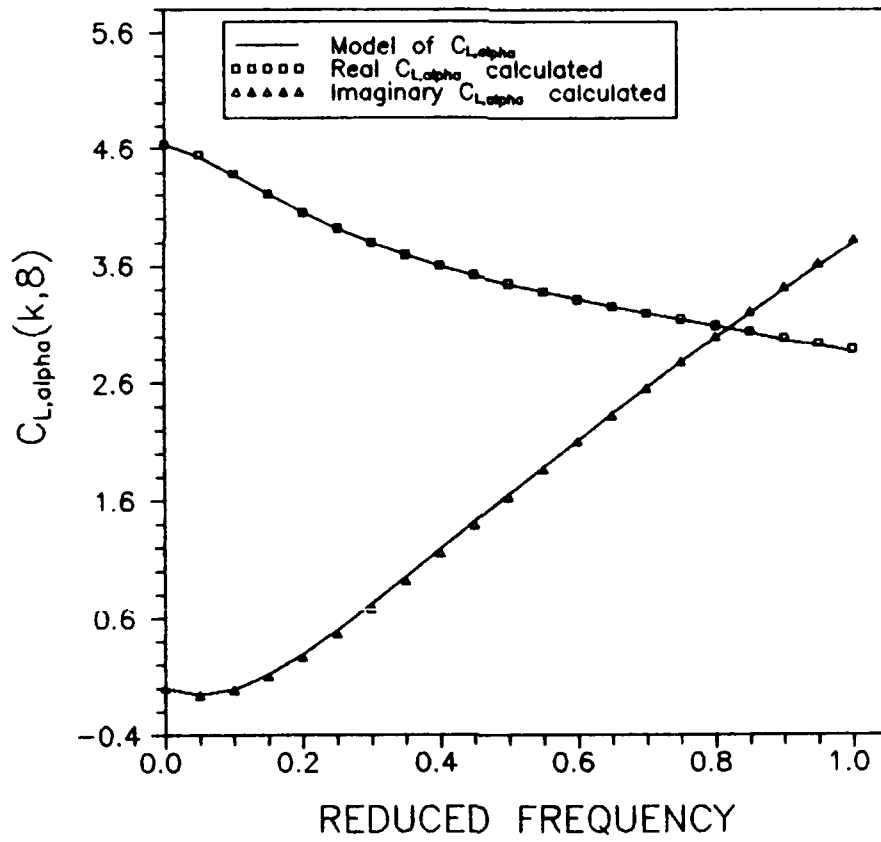$b = 2.85$ $f = 0.0823$
$g = 0.026$

Figure 34: $C_{L,\alpha}$ for Wing of Aspect Ratio 8

$$C_{L_\alpha} = \pi \left\{ ik + 2T(k)\left[1 + \frac{ik}{2}\right] \right\} \qquad (92)$$

$$T(ik) = T_0 + \frac{a(ik)^\mu}{1 + b(ik)^\mu} - g(ik) + f(ik)^2 \qquad (93)$$

where

$T_0=0.739$
$a=0.884$ $\mu=0.911$
$b=3.144$ $f=0.0843$
$g=0.021$
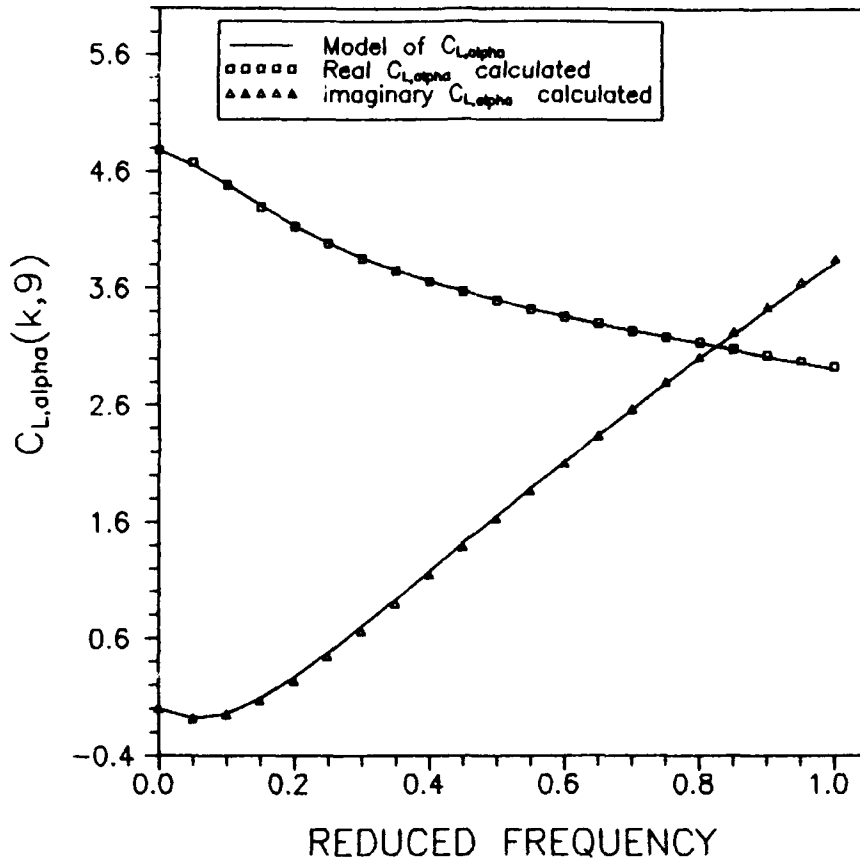
Figure 35: C_{L_α} for Wing of Aspect Ratio 9

$$C_{L_\alpha} = \pi \left\{ ik + 2T(k)\left[1 + \frac{ik}{2} \right] \right\} \tag{94}$$

$$T(ik) = T_0 + \frac{a(ik)^\mu}{1 + b(ik)^\mu} - g(ik) + f(ik)^2 \tag{95}$$

where

$T_0 = 0.7606$
$a = 0.964$ $\mu = 0.907$
$b = 3.24$ $f = 0.0847$
$g = 0.0185$

107

The variation of the parameters of the fractional calculus model
of the coefficient of lift are presented in this appendix. The
parameters and the model are given in equation (61).
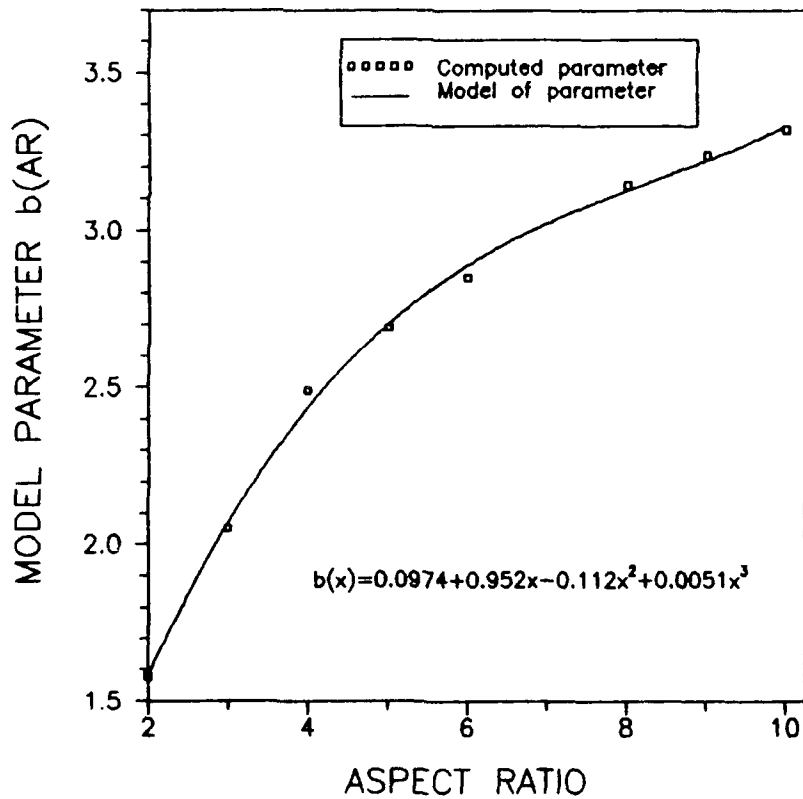
Figure 36: Parameter b vs. Aspect Ratio

Figure 37: Parameter T_0 vs. Aspect Ratio

$$T_0(x) = 0.149 + 0.169x - 0.0173x^2 + 0.00067x^3$$

$$g(x)=0.114-0.0302x+0.0034x^2+0.00014x^3$$

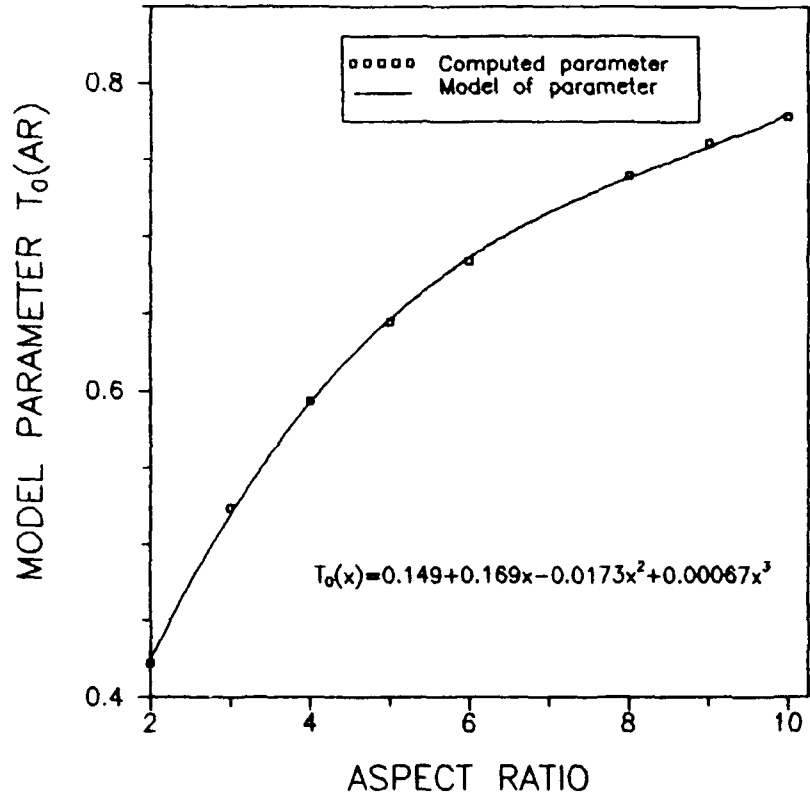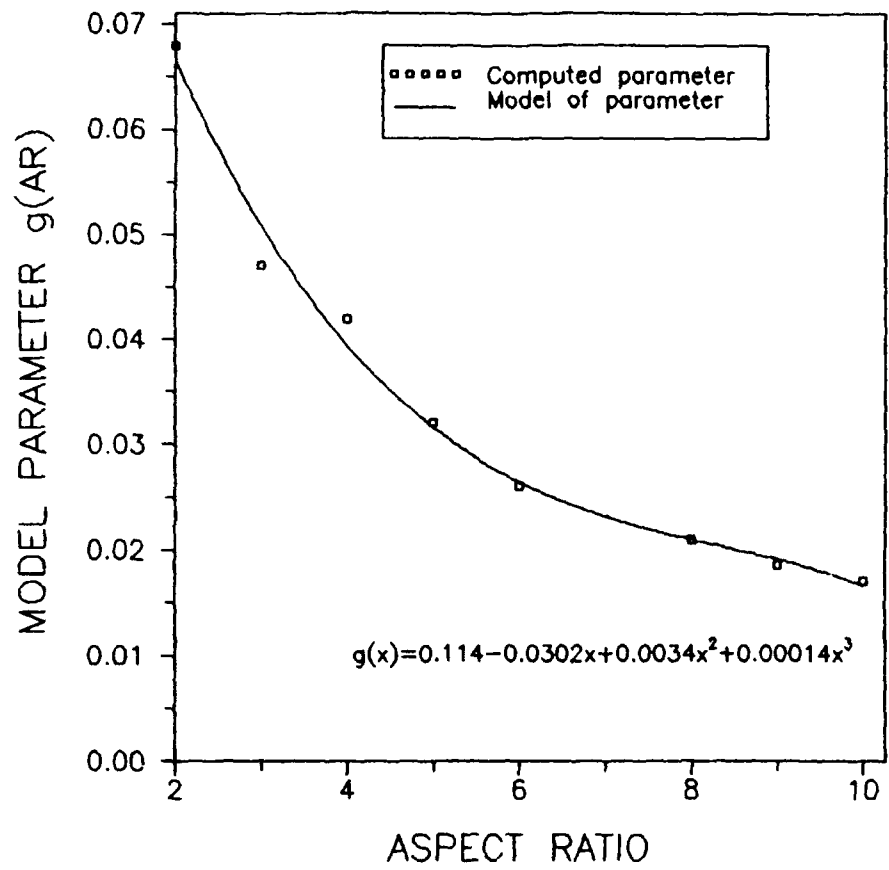**Figure 38: Parameter g vs. Aspect Ratio**
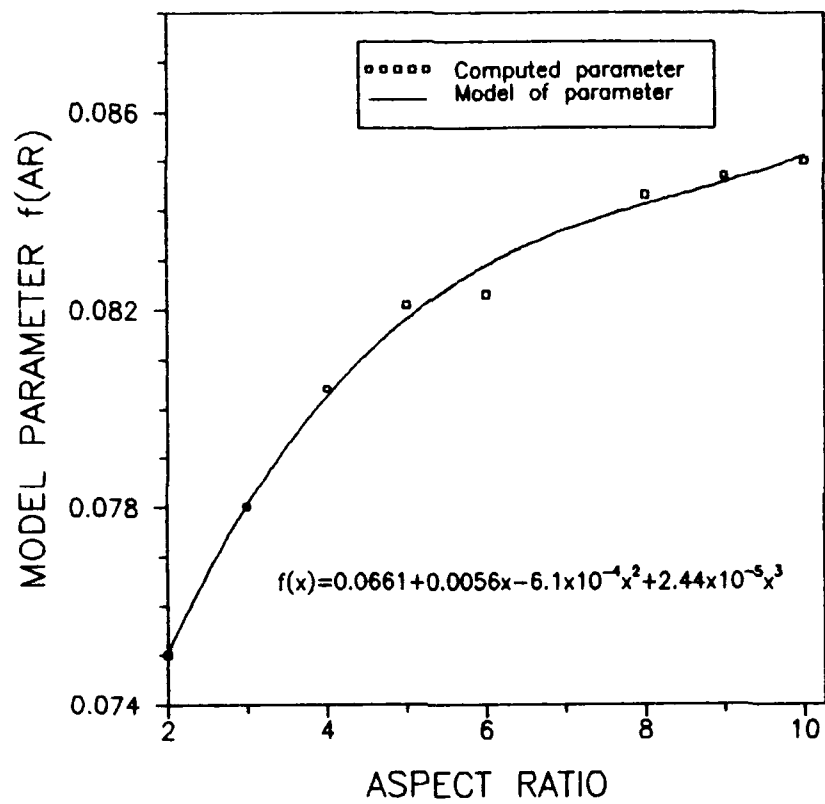
Figure 39: Parameter f vs. Aspect Ratio

The plot shows MODEL PARAMETER f(AR) on the vertical axis (ranging from 0.074 to 0.086) versus ASPECT RATIO on the horizontal axis (ranging from 2 to 10).

Legend:
- Computed parameter
- Model of parameter

$$f(x)=0.0661+0.0056x-6.1\times10^{-4}x^2+2.44\times10^{-5}x^3$$

111

Appendix F: Derivation of the Pressure-Downwash
Integral Equation
Based Upon References 32 and 16

The wing is considered a nearly plane impenetrable surface S consistent with the concepts of linear theory. Let the wing lie nearly in the x-y plane and let it and the x-y-z coordinate system to which it is referred be assumed to move with uniform velocity V in the negative x-direction. Note the positive z-direction is defined opposite to that in Chapter 2. At the same time, let each point of the wing be assumed to undergo small amplitude harmonic translations $Z_a(x,y,t)$ at circular frequency ω and let c represent the speed of sound in the medium.
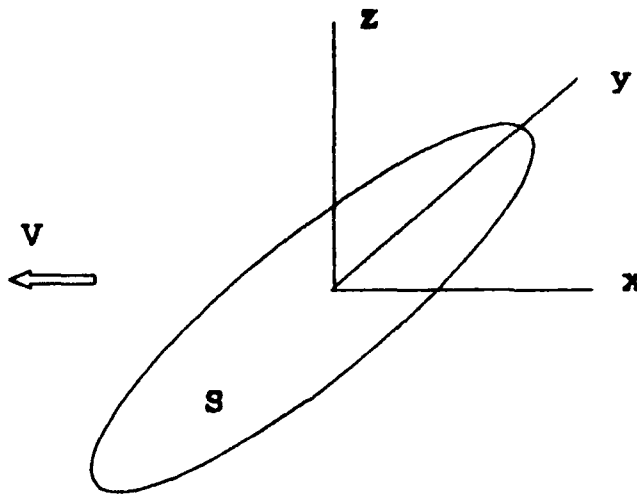
The problem for an oscillating wing consists in solving the wave equation to certain boundary conditions. The wave equation in rectangular coordinates is

$$\frac{\partial^2 \Xi}{\partial x^2} + \frac{\partial^2 \Xi}{\partial y^2} + \frac{\partial^2 \Xi}{\partial z^2} - \frac{1}{c^2}\left(V\frac{\partial}{\partial x} + \frac{\partial}{\partial t}\right)^2 \Xi = 0 \qquad \text{(F1)}$$

The dependent variable Ξ in equation (F1) is regarded as an acceleration potential. The acceleration is directly related to a perturbation pressure field and is related to a velocity potential Φ.

$$\Xi = \frac{\partial \Phi}{\partial t} + V\frac{\partial \Phi}{\partial x} \qquad \text{(F2)}$$

The boundary problem for the wing is completed by calculating the downwash $w(x,y,z,t) = \partial\Phi/\partial z$ associated with Ξ. This downwash is assumed to be harmonic with regard to time which implies that both potentials Ξ and Φ are harmonic with respect to time and as shown in equation (F3).

$$\Xi(x,y,z,t) = e^{i\omega t}\overline{\Xi}(x,y,z)$$

$$\Phi(x,y,z,t) = e^{i\omega t}\overline{\Phi}(x,y,z) \qquad \text{(F3)}$$

With these expressions for Ξ and Φ, equation (F2) becomes independent of time and reduces to an ordinary differential equation with one dependent variable

$$\overline{\Xi} = i\omega\overline{\Phi} + V\frac{d\overline{\Phi}}{dx} \qquad \text{(F4)}$$

This equation can be integrated with respect to x to produce equation (F5).

113

$$\overline{\Phi} = \frac{\exp\left(\frac{i\omega x}{V}\right)}{V} \int_{-\infty}^{x} \overline{\Xi}(\lambda, y, z) \exp\left(\frac{i\omega\lambda}{V}\right) d\lambda \qquad \text{(F5)}$$

The boundary problem for the wing may now be expressed mathematically in the following manner. Assuming simple harmonic motion, equation (F1) becomes

$$\frac{\partial^2 \overline{\Xi}}{\partial x^2} + \frac{\partial^2 \overline{\Xi}}{\partial y^2} + \frac{\partial^2 \overline{\Xi}}{\partial z^2} - \frac{1}{c^2}\left(V\frac{\partial}{\partial x} + i\omega\right)^2 \overline{\Xi} = 0 \qquad \text{(F6)}$$

To insure tangential flow at the wing surface, the potential must satisfy the following downwash condition.

$$\overline{w}(x, y) = \left(\frac{\partial \Phi}{\partial z}\right)_{z=0} = \left(V\frac{\partial}{\partial x} + i\omega\right) \overline{Z}_{a}(x, y) \qquad \text{(F7)}$$

Here w and Z_a are amplitudes of velocity and displacements respectively and are assumed to be known from the motion of the wing. At z=0, the pressure must be zero at all points (x,y) off the wing.

$$p = -\rho (\overline{\Xi})_{z=0} \qquad \text{(F8)}$$

The potential $\overline{\Xi}$ is allowed to be discontinuous at all points on the wing and the value of p is determined by the magnitude of the discontinuity in $\overline{\Xi}$ at the point. In the neighborhood of the trailing edge, p must go to zero to satisfy the Kutta condition. One other condition, that $\overline{\Xi}$ vanish far ahead of the wing is inherently satisfied by the condition given in equation (F5).

114

The potential Ξ_0 at a point (x,y,z) due to a harmonically pulsating doublet located in the x-y plane at a point $(\xi,\eta,0)$ that satisfies equation (F6) is

$$\Xi_0 = A \frac{\partial}{\partial z} \frac{\exp\left(i\omega\left[t + \frac{M}{c\beta^2}(x-\xi) - \frac{R'}{c\beta^2}\right]\right)}{R'} \tag{F9}$$

where

$$R' = \sqrt{(x-\xi)^2 + \beta^2(y-\eta)^2 + \beta^2 z^2}$$

The factor A is a strength and dimensionality factor allowing different uses and interpretations of the potential Ξ_0. If Ξ_0 is considered an acceleration potential and substituted into equation (F5), the corresponding velocity obtained may be written in the following manner.

$$\Phi_0 = A \frac{\partial}{\partial z} e^{\frac{i\omega(x-\xi)}{V}} \int_{-\infty}^{\lambda=x-\xi} \frac{\exp\left[i\omega\left(t + \frac{\lambda}{V} + \frac{M\lambda}{c\beta^2} - \frac{R}{c\beta^2}\right)\right]}{R} d\lambda \tag{F11}$$

where

$$R = \sqrt{\lambda^2 + \beta^2(y-\eta)^2 + \beta^2 z^2}$$

The downwash $\partial\Phi_0/\partial z$ associated with Φ_0 may be written as

$$\frac{\partial\Phi_0}{\partial z} = A \frac{\partial^2}{\partial z^2} e^{-\frac{i\omega x_0}{V}} \int_{-\infty}^{x_0} \frac{e^{i\overline{\omega}(\lambda - M\sqrt{\lambda^2 + r^2})}}{\sqrt{\lambda^2 + r^2}} d\lambda \tag{F13}$$

115

In equation (F13)

$$x_0 = x - \xi$$

$$\omega = \omega / V\beta^2$$

$$r = \sqrt{(y-\eta)^2 + z^2}$$

With the use of equations (F13) and (F14) and the concept of solving linear boundary-value problems by means of superposition of elementary solutions to the governing differential equation, the boundary value problem presented here can be reduced to an integral equation.

$$\bar{w}(x,y) = \lim_{z \to 0} A \iint_S L(\xi, \eta) \, e^{-\frac{i\omega x_0}{V}} \, d\xi \, d\eta \, \frac{\partial^2}{\partial z^2} \int_{-\infty}^{x_0} \frac{e^{i\bar{\omega}(\lambda - M\sqrt{\lambda^2 + r^2})}}{\sqrt{\lambda^2 + r^2}} \, d\lambda$$

(F15)

Here S represents the surface of the wing and $L(\xi, \eta)$ represents an unknown lift distribution or doublet strength on S. This integral equation can be reduced further to the form given in Chapter 2 as shown in Reference 31.

116

Vita

Captain John K. Ryder (Ken) was born on ███████████████████,
███████. He graduated from Lake Forest High School, Felton, Delaware,
in 1982 and entered the University of Delaware from which he received
the degree Bachelor of Mechanical Engineering in 1986. Upon graduation,
he was commissioned a second lieutenant in the USAF through the AFROTC
program. He entered active duty at the Ballistic Missile Office, Norton
AFB, California where he served as the project officer for the third
stage of the Peacekeeper ICBM weapon system. Ken entered the School of
Engineering, Air Force Institute of Technology, in June 1989.

Permanent Address: ██████████████████

REPORT DOCUMENTATION PAGE

Public reporting burden for this collection of information is estimated to average 1 hour per response, including the time for reviewing instructions, searching existing data sources, gathering and maintaining the data needed, and completing and reviewing the collection of information. Send comments regarding this burden estimate or any other aspect of this collection of information, including suggestions for reducing this burden, to Washington Headquarters Services, Directorate for Information Operations and Reports, 1215 Jefferson Davis Highway, Suite 1204, Arlington, VA 22202-4302, and to the Office of Management and Budget, Paperwork Reduction Project (0704-0188), Washington, DC 20503.

1 AGENCY USE ONLY (Leave blank)	2 REPORT DATE	3 REPORT TYPE AND DATES COVERED
	December 1990	Master's Thesis

4. TITLE AND SUBTITLE

Modelling and Analysis of Kernel Function and Development of Equivalent Theodorsen Function for Three-Dimensional Aeroelastic Analysis

5 FUNDING NUMBERS

6. AUTHOR(S)

John Kenneth Ryder, Captain, USAF

7 PERFORMING ORGANIZATION NAME(S) AND ADDRESS(ES)

Air Force Institute of Technology
WPAFB OH 45433-6583

8. PERFORMING ORGANIZATION REPORT NUMBER

AFIT/GAE/ENY/90D-25

9. SPONSORING MONITORING AGENCY NAME(S) AND ADDRESS(ES)

WRDC/FIBRC
WPAFB OH 45433

10. SPONSORING MONITORING AGENCY REPORT NUMBER

11. SUPPLEMENTARY NOTES

12a. DISTRIBUTION AVAILABILITY STATEMENT

Approved for public release; distribution unlimited

12b. DISTRIBUTION CODE

13. ABSTRACT (Maximum 200 words)

A fractional calculus model is developed for the kernel function under incompressible subsonic flow conditions for rectangular planform airfoils with small aspect ratio. A model valid for restricted regions of the kernel function for compressible subsonic flow conditions is also developed. Additionally, a method for numerically solving the pressure-downwash integral equation for rectangular planform wings of aspect ratio two through ten in incompressible flow is developed. An equivalent Theodorsen function for three-dimensional unsteady flow is developed, enabling the use of the simpler two-dimensional aeroelastic equations of motion to fully capture the more complicated three-dimensional effects.

14. SUBJECT TERMS

Aeroelasticity, Three-Dimensional Flow, Unsteady Aerodynamics, Kernel Functions, Fractional Calculus

15. NUMBER OF PAGES

129

16. PRICE CODE

17 SECURITY CLASSIFICATION OF REPORT	18 SECURITY CLASSIFICATION OF THIS PAGE	19. SECURITY CLASSIFICATION OF ABSTRACT	20. LIMITATION OF ABSTRACT
Unclassified	Unclassified	Unclassified	UL